Grant Award 01HQGR0030

Dr. Timothy D. Stark
Stark Consultants, Inc.

Interpretation of Ground Shaking from Paleoliquefaction Features

NEHRP Element: II (Memphis Metropolitan Area)

Research supported by the U. S. Geological Survey (USGS), Department of the Interior, under USGS award number 01HQGR0030. The views and conclusions contained in this document are those of the authors and should not be interpreted as necessarily representing the official policies, either expressed or implied, of the U. S. Government.

Grant Award 01HQGR0030

INTERPRETATION OF GROUND SHAKING FROM PALEOLIQUEFACTION FEATURES

Dr. Timothy D. Stark, Stark Consultants, Inc. 401 W. Indiana Ave. Urbana, IL 61801
Telephone: (217) 840-8263 E-mail: stark@shout.net
Additional Investigators: Dr. S. F. Obermeier, Mr. E. J. Newman, and Ms. J. M. Stark
Reviewers: Dr. Russell A. Green, Dr. Scott M. Olson
NEHRP Element(s): II Keywords: Paleoliquefaction, Paleoseismology, CPT

TECHNICAL ABSTRACT

Evidence in the geologic record, e.g. buried liquefaction features, is used to determine the magnitude of earthquakes that occurred in the New Madrid Seismic Zone before the advent of seismic recording devices. Marginal paleoliquefaction features represent the threshold where the driving forces caused by earthquake shaking are essentially equal to the resisting strength of the soil. If the resisting strength of the soil at a site of marginal liquefaction is known, the driving force and thus the maximum acceleration and magnitude of the earthquake can be back-calculated.

Recent field testing at the Wolf River marginal liquefaction site near Memphis, Tennessee is used to quantify the soil shear strength. These strength values from the 2000 testing must be adjusted to account for changes that have occurred in the soil strength since the occurrence of historic earthquakes. These changes include increases in soil strength due to soil aging and the effects of changes in the location of the water table. Because of the uncertainty in the change in cone penetration resistance with time, the results of the back-analyses conducted herein should be considered to be overestimates.

New liquefaction potential relationships are presented herein for use in the simplified liquefaction evaluation procedure to determine the maximum acceleration (a_{max}) that caused the marginal liquefaction. The analysis indicates that the value of a_{max} to cause the observed marginal liquefaction features is between 0.15 to 0.20 g without considering soil aging effects, respectively. Attenuation and site response analyses are used to show the earthquake magnitudes that correspond to these a_{max} values are 7.9 and 8.4. Analyses of three liquefaction sites in the New Madrid Seismic Zone using the same procedure indicate that values of a_{max} range from 0.16 g to 0.22 g and earthquake magnitudes required to cause the observed liquefaction features are 7.4 and 7.8 without considering aging effects.

An energy-based liquefaction evaluation procedure is presented herein and is also used to estimate the values of a_{max} and earthquake magnitude for the historic earthquakes. This procedure yields back-calculated peak ground accelerations of 0.18 to 0.23 g corresponding to earthquake magnitudes 8.2 and 8.6, respectively. Analysis of the liquefaction sites in the New Madrid Seismic Zone yields peak ground accelerations from 0.19 g to 0.24 g and corresponding magnitudes of 7.6 to 8.1. Further research is necessary to identify the regional behavior in the NMSZ of many of the factors used in the development of the energy-based liquefaction evaluation procedure.

Grant Award 01HQGR0030

INTERPRETATION OF GROUND SHAKING FROM PALEOLIQUEFACTION FEATURES

Dr. Timothy D. Stark, Stark Consultants, Inc. 401 W. Indiana Ave. Urbana, IL 61801
Telephone: (217) 840-8263 E-mail: stark@shout.net
Additional Investigators: Dr. S. F. Obermeier, Mr. E. J. Newman, and Ms. J. M. Stark
Reviewers: Dr. Russell A. Green, Dr. Scott M. Olson
NEHRP Element(s): II Keywords: Paleoliquefaction, Paleoseismology, CPT

NON-TECHNICAL ABSTRACT

Evidence in the geologic record, e.g. buried liquefaction features, can be used to determine the magnitude of earthquakes that occurred before the advent of seismic recording devices. Marginal paleoliquefaction features represent the threshold where the driving forces caused by earthquake shaking are essentially equal to the resisting strength of the soil which allows for back-calculation of the maximum acceleration and magnitude of the earthquake. Recent field testing at a site near Memphis, Tennessee where marginal liquefaction was caused and at four sites in Arkansas where full liquefaction effects were caused are used to quantify the soil shear strength. This field testing was performed in 2000 and must be adjusted for changes in soil strength and the insitu condition since the occurrence of the earthquakes. Back analyses are conducted to estimate the earthquake magnitude that had to occur to cause liquefaction at the marginal liquefaction site as well as at the full liquefaction sites. These back-analyses indicate an earthquake magnitude less than 7.9 for the 1811-1812 new Madrid earthquakes.

TABLE OF CONTENTS

TECHNICAL ABSTRACT 3
NON-TECHNICAL ABSTRACT 5
INTRODUCTION 9
PALEOLIQUEFACTION SITES AND TESTING 11
Epicentral Locations 11
Memphis 12
Memphis Site Selection 12
Wolf River Test Site Description 13
Memphis Field Testing – Wolf River Sites 15
Cone Penetration Testing (CPT) 15
Portable Dynamic Cone Penetrometer (DCP) 16
Calibration of Portable DCP Data to CPT Data at Wolf River Sites 17
Grain Size Analysis of Wolf River Sands 18
New Madrid Seismic Zone 19
Walker Farm Site 19
Nodena Farm Site 20
Hillhouse Farm Site 21
Dexter, MO Sites 23
Other Sites 24
DETERMINATION OF HISTORICAL IN SITU CONDITION 24
Densification Caused by Liquefaction 24
Strength Increase Due To Soil Aging 25
Strength Increase Due To Earthquake Shaking 27
Change in Penetration Resistance Caused by Changes in Ground Water Surface 28
1811-1812 Ground Water Surface Location – Memphis 28
1811-1812 Water Table Location – New Madrid Seismic Zone 28
BACK CALCULATION OF a_{max} USING THE SIMPLIFIED PROCEDURE 30
Overview of Evaluation Procedure for Use of the Simplified Procedure 30
Determination of SSR to Develop Liquefaction Potential Relationships 31
Update of CPT Liquefaction Potential Database 33
Update of Liquefaction Potential Relationships 38
Liquefaction Potential of Sandy Soils Based On Cyclic Stress Ratio 38
Soil Group 1 - Fines Contents less than 12% 38
Soil Group 2 - Fines Contents greater than or equal to 12% and less than 20% 39
Soil Group 3 - Fines Content greater than or equal to 20% and less than 35% 40
Soil Group 4 - Fines Content greater than or equal to 35% 41
New Liquefaction Potential Relationships 43
Comparison of Proposed and NCEER CPT-Based Liquefaction Potential Relationships 44
Comparison of Measured and NCEER Fines Contents 48
Determination of a_{max} at a Paleoliquefaction Site Using Proposed Liquefaction Potential Relationships 49
Determination of a_{max} at Wolf River Liquefaction and No Liquefaction Sites Using Simplified Procedure 52
Determination of a_{max} In the NMSZ Using Simplified Procedure 55
USE OF ENERGY-BASED LIQUEFACTION EVALUATION PROCEDURE 59

Overview of Energy-Based Procedures for Liquefaction Assessment 59
Development of Mathematical Expression for Normalized Energy Demand 62
Determination of Soil Shear Modulus 63
Determination of Shear Strain for τ_{avg} 65
Determination of Normalized Energy Demand (*NED*) 66
Development of Relationship between Cone Tip Resistance and Soil *Capacity* 70
Liquefaction Potential of Sandy Soils Based on Normalized Energy Demand 70
Group 1 – Fines Contents less than 12% 70
Group 2 – Fines contents greater than or equal to 12% and less than 20% 71
Group 3 – Fines contents greater than or equal to 20% and less than 35% 72
Group 4 – Fines contents greater than or equal to 35% 73
New Liquefaction Potential Relationships 74
Comparison With SPT *Capacity* Curve 75
Energy Back-Analysis at Wolf River 77
Energy Back-Analysis at NMSZ Sites 79
DETERMINING MAGNITUDE OF HISTORIC EARTHQUAKES 81
Ground Motion Attenuation and Site Response Model 83
Site Response Analysis 85
Paleoliquefaction Site Amplification Factors 89
Magnitude Back-Calculated at Wolf River 94
Magnitude Back-Calculated in NMSZ 97
SUMMARY 100
RECOMMENDATIONS FOR FUTURE RESEARCH 101
APPENDIX A 103
GRAIN SIZE DISTRIBUTION CURVES FOR WOLF RIVER LIQUEFACTION SITES 103
APPENDIX B 107
LIQUEFACTION CASES UTILIZED IN DATABASE FOR CPT LIQUEFACTION POTENTIAL RELATIONSHIPS 107
APPENDIX C 113
DATABASE FOR CPT LIQUEFACTION POTENTIAL RELATIONSHIPS 113
APPENDIX D 119
DENSIFICATION CAUSED BY LIQUEFACTION 119
Change in N Value 120
Change in Void Ratio 124
Relating Liquefaction Decrease in Void Ratio to Increase in N Value 125
APPENDIX E 129
GROUND MOTION ATTENUATION AND SITE RESPONSE MODEL 129
Frequency Spectrum At the Earthquake Source 132
Attenuation of Frequency Spectrum From Source To Site 134
Low Pass Filter 136
Site Amplification Spectrum 138
REFERENCES 139

INTRODUCTION

Regions where earthquakes of high magnitudes are a rare occurrence provide a challenge to engineers when designing structures to resist seismic forces. The low rate of occurrence means that it is likely that no measurements or recordings of earthquake motions in the region are available. In order to determine how large of an earthquake might be expected in a region like this, evidence from previous earthquakes must be examined.

Studies performed by many researchers (Tuttle et al. 2000, Tuttle 1999, Vaughn 1994, Barnes 2000) have identified the historical seismicity in the New Madrid Seismic Zone through the dating of paleoliquefaction features. The major periods of seismicity prior to 1811-1812 that have been identified are approximately AD 900 and AD 1530. Figure 1 shows the locations and ages of paleoliquefaction features studied in the NMSZ. Paleoliquefaction features corresponding to all three major periods of seismicity have been found throughout the region, and sometimes at the same sites. This indicates that the historic earthquakes share similar fault rupture behavior and energy centers, as well as being similar in magnitude.

Evidence in the geologic record, e.g. buried liquefaction features, can be used to determine the magnitude of earthquakes that occurred in the New Madrid Seismic Zone. The spatial distribution and size of liquefaction features can indicate the magnitude of the event that caused them (Obermeier et al. 1993, Pond 1996, Pond and Martin 1997), though this behavior varies from region to region. As an alternative, an insitu measurement of the strength of the soil can provide an indicator of the intensity of ground shaking required to cause liquefaction at a particular site.

Marginal paleoliquefaction features represent the threshold where the driving forces caused by earthquake shaking are essentially equal to the resisting strength of the soil. Marginal liquefaction sites provide the best estimate of strong motion parameter in the back-calculation because these driving and resisting forces are essentially equal. Sites of no liquefaction and extensive liquefaction are also useful in the paleoliquefaction analysis because the back-calculation provides an upper bound and lower bound, respectively, of strong motion parameters. These upper and lower bounds provide a range for the back-calculated magnitude of a prehistoric earthquake and more importantly, they provide an independent verification of the values obtained for the marginal liquefaction features. The main objectives of the study are to develop and apply a procedure to back-calculate the peak ground acceleration and magnitude of the 1811-1812 New Madrid earthquakes, as well as other historic earthquakes in the region, using marginal paleoliquefaction features near Memphis, Tennessee and sites of extensive and no liquefaction within the New Madrid Seismic Zone (NMSZ).

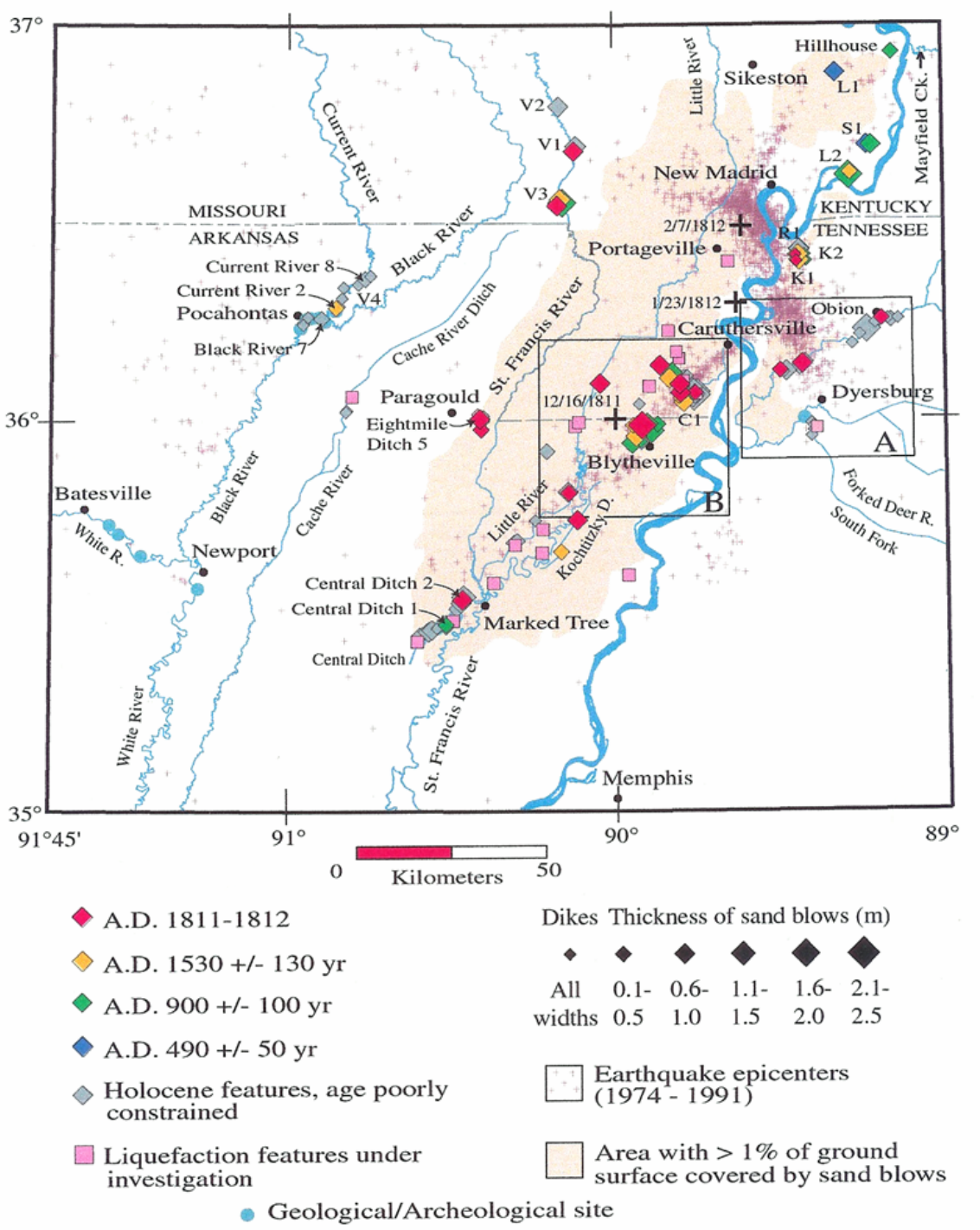

Figure 1. Map of NMSZ showing locations and age of paleoliquefaction features (from Tuttle 1999)

PALEOLIQUEFACTION SITES AND TESTING

Epicentral Locations

Table 1. Estimated epicenter locations of 1811-1812 earthquakes and distances to Wolf River test site

Date of Earthquake	Name	Location of Epicenter	Epicentral Distance to Wolf6
December 16, 1811	Blytheville, AK	35.95N/89.95W	95 km
January 23, 1812	New Madrid, MO	36.67N/89.55W	175 km
February 7, 1812	Tiptonville, TN	36.40N/89.50W	140 km

The epicentral locations and dates of the three New Madrid earthquake events of 1811 – 1812 shown in Figure 2 were given by Dr. Arch Johnston of the University of Memphis (e-mail communication to Dr. Timothy Stark on March 11, 2002). Dr. Johnston stated that the December 16, 1811 event is somewhat constrained to the Blytheville arch right at Blytheville, the epicentral location of the January 23, 1812 event is a best guess, and the February 7, 1812 event is fairly well constrained to the mid-section and down dip on the Reelfoot fault, leading to the values of latitude and longitude given in the table.

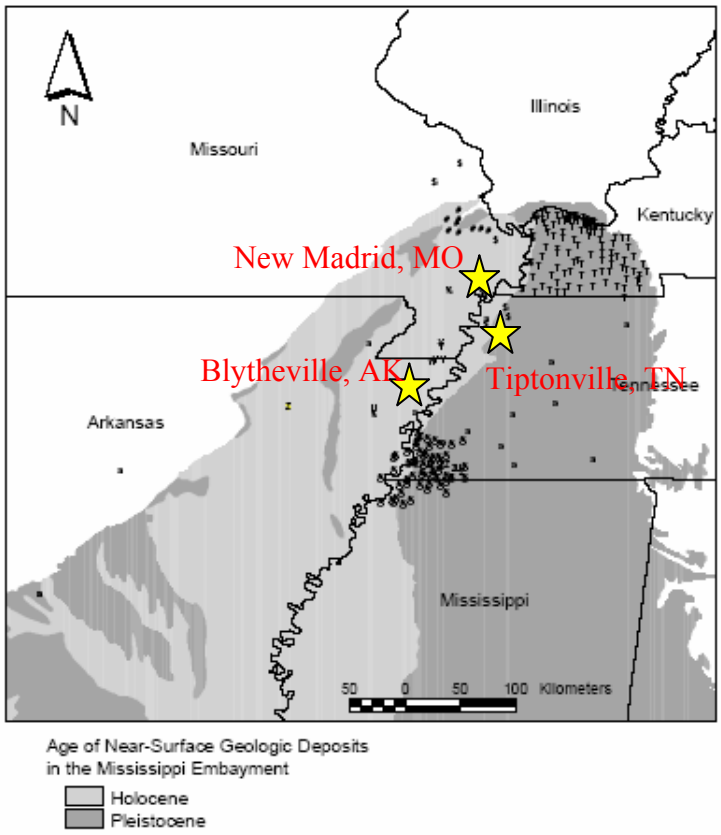

Figure 2. Map of the Upper Mississippi Embayment showing epicentral locations listed in Table 1 (after Romero and Rix 2001)

Memphis

Memphis Site Selection

The city of Memphis, Tennessee, is in such proximity to the NMSZ as to be susceptible to severe damage from strong earthquakes originating there. Liquefaction features of young age, and likely caused by the 1811-1812 earthquakes, have recently been discovered at scattered locales in the Memphis area (Broughton et al. 2001). These liquefaction features were exposed in near-vertical river banks in a variety of field settings. There are no reports of locales in the Memphis region where liquefaction effects can be observed in plan view. The search for a field test site for this study concentrated on river banks that have thick deposits of clean sand that were potentially liquefiable at the time of an earthquake and have an overlying cap thickness that is quite variable. A variable cap thickness is used to bracket the depth of water table at the time of the earthquake(s). Based on Broughton et al. (2001) and communications with Professor Roy Van Arsdale of the University of Memphis, co-author of the Broughton et al. (2001) paper, a decision was made to focus on a portion of the Wolf River in the eastern suburbs of Memphis, between the towns of Germantown and Collierville (see Figure 3), where Professor Van Arsdale has found paleoliquefaction features. The primary author visited this Wolf River site in 1998.

Figure 3. Area of field study indicated by star
(www.ce.gatech.edu/~geosys/Faculty/Mayne/Research/summer2000/wolf/map.htm)

The selected area of the Wolf River lies just upstream from a portion that was channelized (straightened) about 20 years ago by the U. S. Army Corps of Engineers. In response to channelization, the river has been eroding down and laterally exposing the soil profile in the banks. A field search, conducted by Dr. Stephen Obermeier during this

study, entailed a continuous examination of the river banks, mainly from a canoe, extending for about 8 km from S. Collierville Arlington Road to Houston Levee Road (see Figure 4). Recent downcutting along the first few km was only about a meter at the time, but after encountering an erosional nickpoint, the downcutting for the next 5 to 6 km increased rather abruptly to about 3 m. Examination of the river banks in the selected area revealed that the lower portions of the bank exposures extend below the depth of oxidization, and thus below the depth of the water table. Also, the exposed banks show sand deposits immediately beneath the clay cap, that are typically thick, clean, and medium grained. These sands appear to be not more than moderately dense at many places, and thus they are judged likely to be susceptible to liquefaction during moderate levels of shaking. Additionally, the thickness of the fine-grained cap was seen to be quite variable, ranging from 1.7 m to 3 m. In summary, this portion of the Wolf River was judged to be suitable for this paleoliquefaction study.

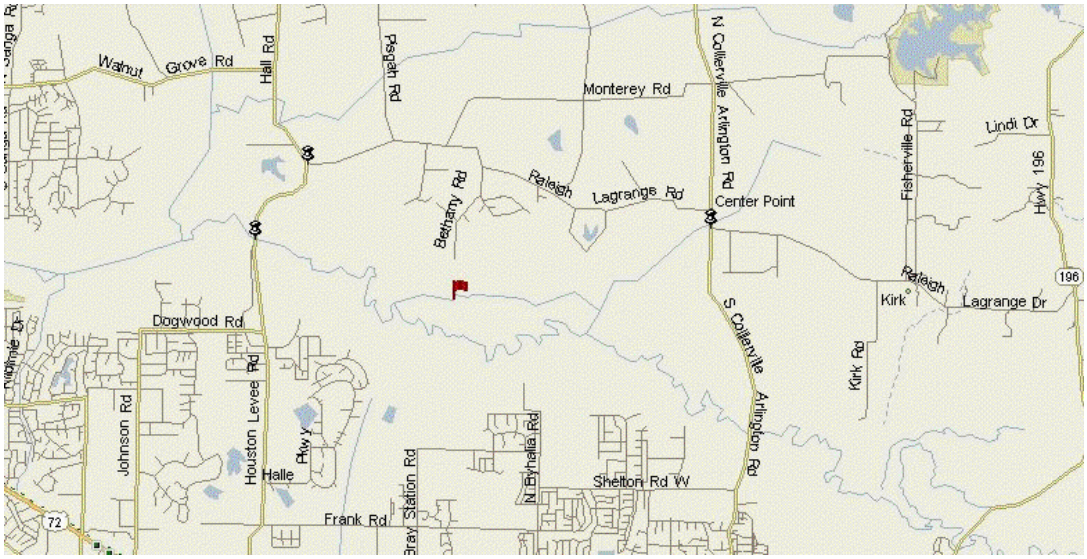

Figure 4. Area of field search along Wolf River
(Selected test site indicated by flag.)
(www.ce.gatech.edu/~geosys/Faculty/Mayne/Research/summer2000/wolf/map2.jpg)

Wolf River Test Site Description

The search for a test site along this portion of the Wolf River concentrated on locating marginal liquefaction-induced features. A marginal liquefaction feature, as defined for this field search, is a small liquefaction-induced effect (e.g., small non-horizontal sand deposits accompanied by fluidization features or ground-failure features) caused by liquefaction of a zone of sediment that is relatively thick in relation to the size of the observed liquefaction-induced features within it. This definition takes into consideration all mechanisms of ground failure, whether from hydraulic fracturing, lateral spreading, or surface oscillations. An area of scattered small dikes was discovered and chosen as the field test site for this study (Figure 4).

A schematic elevation of the river bank at the test site area is shown in Figure 5 along with a photograph of one of the marginal liquefaction features. At the ground surface is a clay-silt cap, probably derived from loess washed into the river valley from uplands and later deposited as overbank deposits. The uppermost portion of the cap, about 0.5 m thick, is quite young and almost certainly postdates the 1811-12 earthquakes. As a result, this upper 0.5 m of clay-silt is not incorporated in the liquefaction and site response analyses.

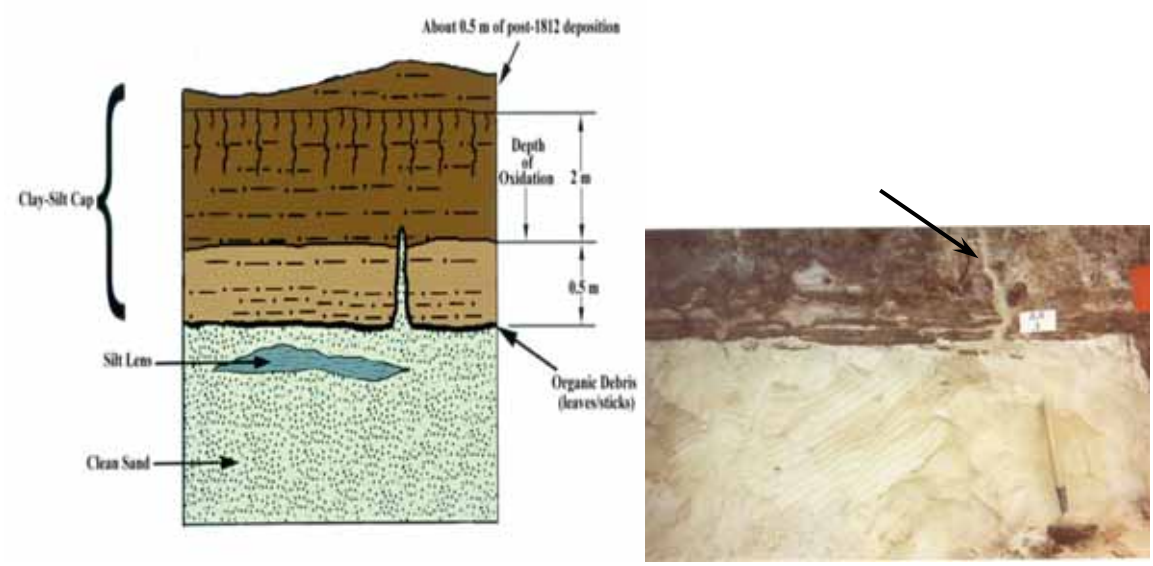

Figure 5. River bank schematic and photographic elevations at Wolf River marginal liquefaction test site AA3

The base of the cap is underlain by either a thick deposit of clean, medium-sized quartz sand, with no more than a few percent silt; or a transition zone of fine-to medium grained sand with silt lenses, which typically extends from the base of the cap to less than a meter below, whereafter the clean, medium-grained, thick sand deposit is present.

The uppermost 2 m of the cap beneath the very young surficial veneer is commonly oxidized, and the degree of oxidization diminishes rather abruptly with depth. Along the base of the cap, sticks and leaves were encountered at many locations. These were probably deposited slightly before the soil layers comprising the fine-grained cap.

Seven sites of liquefaction features were identified along a half-kilometer length of the south bank of the Wolf River, indicated as AA1 through AA7 in Figure 6. Some of the features have small dikes (<2.5 cm in width) such as the one shown in Figure 5 extending into the cap or cutting thin silt stringers just beneath the cap. In some cases fluidization had caused the silt stringers to be broken into clasts and distributed into the overlying clean sand. On the northern bank, only one small dike in the cap was found (Figure 6), located where the river turns from north to west. Other small effects of liquefaction were observed on the northern bank, at the westernmost portion of the area shown on Figure 6.

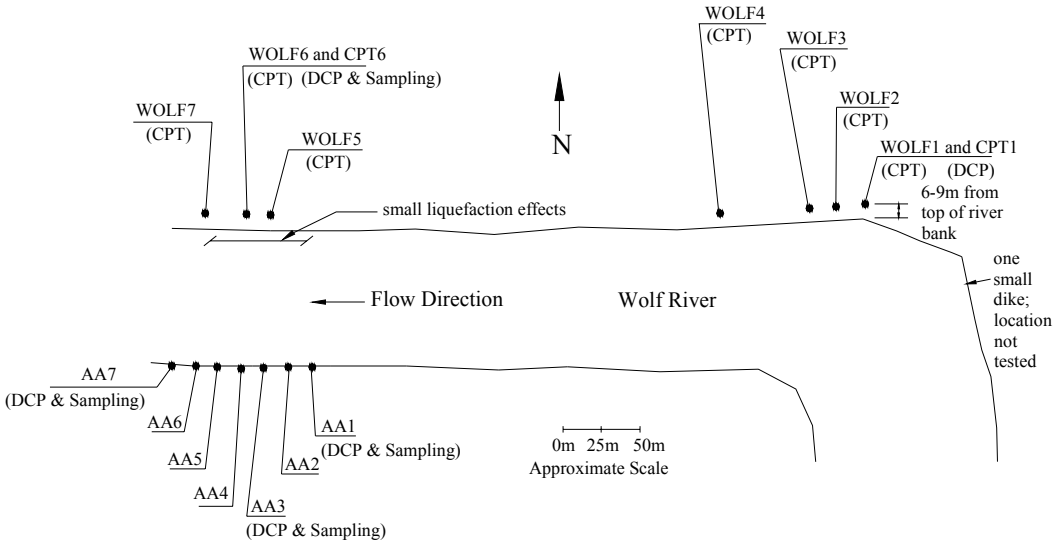

Figure 6. Map showing individual testing locations at the Wolf River site

The largest dikes extend up into the cap only about 1-1.5 m and all of the dikes in the cap pinch together completely. This pinching together made it impossible to accurately date when any of the dikes formed, but it was noted that the sand filling in the dikes is very loose and unoxidized, thus making it a relatively young deposit. An origin during the 1811-1812 New Madrid earthquakes seems plausible and likely for all the observed liquefaction effects, which is consistent with the degree of weathering and the looseness of the sand filling in the dikes.

Memphis Field Testing – Wolf River Sites

Cone Penetration Testing (CPT)

A truck-mounted CPT rig, owned and operated by the Georgia Institute of Technology School of Civil and Environmental Engineering, tested seven sites along the northern bank of the Wolf River in the summer of 2000. These sites were chosen by Dr. Obermeier and are shown as Wolf1 through Wolf7 in Figure 6. The CPT truck was not able to get closer than about 6 – 9 meters to the top of the river bank, nor was it able to access the southern bank of the river. Therefore, CPT soundings were recorded a distance from the paleoliquefaction features on the northern bank. A portable cone penetrometer, described subsequently, was used to obtain information closer to the liquefaction features along the southern bank. Records of the soundings taken at sites Wolf1 through Wolf7 were obtained from:

http://www.ce.gatech.edu/~geosys/Faculty/Mayne/Research/summer2000/wolf/wolf.htm.

Sites Wolf1 through Wolf3 are clustered within 30 m of each other along the northern river bank (see Figure 6). Bank exposures were excellent at the time of this investigation and revealed no clear-cut effects of liquefaction. The Wolf4 site is located another 60 m downstream, where no liquefaction or fluidization effects were observed. The bank exposure at Wolf4 was only fair, but if significant liquefaction features were present they would have been seen. Wolf5 and Wolf6 are 300 m farther downstream and 15 m apart from one another. Liquefaction effects were observed at both of these sites and source beds of liquefaction were identified at site Wolf6. Site Wolf7 was another 30 m downstream from Wolf6, and this site was judged not to exhibit any evidence of liquefaction. The location of sites Wolf5 through Wolf7 were selected partly to provide data for the liquefaction features previously observed on the opposite (south) bank of the Wolf River (about 100 m away) that was inaccessible by the CPT truck. As a result, only portable dynamic cone penetrometer tests were conducted on the south bank of the Wolf River.

Portable Dynamic Cone Penetrometer (DCP)

A portable dynamic cone penetrometer (DCP) was used to gather data at three of the paleoliquefaction sites discovered along the south bank of the Wolf River. These sites are denoted as AA1, AA3, and AA7 on Figure 6. These sites are of most interest because they contain the best examples of marginal liquefaction, and they were inaccessible to the truck-mounted CPT rig. The DCP, as described by Sowers and Hedges (1966), is manufactured by Durham Geo-Enterprises of Stone Mountain, GA and shown in Figure 7 and Figure 8. It is comprised of a 15 lb (6.8 kg) steel ring that drops 20" (0.5 m) along a sliding rod with a 45^{o} cone-shaped drive tip. Penetration resistance is measured as a blow-count value. According to Sowers and Hedges (1966), use of the DCP involves seating the cone tip 2" (5 cm) into the undisturbed bottom of an augured hole and recording the number of drops of the 15 lb (6.8 kg) weight required to drive the cone tip 1-3/4" (4.5 cm) into the sampled material. The drop test can be repeated for 2 to 3 more 1-3/4" (4.5 cm) lengths, after which the side friction of the shaft and the altered shape of the shear zone around the cone tip may jeopardize the value of the blow count readings. The DCP can be effectively used in augured holes to depths of 15 to 20 feet (4.5 to 6 m). The values recorded using the DCP can then be correlated to equivalent penetration values as measured by the standard penetration test (SPT) or by CPT. The main benefits of the DCP are: (1) it is portable; (2) it can be used at the edge of a river bank without causing bank instability; (3) it is less expensive than a CPT truck; (4) soil samples can be obtained for grain size analyses; and (5) lower maintenance costs. The main disadvantages are that it is somewhat labor intensive and the allowable testing depth is limited by the weight of the equipment. These limitations prevented DCP measurements from being made in the soil layers most critical to liquefaction. Measurements were made as deep as the equipment and soil allowed to verify the stratigraphy from the CPT as well as to recover samples for grain size analysis.

DCP measurements were made next to CPT test sites Wolf1 and Wolf6, as shown on Figure 6, for calibration purposes. Calibration of the DCP measurements at the Wolf River test sites with corresponding CPT values is discussed subsequently.

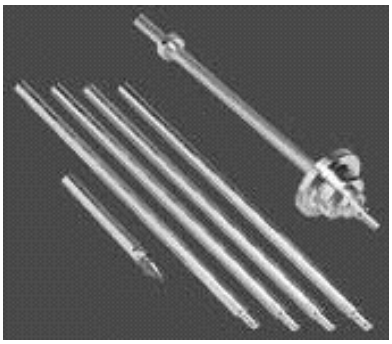

Figure 7. Portable dynamic cone penetrometer components
(www.durhamgeo.com/testing/soils/field-testing1.html)

Figure 8. Portable dynamic cone penetrometer in use at a Wolf River test site

Calibration of Portable DCP Data to CPT Data at Wolf River Sites

The blow count values recorded using the DCP, N_{DCP}, at the CPT6 test site were compared to the penetration resistance values, q_c, recorded using the CPT device at the Wolf6 site to develop a calibration relationship. Figure 9 shows a graph of N_{DCP} values versus q_c values recorded at corresponding depths. The N_{DCP} values plotted in Figure 9 are average blow counts from 2-3 adjacent drop tests and the q_c values are an average of six adjacent CPT resistance values in the same sounding. Averaging of the N_{DCP} and q_c values is used to reduce the effects of small-scale or local soil variability.

The resulting relationship and equation in Figure 9 can be used in other projects to convert N_{DCP} blow count values to equivalent values of q_c for sands having grain size characteristics similar to the Wolf River test site sands, as given in Figure 10 below.

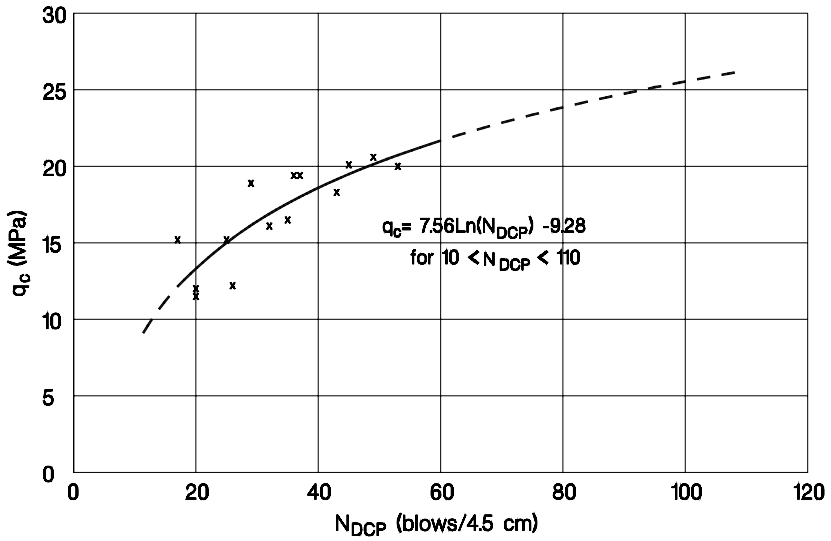

Figure 9. Calibration curve of q_c and N_{DCP} for Wolf River test site

Grain Size Analysis of Wolf River Sands

During DCP testing, soil samples were collected at sites CPT6, AA1, AA3, and AA7, which are shown on Figure 6. Samples were taken at 2" depth intervals in the zones that contained evidence of marginal liquefaction. Samples were collected at site CPT6 to support the development of a correlation for the DCP measurements with CPT readings. Samples were collected along with DCP measurements at liquefaction sites AA1, AA3, and AA7.

Results of grain size analyses conducted on the samples are shown in Figure 10 for the Wolf River sites noted above. Grain size distributions for individual sites are included in Appendix A.

Figure 10 shows the soils in the zones of marginal liquefaction at the sites tested during this study can be classified as clean sands, having D_{50} = 0.33- 0.68 mm and a fines content of 0 – 5%. Ishihara et al. (1989) defines the range of grain size distributions most susceptible to liquefaction and these range boundaries are included in Figure 10 as dashed lines. The grain size distributions for the sands in the zones of marginal liquefaction at the Wolf River test sites fall completely within the boundaries for the most liquefiable soils defined by Ishihara et al. (1989). This supports field observations that liquefaction could occur at these sites if the sand was saturated at the time of shaking, the sand was loose to medium dense, and the earthquake was large enough.

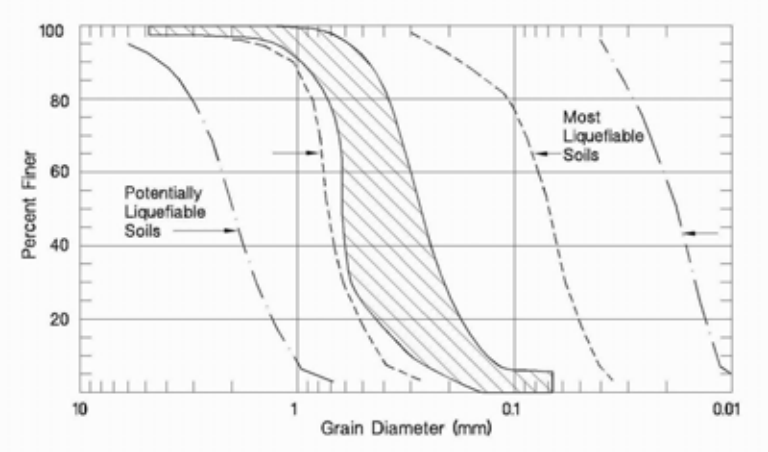

Figure 10. Grain size distribution curves for sand samples taken at the Wolf River test sites CPT6, AA1, AA3, and AA7

New Madrid Seismic Zone

Professor Paul W. Mayne of the Georgia Institute of Technology School of Civil and Environmental Engineering has directed features such as sand blows are visible at the ground surface or visible in near surface trenches) in the New Madrid Seismic Zone. Data from these sites can be used to provide a lower bound to the values of earthquake magnitude and acceleration in a back-calculation. Table 2 gives a summary of the cone penetration testing performed by the Georgia Institute of Technology at several sites of extensive liquefaction in the New Madrid Seismic Zone that were considered in this study. Figure 11 shows a map of the location of the sites listed in Table 2 as well as the location of other CPT sites investigated by the Georgia Institute of Technology. The raw data from all of the soundings is available from the following URL:

<http://www.ce.gatech.edu/~geosys/Faculty/Mayne/Research/>

Walker Farm Site

The Walker Farm site in Marked Tree, Arkansas contains several major sand dikes caused by liquefaction. Tuttle et al. (2000) used aerial photography and geophysical mapping to locate these liquefaction features. To examine them, trenches were excavated through two of the dikes to map the liquefaction features in cross-section as well as to recover archeological samples for dating. Analyses of the recovered archeological samples date the formation of the liquefaction features to sometime after AD 1420. For all of the paleoliquefaction sites, the dates estimated using radiocarbon methods correspond to the formation of the large, surficial paleoliquefaction features and do not identify any liquefaction of lack thereof that may have occurred after the formation of these features.

Because the liquefaction features at this site are severe, the back-analysis is only providing a lower bound on the ground shaking experienced there during that particular seismic event. Although not directly comparable with the event that caused the

liquefaction features at the Wolf River site, data from older sites can still provide lower bounds for seismicity of the region in general.

A map of the Walker Farm test site is shown in Figure 12. As seen in Figure 12, the CPT testing was performed in two linear arrays perpendicular to the main direction of the sand dikes. Soundings MTREE02 to MTREE08 were performed across a dike on the south and soundings MTREE09 to MTREE14 were performed across a sand dike to the north. Sounding MTREE01 is a reference sounding. The locations of the soundings were chosen with input from Dr. Martitia Tuttle and Laurel Clark working with Dr. Buddy Schweig (Liao et al 2001).

Table 2. Summary of cone penetration testing in the New Madrid Seismic Zone performed by the Georgia Institute of Technology and considered in this study

Test Sites	Severity of Liquefaction	Date of CPT Sounding	Approximate Date of Formation of Liquefaction Features
Walker Farm (Marked Tree, AR)	Extensive	July 2000	after AD 1420
Nodena Farm (Wilson, AR)	Extensive	March 2001	AD 1470
Hillhouse Farm (Wyatt, MO)	Extensive	March 2001	AD 900
Wilhelmina Cutoff (Dexter, MO)	Small to Extensive	June 2001	possible 1811-1812 AD 1440-1540 AD 240-1020
Dudley main ditch (Dexter, MO)	Extensive	June 2001	10,000BC-AD 400 ca. 15,000 BC
Clodfelter ditch (Dexter, MO)	Extensive	June 2001	no radiocarbon dating, probably pre-1811

Nodena Farm Site

The Nodena Farm site northeast of Wilson, Arkansas contains several sand blows identified using aerial photography by Tuttle at al. (2000). Three trenches were excavated and logged and artifacts were recovered for radiocarbon dating and archeological examination. Based on this dating, the liquefaction features have been dated to a max age of AD 1470 (Tuttle et al. 2000). Four CPT soundings were performed in a linear array at this site. Though a small number of CPT soundings were performed at this site, it was also judged to be suitable for this study. Because the liquefaction features

at this site are severe, back-analysis of this site only provides a lower bound on the ground shaking experienced there during that particular seismic event.

Hillhouse Farm Site

The severe liquefaction feature at the Hillhouse Farm site in Wyatt, Missouri has been dated to around AD 900 (Barnes 2000). It can be seen from Figure 11 that this site is located a distance north of the liquefaction occurrences discussed in this report. The liquefaction features at this site are dated older than the Walker and Nodena Farm sites.

Figure 11. Locations of testing performed by the Georgia Institute of Technology in the New Madrid Seismic Zone (after Liao et al. 2002)

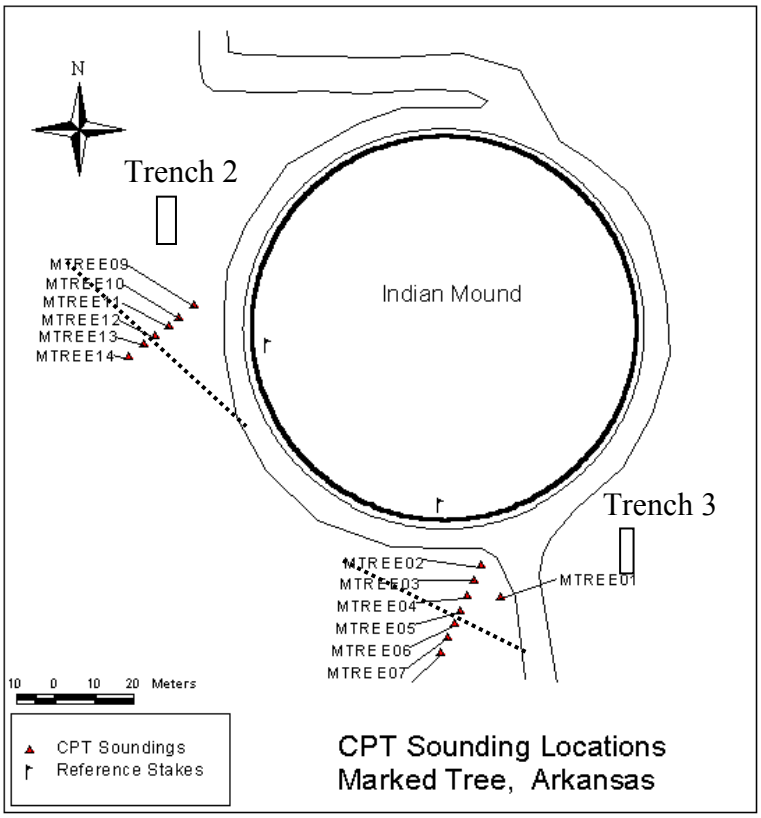

Figure 12. Map of CPT soundings performed by the Georgia Institute of Technology at the Walker Farm site in Marked Tree, Arkansas with approximate orientations of major sand blows, and approximate locations of trenches studied by Tuttle et al (2000) (after Liao et al. 2001).

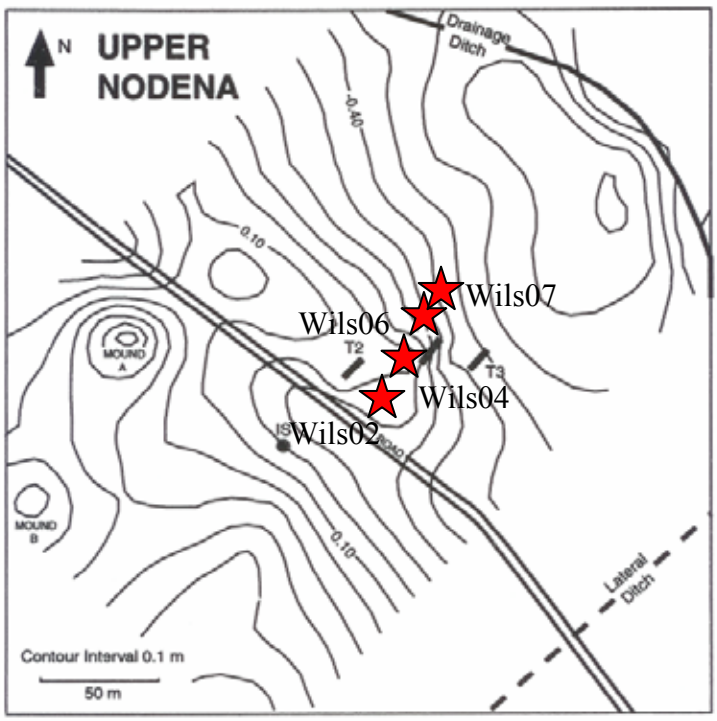

Figure 13. Map of Nodena Farm paleoliquefaction site with approximate locations of CPT soundings performed by Georgia Institute of Technology (after Tuttle et al. 2000).

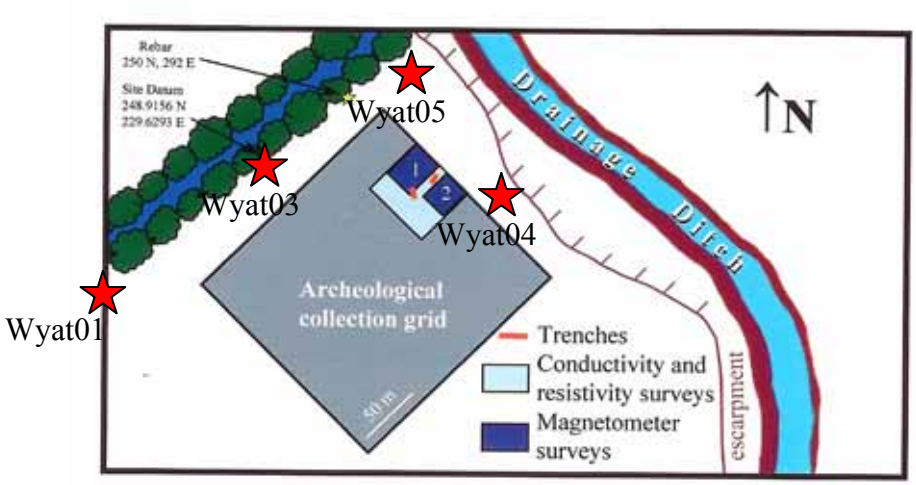

Figure 14. Map of Hillhouse Farm paleoliquefaction site with approximate locations of CPT soundings performed by Georgia Institute of Technology (after Barnes 2000).

Dexter, MO Sites

The paleoliquefaction site along the Wilhelmina Cutoff of the St. Francis River studied by Vaughn (1994) has several dikes and sand boils. A small sand boil is of probable

1811-1812 age, but had no organic material for radiocarbon dating. Organic material recovered from beneath larger sand boils yielded dates of AD 240-560, AD 770-1020, and AD 1440-1540. No information was available to identify the locations of the two CPT soundings relative to the liquefaction features studied by Vaughn (1994). The Wilhelmina Cutoff site was the best-documented of the Dexter, MO sites. Thus the CPT data from the Wilhelmina Cutoff was chosen over the other sites.

Other Sites

The other CPT soundings shown in Figure 11 were not considered for this study because they were performed either as part of a project to evaluate liquefaction hazards in the Memphis area or are located too close to the epicentral areas to be useful in cobination with attenuation and site response analyses.

DETERMINATION OF HISTORICAL IN SITU CONDITION

In order to determine the seismic forces required to cause liquefaction at a given site during previous earthquakes, it is necessary to determine the resisting shear strength of the soil deposit at the time of the earthquakes (Obermeier and Pond 1999 and Olson, Obermeier, and Stark 2001). Cone penetration testing, as well as standard penetration testing, can be used to estimate the current shear strength of a soil deposit that liquefied in the past. To relate the current strength of the soil to the strength of the soil at the time of liquefaction, it is necessary to account for the processes that the soil has undergone since the liquefaction occurred. These processes include earthquake densification, soil aging, and raising or lowering of the ground water surface. Aging of the soil describes the increase in shear strength caused by soil grain interaction and/or bonding over time. The depth of the ground water at the time of liquefaction is important because the effective stress is a key parameter in determining the shear strength of a soil

Densification Caused by Liquefaction

After liquefaction severe enough to create the dikes and sand boils studied at paleoliquefaction sites, large portions of the sandy layers at these sites can be essentially a new or fresh deposit. After the shaking has stopped, the excess pore water pressures that caused the liquefaction and the sand flow start to dissipate. Depending on the permeability of the sand and the clay cap, as well as the thickness of the sand layer, the thickness of the clay cap, the size of the liquefied area, and the availability of drainage outlets through the clay cap, this pore water pressure might take hours to days to dissipate. While this is happening the sand is consolidating or settling and gaining strength.

The time required for the primary consolidation to occur is difficult or impossible to calculate because of the uncertainties involved in each case. In the discussion on aging relationships presented subsequently, a reference time of 6 months after liquefaction is used for comparison purposes. This time is chosen somewhat arbitrarily, but is related to the timing of the field testing done to develop the liquefaction triggering relationship.

The majority of the field testing used in developing the liquefaction triggering relationships was performed anywhere from months to years after the occurrence of the liquefaction and thus a variable amount of time was allowed to pass between the end of primary consolidation at each site and the insitu testing performed at that site. This database primarily consists of post-earthquake measurements and thus changes to the soil during the earthquake that caused the liquefaction are not relevant to this study.

Strength Increase Due To Soil Aging

The phenomenon of soil aging, which results in soils gaining strength over time, is well recognized in the literature, although attempts to quantify this change are preliminary and ongoing. Three different soil aging theories are reviewed and applied to the 1811 – 1812 New Madrid earthquakes and the results of each theory are presented below.

First, Mesri et al. (1990) attribute this aging strength gain in sands to secondary compression. Secondary compression is defined as the gradual readjustment of soil particles to a more stable equilibrium position. The readjustment causes an increased number of interparticle contacts and surface interactions after a disruption caused by blasting or dynamic loads, which leads to a higher shear strength. Laboratory consolidation tests and field measurements of penetration resistance after ground densification were used by Mesri et al. (1990) to propose the following relationship to estimate the time-dependent increase in q_c beyond a reference time, t_R:

$$\frac{q_c}{q_{cR}} = \left(\frac{t}{t_R} \right)^{C_D \left(\frac{C_\alpha}{C_c} \right)} \tag{1}$$

where q_c is the cone resistance at any time $t > t_R$; q_{cR} is a reference cone resistance at a reference time, $t_R > t_p$; and t_p is the time of the end of primary consolidation. The reference time is any time selected after the disturbance and is discussed subsequently. The parameter C_D is defined as reflecting any densification by such disturbance mechanisms as vibration and blasting, which are not related to a static increase in effective vertical stress. C_α/C_C is a compression index parameter, equal to 0.02 for granular soils (Terzaghi et al. 1996). Mesri et al. (1990) recommend that a value of C_D = 7 with C_α/C_C = 0.02 be used in Equation (1) to estimate the time-dependent increase in q_c at times greater than t_R at sites with an average decrease in void ratio of about 10% (see Appendix D). However, Mesri et al. (1990) state that further study of the C_D parameter is needed.

It has been 189 years or approximately 69,000 days since the New Madrid earthquakes of 1811 – 1812 occurred. Using a reference time of 180 days (approximately 6 months) after the earthquakes, Equation (2) gives an increase in penetration resistance of 230% due to soil aging. For the Arkansas sites dated to earlier than 1811-1812 (approximately 550 years old) an increase in penetration resistance of 270% is calculated.

Second, Charlie et al. (1992) conducted CPT testing before and after blasting at a test site of saturated sand along the Platte River to develop the following expression for the time-dependent change in cone tip resistance:

$$\frac{(q_c)_{N-weeks}}{(q_c)_{1-week}} = 1 + K(\log_{10} N) \tag{2}$$

where N is the number of weeks after disturbance and K is an empirical constant, ranging from 0.02 to 1.0. Subsequent to this study, these same investigators reported in Clark et al. (1993): "After our paper was published we were able to obtain funding to conduct an additional CPT test …at our Platte River test site. At 5.5 years after the blast, tip resistance had increased to 211%…of the one week values." Substitution of these values into Equation (2) yields value of K = 0.45.

Using this value of K and N = 9828 weeks (189 years) since the New Madrid earthquakes of 1811 – 1812 leads to an expected tip resistance increase due to soil aging of 280% from Equation (2), which is in agreement with the 230% estimated using the methodology presented by Mesri et al. (1990).

Third, Joshi et al. (1995) present laboratory experiments to investigate the time-dependent increase in penetration resistance of sand and to study the effect of three different environmental conditions (dry sand, saturated sand in distilled water, and saturated sand in sea water) on the penetration resistance. They report that the increase in penetration resistance of sand submerged in water is not only caused by particle rearrangement, as in the case of dry sand, but is also due to dissolution and precipitation of salts and other impurities and possibly silica at the particle contacts and in the interspaces. For sand submerged in distilled water, the penetration resistance increased more than in the case of dry sand, and thus it is concluded that dissolution and precipitation of salts present in the sand grains affect the penetration resistance. (The precipitation of salts and other impurities may be especially relevant to the Wolf River sites because of the low ground water surface which allows surface water to infiltrate the upper partially saturated sand.) The aging phenomenon in the sands studied by Joshi et al. (1995) is approximated by the following exponential equation:

$$\frac{P_t}{P_1} = a(t)^b \tag{3}$$

where P_t is the penetration resistance at age t, P_1 is the penetration resistance of freshly deposited sand on the first day, t is the aging period expressed in days, and a and b are constants equal to 0.9 and 0.06, respectively, for dry sand, and 0.75 and 0.15, respectively, for saturated sand in distilled water. Using t = 68,985 days (189 years) and the coefficients a and b equal to 0.75 and 0.15, respectively for the condition of saturated sand in distilled water, the expected increase in penetration resistance is 399% due to aging since the 1811 – 1812 New Madrid earthquakes. Note that this increase does not include any effects of dry aging that may have occurred at the Wolf River test sites during the 20 years the sand deposits have been above the ground water surface.

Table 3 shows the range of time-dependent increase in cone penetration resistance caused by soil aging using these three prominent soil aging theories. These methods provide a range of increase in penetration resistance of 176% for dry aging conditions and 230 to 399% increase in penetration resistance for saturated aging conditions.

The length of time over which the strength gain was measured in the three studies ranges from 4 months in the Mesri et al. (1990) study, to 2 years and 9 months in the Joshi et al. (1995) study, to a maximum of 5.5 years for the Charlie et al. (1993) study. It may not be prudent to extrapolate the relationships obtained from these studies to the 189-year time frame since the New Madrid earthquakes of 1811 - 1812. It is conceivable that the rate of soil aging may decrease over longer periods of time and thus the methods over-predict the increase in penetration resistance. However, these studies represent the current state-of-the-art on the increase in cone penetration resistance with time and all three studies show a tip resistance increase greater than 200% over their relatively short time frames, i.e., less than 5.5 years. The correction of the cone resistance values for soil aging is thus a significant source of uncertainty in the estimate of the 1811 – 1812 level of shaking.

Table 3. Results Estimated increase in penetration resistance due to saturated aging

Method Used	Expected Increase since 1811 -1812
Mesri et al. (1990)	230%
Charlie et al. (1992)	280%
Joshi et al. (1995) Distilled Water	399%

Strength Increase Due To Earthquake Shaking

In addition to the gradual aging or secondary compression effects discussed above, earthquake shaking not severe enough to induce paleoliquefaction features can cause densification or increased particle interaction and increase the strength of the soil. In addition to the magnitude 7-8 earthquakes being studied herein, sites located in the NMSZ are subjected to lower magnitude earthquakes on a more frequent basis than the severe events that cause widespread liquefaction. The number of these earthquakes to which a paleoliquefaction site has been subjected and the effect of these earthquakes on the strength of the soil is another uncertainty in the change in insitu condition between the present day and the occurrence of a past earthquake.

For the reasons discussed above, strengths measured in a soil deposit in the present are likely to be higher than what would have been measured at the time of the earthquake or shortly after. Thus, strong-motion parameters back calculated based on present-day soil strengths will over-estimate the forces that caused liquefaction at the paleoliquefaction sites studied herein. The large uncertainties in the changes to the strength of the soil make it difficult to quantify the effect that these changes will have on the back-analysis of ground shaking. Therefore, back-analyses with varying reductions in strength to account for changes in the soil will be performed to illustrate the potential range of back-calculated values with and without these effects accounted for.

Change in Penetration Resistance Caused by Changes in Ground Water Surface

1811-1812 Ground Water Surface Location – Memphis

At the Wolf River study area just east of Memphis, the location of the ground water surface at the time of the 1811 – 1812 earthquakes has been estimated by field observation. Prior to the recent downcutting, the ground water surface through time has been relatively shallow, as indicated by the observed depth of oxidization to about 2.5 m below the ground surface and the presence of organic debris at many places along the base of the fine-grained cap, which is located at depths greater than about 3 m. This organic debris is susceptible to oxidization when above the ground water surface for only a few tens of years. If this oxidation occurs, all indicators of the organic debris' presence would be eliminated. (The only reason the organic debris is still present is that river downcutting due to channelization of the Wolf River only started occurring a few years ago.) Another indication of the depth of the ground water surface prior to the 1811 – 1812 earthquakes was obtained from the observation of the minimum depth of the bases of liquefaction dikes along the river. This procedure is the same as that used by Pond (1996) in the Wabash Valley of Indiana-Illinois to estimate the depth of the ground water surface. The uppermost base of these marginal dikes gives a lower bound to the historic depth of the ground water surface, i.e. the ground water surface could not have been any lower than the shallowest dike base to cause liquefaction, and may have been higher. No dikes were observed to originate in sands less than about 3.5 m below the current ground surface. Accounting for 0.5 m of deposition of sediment in the intervening 189 years, the maximum depth of the ground water surface at the time of the 1811 – 1812 earthquakes is estimated to be about 3 m below the ground surface at the Wolf River sites. In contrast, the depth of the ground water surface measured during CPT testing in the summer of 2000 is 6 m. Therefore, the state of stress in the soil profile used in the back-analysis must consider this decrease in the ground water surface from a depth of 3 m to 6 m.

1811-1812 Water Table Location – New Madrid Seismic Zone

At the time of the 2000-2001 testing program described in Table 2, the location of the ground water surface at the New Madrid Seismic Zone test sites was found to vary between 2.4 and 9.8 m below the ground surface. However, there is historic evidence that indicates at the time of the 1811-1812 New Madrid earthquakes this area was predominantly swampland, with the ground water surface located essentially at the ground surface, e.g., Penick (1976).

Penick (1976, pages 91-92) describes a report completed by army officer Amos Stoddard just before the New Madrid earthquakes of 1811-1812, in which he describes the condition of the land obtained in the Louisiana Purchase in the area now known as the New Madrid Seismic Zone, (see Figure 15). Of the region between the St. Francis and Mississippi Rivers, Stoddard wrote, “Nearly half of the lands between these two rivers are covered with swamps and ponds, and periodically inundated. These swamps, filled with cypress, are mostly dry in summer; though, unless they be drained at great expense,

or banks constructed to keep the water from them, they will never be of any service to agriculturalists, other than as ranges for cattle. Many creeks or bayous take their rise in them, and they flow into both rivers; and it is calculated, that there are as many of them as one to every fifteen miles. These swamps are generally in a central position between the two rivers; they mostly communicate with both by forming creeks or bayous, which are navigable in the time of freshes."

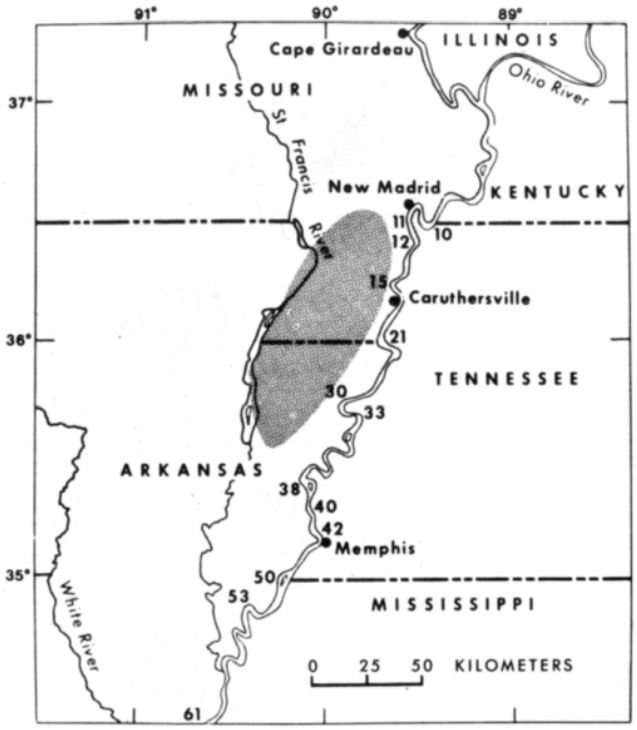

Figure 15. The New Madrid Seismic Zone (from Nuttli, (1974) page 10)
The shaded area is the region where numerous sand blows occurred during the 1811-1812 earthquakes. Numbers along the Mississippi River refer to islands.

In addition, Penick (1976, page 92) reports that before the 1811-1812 earthquakes, the region had earned a deserved reputation as the "sunk country". In the spring of 1811, the flood waters were so high in the Ohio and Mississippi valleys, that it was remembered as the "year of waters" (Penick 1976, page 11). This accumulated evidence indicates that the location of the ground water surface was at or near the ground surface in the New Madrid Seismic Zone at the time of the 1811-1812 earthquakes. Since 1812 a number of measures have been implemented to make the area between the St. Francis and Mississippi rivers more usable. These measures include subsurface drainage, levees to prevent flooding from the rivers, and ground water pumping. Now it is not uncommon to see irrigation activities during the summer in this area even though it was once a swamp.

BACK CALCULATION OF a_{max} USING THE SIMPLIFIED PROCEDURE

Overview of Evaluation Procedure for Use of the Simplified Procedure

A methodology known as the simplified procedure for liquefaction assessment is a standard of practice for evaluating the liquefaction resistance of soils using the cyclic stress method. It was first proposed by Seed and Idriss (1971) from empirical evaluations of field observations and field and laboratory test data. It has been modified and updated periodically since that time, most recently in Youd et al. (2001). The Simplified Procedure was originally developed for use with penetration values measured using the Standard Penetration Test (SPT), or N values. Stark and Olson (1995) extended the simplified procedure to use cone tip resistance.

The Simplified Procedure utilized the cyclic stress method which requires calculation, or estimation, of two variables for evaluation of the liquefaction potential of a soil: (1) the seismic *Demand* on a soil layer, expressed as the driving seismic stress ratio, $SSR_{driving}$ herein and cyclic stress ratio, $CSR_{driving}$, and (2) the *Capacity* of the soil to resist the seismic demand, expressed as the resisting seismic stress ratio, $SSR_{resisting}$ herein and cyclic stress ratio, $CSR_{resisting}$.

Seed and Idriss (1971) relate $CSR_{driving}$ to a certain number of equivalent laboratory loading cycles in a cyclic triaxial compression test that correspond to an earthquake magnitude. Thus, Seed and Idriss (1979) refer to the method as the cyclic stress method and use the cyclic stress ratio in the method. Because liquefaction is induced in the field by a seismic shear stress, Stark and Olson (1995) propose to refer to the field earthquake loading as the seismic shear stress ratio, SSR and not CSR. Stark and Olson (1995) suggest that the term "SSR" is more descriptive of field earthquake loading than cyclic stress ratio. This is also suggested because liquefaction potential is now being evaluated based on field performance data and not laboratory test results as initially proposed. As a result, the proposed relationships described subsequently utilize SSR and CPT tip resistance to estimate the liquefaction potential of sandy soils instead of CSR.

When $SSR_{driving}$ is equal to $SSR_{resisting}$, liquefaction begins to occur. $SSR_{driving}$ is a function of the maximum acceleration, a_{max}, of the earthquake. Relationships have been developed that correlate $SSR_{resisting}$ to the penetration resistance of a soil, e.g. Seed and Idriss (1971). With known values of penetration resistance, and thus $SSR_{resisting}$, at a site of marginal liquefaction (i.e. liquefaction beginning to occur), the maximum earthquake acceleration, a_{max}, that caused the marginal liquefaction can be estimated by equating $SSR_{driving}$ to $SSR_{resisting}$ and solving for a_{max}, as described subsequently. At sites of full liquefaction, the maximum earthquake acceleration cannot be estimated because the relationship between $SSR_{driving}$ and $SSR_{resisting}$ is not known. For example, $SSR_{driving}$ could be 1.1, 1.5, or more times greater than $SSR_{resisting}$. Therefore, back analysis of full liquefaction sites only provides a lower bound estimate of a_{max}. At sites of no liquefaction, the value of $SSR_{resisting}$ is greater than $SSR_{driving}$ but again the difference is not known. Thus, sites of no liquefaction can be used to estimate an upper bound value of a_{max} by setting $SSR_{driving}$ equal to $SSR_{resisting}$. These upper and lower bound values can be used to verify and bracket the acceleration back-calculated for the marginal liquefaction site.

Determination of SSR to Develop Liquefaction Potential Relationships

Because of limitations with the SPT, Stark and Olson (1995) and Olson and Stark (1998) present a set of liquefaction potential relationships for sandy soils based on corrected CPT tip resistance values, q_{c1}. These relationships were developed based on 180 field case histories where cone penetration tests were performed at sites of liquefaction and no liquefaction. The relationships are reproduced in Figure 16 .

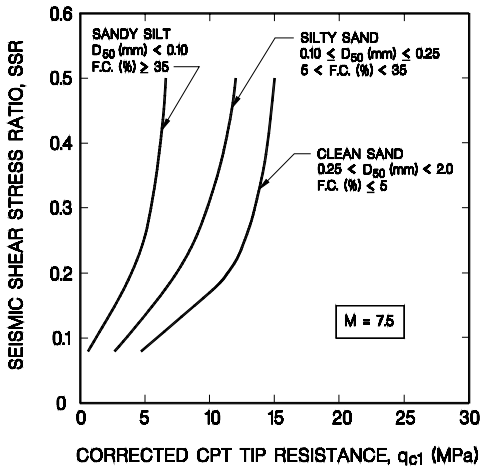

Figure 16. Liquefaction potential relationships based on CPT (Olson and Stark (1998)

Because q_c values measured by the CPT increase with increasing effective overburden stress, a correction factor, C_q, is applied to normalize the measured penetration resistance to an effective overburden pressure of 100 kPa (1 atm). The corrected CPT tip resistance, q_{c1}, used in Figure 16 is obtained by:

$$q_{c1} = C_a q_c \tag{4}$$

where C_q is defined by the following equation proposed by Kayen et al. (1992):

$$C_q = \frac{1.8}{0.8 + \left(\sigma'_{vo} / 100kPa\right)} \tag{5}$$

where σ'_{vo} is the effective overburden pressure.

The penetration values measured using the CPT should in some cases be corrected for the effects of pore water pressures on unequal cone tip areas, which are a function of the geometry of the testing apparatus. This correction is given by Lunne et al. (1997) as:

$$q_c = q_{c\,\text{uncorrected}} + (1 - a)u_2 \tag{6}$$

where

$q_{c\ uncorrected}$	=	measured cone resistance,
u_2	=	measured pore pressure between cone tip and friction sleeve,
a	=	net area ratio $\cong d^2/D^2$,
d	=	diameter of load cell support, and
D	=	diameter of the cone penetrometer.

The correction for $q_{c\ uncorrected}$ to q_c is appropriate in soft clayey soils or other very loose materials where penetration-induced excess pore water pressure is several times the hydrostatic pressure and is significant with respect to the value of tip resistance. This is only occasionally the case in liquefaction problems. Excess penetration-induced porewater pressures are typically small to negligible in sandy soils with fines contents less than 35% and plasticity indices less than 10. Further, in the sandy soils present at the study sites, any excess porewater pressure that is produced is small compared to typical values of tip resistance because of the strength of sandy soils and, as such, there is a negligible change from $q_{c\ uncorrected}$ to q_c. For this study, values of $q_{c\ uncorrected}$ and q_c were found to be nearly identical, with the difference between the two values typically being less than 1%.

In developing Figure 16, Stark and Olson (1995) calculated the seismic shear-stress ratio, $SSR_{driving}$, (equivalent to $CSR_{driving}$) for each case history from the following equation:

$$SSR_{driving} = 0.65\left(\frac{a_{\max}}{g}\right)\left(\frac{\sigma_{v0}}{\sigma'_{v0}}\right) * r_d \qquad (7)$$

where

$a_{\max}$	=	peak acceleration at the ground surface of the site,
g	=	acceleration due to gravity
σ_{vo}	=	total vertical overburden stress at depth, z, being considered,
σ'_{vo}	=	effective vertical overburden stress at depth, z,
r_d	=	depth reduction factor, equal to 1-0.012*z (Kayen et al. 1992).

The value of $SSR_{driving}$ is also corrected to an earthquake magnitude of 7.5, using the magnitude correction C_m proposed by Seed, et al. (1985).

As shown in Figure 16, Stark and Olson (1995) found that the liquefaction potential of a sandy soil is dependent upon its fines content or grain size. For each soil type shown, the corresponding relationship separates regions of liquefaction (to the left of each curve) from regions of no liquefaction (to the right of each curve) as documented in the case histories. Equations approximating the relationships shown in Figure 16 are as follows:

$$SSR = 0.017q_{c1} \quad \text{for clean sands, } 4.5 \le q_c \le 12.22 \text{ MPa} \qquad (8)$$

$$SSR = 0.0935q_{c1} - 0.935 \quad \text{for clean sands, } 12.22 < q_{c1} \le 15 \text{ MPa} \qquad (9)$$

$$SSR = 0.0505e^{0.1855q_{c1}} \quad \text{for silty sands, } 2.6 \le q_{c1} \le 12.1 \text{ MPa} \qquad (10)$$

$$SSR = 0.0674e^{0.2861q_{c1}} \quad \text{for sandy silts, } 0.6 \le q_{c1} \le 6.1 \text{ MPa} \qquad (11)$$

Update of CPT Liquefaction Potential Database

During this study, the database of liquefaction case histories used in Stark and Olson (1995) and Olson and Stark (1998) was reviewed, revised, and updated because these relationships are used to estimate a_{max} from a paleoliquefaction feature in both the cyclic stress and energy-based liquefaction evaluation procedures. Thus, these relationships had to be updated and verified using data from earthquakes collected since publication of the relationships in Olson and Stark (1998).

Each of the individual data points used to develop the liquefaction potential relationships shown in Figure 16 is re-examined based on a new selection criteria described subsequently. In addition, appropriate data from recent earthquakes in Imzit, Turkey (1999), Chi-Chi, Taiwan (1999), and Northridge, California (1994) as well as data points from the Westmorland, California (1981) and the Imperial Valley, California (1979) earthquakes are added to the database. Also included in the new database are additional cases from the Loma Prieta, California (1989) earthquake that were not examined in Olson and Stark (1998). The database developed during this study is included in Appendices B and C.

To reduce potential biases or inconsistencies by researchers in the data before inclusion in the database, the following guidelines are adopted to screen the data. First, for a CPT sounding to be included in the database, there must be a record of a nearby SPT boring to confirm soil stratigraphy information from the CPT. Second, there must be a value of fines content measured from a soil sample taken from the layer under consideration in the nearby SPT boring. Third, in groups of closely spaced CPT soundings, the critical combination of q_c and fines content for initiation of liquefaction is used. The critical combination is the combination that best represents the strength of the soil where the liquefaction initiated. More than one data point from a group of closely-spaced soundings is used if the layer has a large range of fines contents and it is not possible to determine the critical combination. This is commonly the situation in cases where the fines content of the soil is greater than 35%. Some of the data points in the Olson and Stark (1998) database did not meet these criteria and are not included in the new database.

In general, only one representative q_c value from the liquefied layer of each sounding is used in the new database. For cases where the cone resistance is relatively consistent through the liquefied layer, such as shown in Figure 17, an average value of q_c from that layer is used to represent the soil. This average q_c value is calculated over a 0.75 m interval, which is consistent with the minimum thickness of the strata that is usually the source of significant deformations (Boulanger et al. 1997). The dashed line in Figure 17 corresponds to the average q_c value.

For cases where the cone resistance increases with depth through the liquefied layer, such as shown in Figure 18, a representative value of q_c in the 0.75 meters of the layer in

question is used in the new database because liquefaction usually occurs at the top of a layer.

If the CPT sounding shows a single peak in the liquefied layer, such as shown in Figure 19, the interpretation is more complex because the layer occurs near a contact between soft layer and stiffer underlying material. Most of the steep portion of the tip resistance at the top of the stiffer liquefiable layer is due to the displacement required to mobilize this high resistance. As a result, an average value of the upper portion of the peak q_c value is used in the upper portion of the layer. The initial q_c value is ignored because it may be related to the overlying weak layer. Thus, the average of the peak q_c value, see Figure 19, is used.

Similar to soundings with a single peak q_c value in a layer are soundings that have several closely-spaced peaks and valleys in the cone resistance. Cases where the cone resistance varies with several alternating peaks and valleys in the sounding within the liquefied layer are not included in the revised database. These locations probably consist of thin (less that 0.25 m) interbedded sand and silt layers or sand layers of varying density and fines content. Even if a sample was obtained from a nearby boring at the right depth to measure the fines content, it is difficult to identify which of the q_c values from the several thin layers should be associated with the measured fines content from the nearby sample. If the layer thickness is less than 0.25 m, it is ignored because the layer is too thin to develop a representative q_c value (Boulanger et al. 1997).

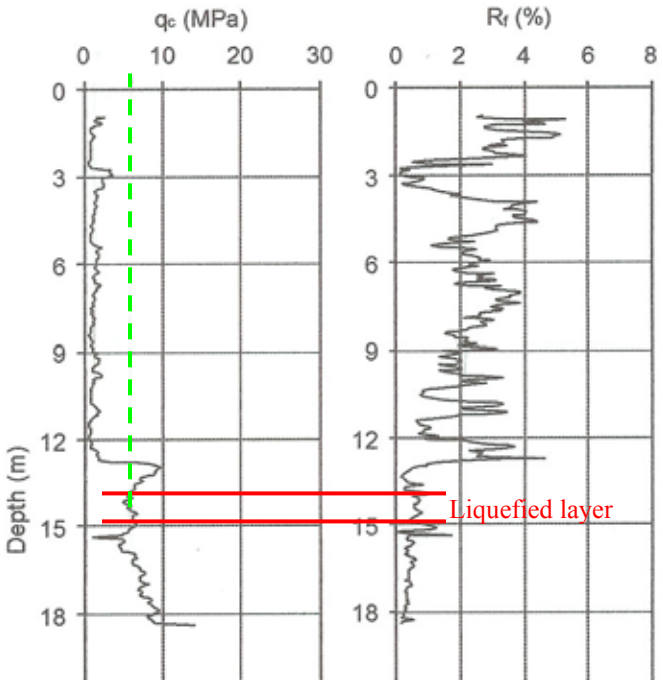

Figure 17. Partial CPT sounding with q_c consistent over the liquefied layer.

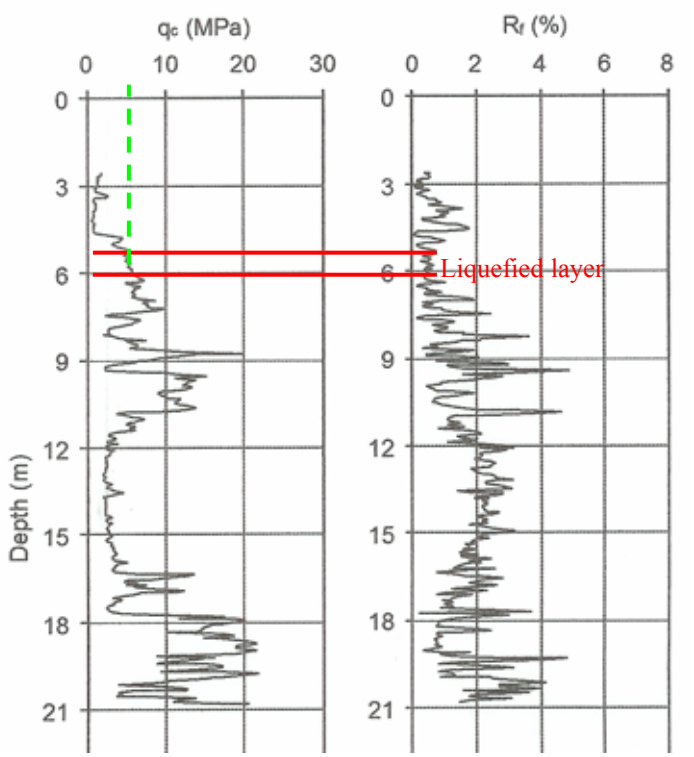

Figure 18. Partial CPT sounding showing q_c increasing with depth through the liquefied layer.

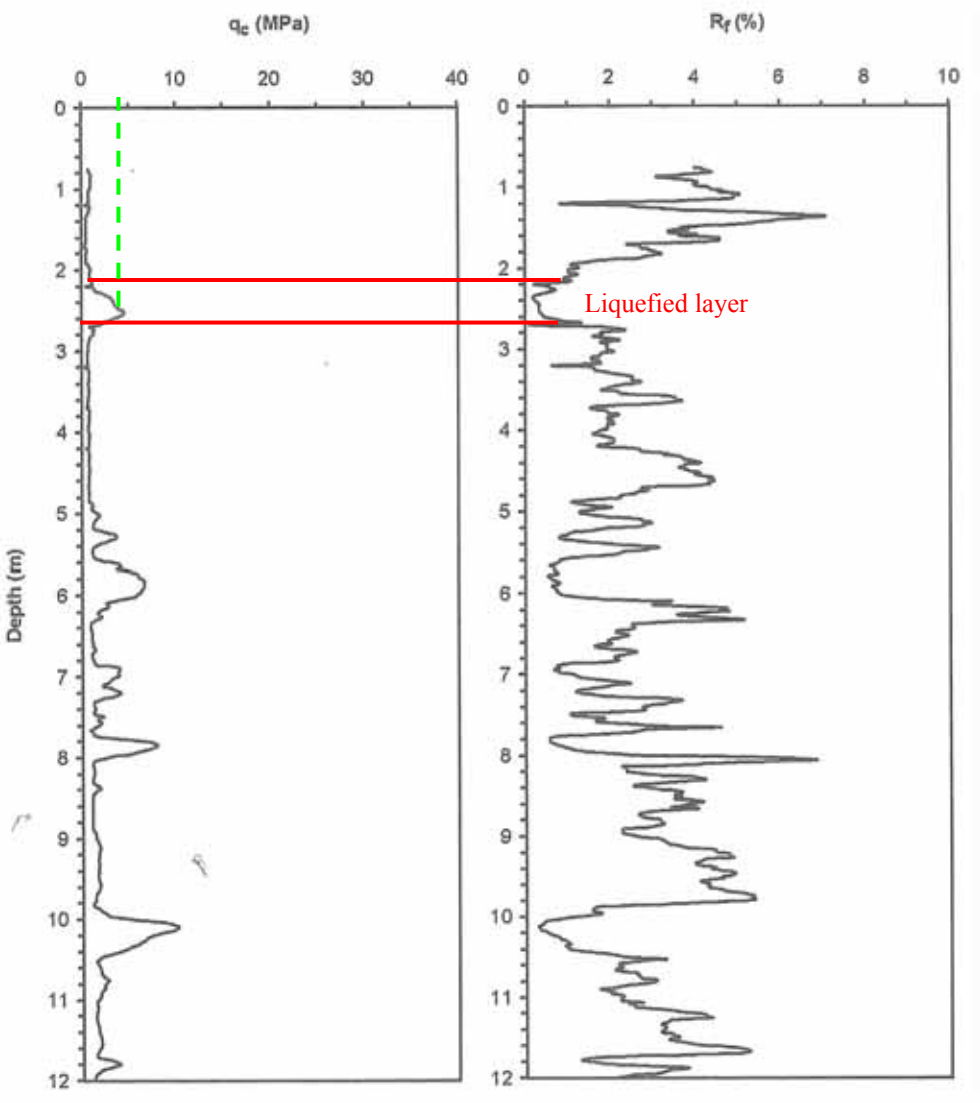

Figure 19. Partial CPT sounding showing a single peak in q_c value in the liquefied layer.

Appendix B presents the new database of 115 data points which contain a suitable value of q_{c1} and a reliable fines content for use in the liquefaction potential relationships. These data points correspond to 11 earthquakes and 76 different sites. For comparison purposes, Olson and Stark (1998) utilize 172 data points, 12 earthquakes, and at least 37 sites. The number of data points is reduced in the new database because some of the data points used by Olson and Stark (1998) do not meet the new criteria used herein. For example, Suzuki et al. (1995) do not present any data on fines content nor have adjacent SPT data. Thus, the data from the 1993 Kushiro-Oki, 1993 Hokkaid-Nansei-Toho-Oki, and 1994 Hokkaido-Toho-Oki earthquakes (55 data points) presented by Suzuki et al. (1995) are not used in the new database. Olson and Stark (1998) state that the reason three liquefied points lie outside of the clean sand liquefaction potential relationship is that Suzuki et al. (1995) do not report any fines content values and thus "no further scrutiny of the data was possible". Because the new relationships are a function of only fines content and not D_{50}, these 55 data points are not used herein.

Another example of the stricter selection criteria in the new database is cases where only the lowest q_{c1} value is used for a particular site even though a number of CPT soundings are available. This is illustrated by the State Beach site at Moss Landing described by Boulanger et al. (1997) because there are six CPT soundings. Five CPT soundings are in the liquefied area and one is outside the liquefied area. Olson and Stark (1998) use data from all six CPT soundings in their liquefaction potential relationships. Because the seismic shear stress ratios are similar (0.15 to 0.18) for all six soundings, the use of all of the data tends to shift the liquefaction potential relationship towards the right, making more material potentially liquefiable and increasing the variability in the data separating the three soil type groups.

In summary, in the new liquefaction potential database, only the minimum q_c value is used for a particular site, i.e., there is only one data point for a particular site and fines content. However, more than one data point may be used for a particular site if the CPT soundings are widely spaced or if there is a significant difference in the fines content and/or q_{c1} values between two soundings. The required separation of soundings depends on the variability of the soil at the site, i.e., if the occurrence of liquefaction at one sounding could affect the pore water pressure or state of stress at another sounding. For example, soundings UC-14 and UC-15 at the State Beach site are located only 25 meters apart and have the same fines contents but different values of q_{c1}. The same is true for soundings UC-16 and UC-17 at this site. Thus, only two data points corresponding to CPT soundings UC-15 and -17 from the State Beach site at Moss Landing are used in the new database instead of the four liquefaction data points used by Olson and Stark (1998). Soundings UC-15 and UC-17 are used in the database because they are located approximately 150 meters from each other and are likely to be representing different areas of liquefaction. The non-liquefaction data point for the State Beach site used by Olson and Stark (1998) is also used in the new database. Thus, the new data selection criteria reduced the number of liquefaction and non-liquefaction data points from this and other sites.

Another example of where more than one CPT sounding is used in the new database is Juvenile Hall (Bennett 1989). In this case five cone soundings are included in the new database because there is a corresponding SPT boring for each sounding. In addition, the CPT soundings are separated by approximately 100 m. Finally, the fines content for the critical layer in each CPT sounding varies from 50 to 74%. Thus, it was determined that the range of soil types thought to have initiated the liquefaction could not be adequately represented by only one data point.

In summary, the number of data points (172) used in Olson and Stark (1998) are reduced to 51 because of the new site criteria implemented herein. An additional 64 data points from recent earthquakes are combined with the approved 51 data points to produce the updated database of 115 points. The new selection criteria are satisfied if there is an adjacent SPT for stratigraphy, a reliable fines content measurement, and the critical combination of q_c and fines content adequately describe a layer that is most likely to have been involved in the initiation of liquefaction.

Update of Liquefaction Potential Relationships

Figure 16 shows the liquefaction potential relationships from Olson and Stark (1998) that utilize three groups of soil types to model liquefaction potential. These groups are delineated using fines content and D_{50}. The median grain size, D_{50}, was used by Olson and Stark (1998) for soil classification where the fines content was not available. Because the new selection criteria requires a reliable value of fines content, the median grain size is omitted from the soil groupings presented herein.

The three groups of soil type used by Olson and Stark (1998) to model liquefaction potential are clean sand, silty sand, and silty sand-sandy silt groups which correspond to a fines content of less than or equal to 5%, between 5 and 35%, and greater than or equal to 35%. Application of the liquefaction potential relationships in Figure 16 has been somewhat problematic in practice because of the large gap in fines content for the silty sand group, which ranges from 5 to 35%. In general, soils with a fines content greater than 35% exhibit low liquefaction potential and thus the large range of fines contents for the silty sand-sandy silt group (> 35%) did not matter. However, the large range for the silty sand group, 5 to 35%, is significant because this range encompasses a wide range of natural soils and q_c values (about 5 to 12 MPa) that are liquefiable. Thus, it was determined that the three soil type groups had to be refined to facilitate use of the liquefaction potential relationships in practice and in interpretation of paleoliquefaction features.

The new liquefaction database in Appendix B was sorted in many ways to develop a new set of liquefaction potential relationships to facilitate their use in practice and the interpretation of paleoliquefaction sites. Afterwards, it was decided to use four fines content or soil groups instead of the three groups presented by Olson and Stark (1998). These fines content groups are: (1) less than 12%, (2) greater than or equal to 12% and less than 20%, (3) greater than or equal to 20% and less than 35%, and (4) greater than or equal to 35%. Thus, the new fines content groupings refine the liquefaction potential relationships for fines contents between 5 and 35%. It is important to note that the Unified Soil Classification System (USCS) (ASTM D 2487-98) defines "sands with fines" as sands with fines contents of more than 12%. A clean sand is defined in the USCS as a sand with less than 5% and thus a fines content between 5 and 12% is a transition zone between clean sand and sand with fines in the USCS. Because the median grain size and the soil type descriptions (clean sand, silty sand, and silty sand-sandy silt) used in Olson and Stark (1998) are not relevant to the new liquefaction potential relationships, the new groups are only defined using a fines content and a soil group number.

Liquefaction Potential of Sandy Soils Based On Cyclic Stress Ratio

Soil Group 1 - Fines Contents less than 12%

Figure 20 presents a compilation of 27 liquefaction and 22 non-liquefaction field case histories involving soils with fines contents less than 12% where CPT, an adjacent SPT boring, and reliable fines content data are available. This soil group is referred to as Soil

Group 1. From the field data, a boundary line is drawn between liquefied sites and non-liquefied sites. This boundary defines a relationship between the seismic stress ratio necessary to cause liquefaction and CPT q_{c1}-values for clean sand (fines content less than 12%) and an earthquake magnitude of 7.5. This boundary represents a lower bound of the liquefied data to be consistent with the concept of the mobilized undrained yield strength ratio (Stark and Olson 1995). Figure 20 shows that the proposed liquefaction potential relationship is in good agreement with the field case history data. This relationship describes soil capacity in terms of q_{c1} for use in the Simplified Procedure. Shown for comparison in Figure 16 is the relationship from Olson and Stark (1998), which is shown by the thinner line. The proposed relationship is only slightly different than the clean sand relationship presented in Stark and Olson (1995) and Olson and Stark (1998). The slight difference in the two relationships is due to the removal and addition of points to the database.

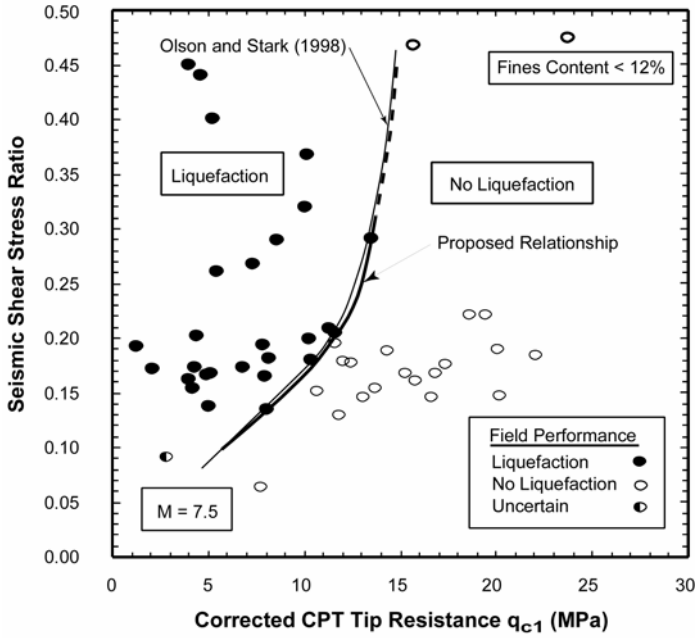

Figure 20. Relationship between Seismic Shear Stress Ratio triggering liquefaction and q_{c1} values for Soil Group 1 and M=7.5 earthquakes

Soil Group 2 - Fines Contents greater than or equal to 12% and less than 20%

Figure 21 presents a compilation of 16 liquefaction and 10 non-liquefaction field case histories involving sands with fines contents greater than or equal to 12% and less than 20% where CPT, an adjacent SPT boring, and reliable fines content data are available. This soil group is referred to as Soil Group 2. From the field data, a boundary line between liquefied sites and non-liquefied sites is established and defines a relationship between the seismic stress ratio necessary to cause liquefaction and CPT q_{c1} values for magnitude 7.5 earthquakes. This boundary line is similar to the boundary for silty sand presented in Olson and Stark (1998), which corresponds to a fines content between 5 and 35%. The relationship for Soil Group 2 plots to the left of the relationship for fines contents less than or equal to 12%. It is anticipated that the plasticity of the fines reduces

the liquefaction potential during earthquake shaking because the fines reduce soil particle movement and pore-water pressure generation during shaking. Thus, a higher Seismic Shear Stress Ratio (SSR) is required to cause liquefaction in a Soil Group 2 soil than in a Soil Group 1 soil of equal CPT tip resistance or density. In addition, the fines may cause a partially undrained condition during penetration, which can lead to a decrease in CPT tip resistance as compared to a clean sand with equal relative density. These two factors result in a Soil Group 2 soil appearing more resistant to liquefaction than a Soil Group 1 soil of equal relative density.

Seven of the non-liquefaction case histories plot inside the proposed boundary in Figure 21. Three of the points are close to the boundary, while the other four are further inside the proposed boundary. The four case histories inside the boundary are from the 1999 Chi-Chi, Taiwan earthquake and are classified as "uncertain" with respect to whether or not they are in liquefied areas by Juang et al. (2003).

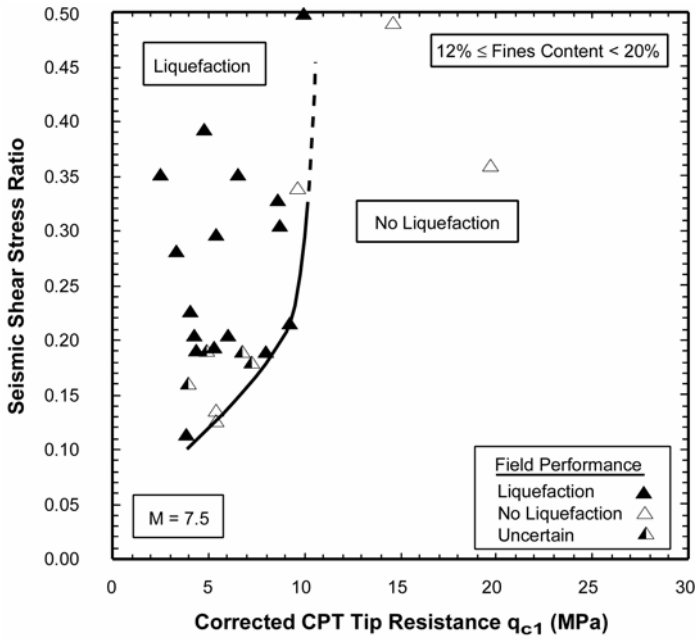

Figure 21. Relationship between Seismic Shear Stress Ratio triggering liquefaction and q_{c1} values for Soil Group 2 and M=7.5 earthquakes

Soil Group 3 - Fines Content greater than or equal to 20% and less than 35%

Figure 22 presents a compilation of 7 liquefaction and 6 non-liquefaction field case histories involving sands with fines contents greater than or equal to 20% and less than 35% where CPT, an adjacent SPT boring, and fines content data are available. From the field data, a boundary line between liquefied sites and non-liquefied sites is established in the same manner as the boundary for Soil Groups 1 and 2 and defines a relationship between the seismic stress ratio necessary to cause liquefaction and CPT q_{c1} values for appropriate sand and magnitude 7.5 earthquakes.

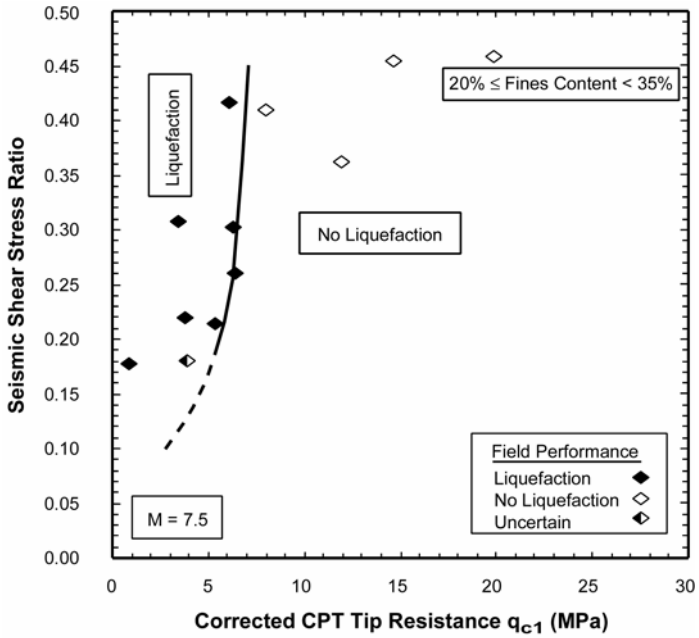

Figure 22. Relationship between Seismic Shear Stress Ratio triggering liquefaction and q_{c1} values for Soil Group 3 and M=7.5 earthquakes

The "uncertain" point located inside the boundary is from the 1999 Chi-Chi, Taiwan earthquake. The reported q_{c1} and fines content are from a silty fine sand layer with clay layers above and below it. The CPT friction ratio measurements indicate that there may be thin clay layers interbedded in the silty sand layer. The presence of these clay layers could increase the resistance of the soil to liquefaction without increasing the value of q_{c1}. The point also has a fines content of 33%, putting it close to being in Soil Group 4 with fines contents greater than 35%. Thus, this data point is included but classified as uncertain.

Soil Group 4 - Fines Content greater than or equal to 35%

Figure 23 presents a compilation of 19 liquefaction and 8 non-liquefaction field case histories involving sands with fines contents greater than or equal to 35% where CPT data are available. From the field data, a boundary line between liquefied sites and non-liquefied sites was established. In the same manner as the boundary for sands with other fines contents above, the boundary in Fig. 19 defines a relationship between the seismic stress ratio necessary to cause liquefaction and CPT q_{c1}-values for magnitude 7.5 earthquakes.

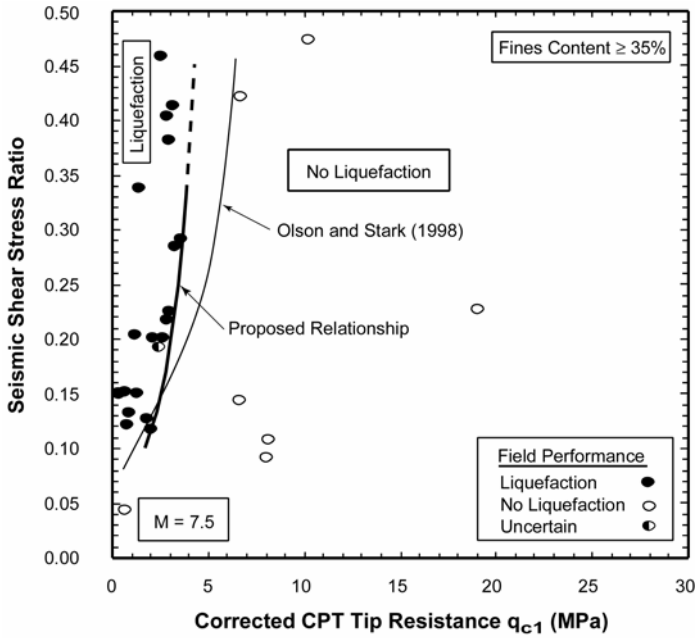

Figure 23. Relationship between Seismic Shear Stress Ratio triggering liquefaction and q_{c1} values for Soil Group 4 and M=7.5 earthquakes

The point that lies inside the boundary at a q_{c1} of 3.6 MPa and a SSR of 0.2 is a case from the 1999 Chi-Chi, Taiwan earthquake that is classified as "uncertain" with respect to liquefaction or non-liquefaction by Juang et al. (2003).

The liquefaction potential relationship for soils with fines contents greater than or equal to 35% from Olson and Stark (1998) is also plotted in Figure 23 and it plots to the right of the new boundary. This difference is caused by the use of only the most critical CPT sounding (or soundings) for a given liquefaction case. The inclusion of extra soundings with higher q_{c1} values than the critical sounding (or soundings) for a given liquefaction case in the Olson and Stark (1998) database tends to shift the trend line to the right.

The liquefaction potential relationships for Soil Groups 3 and 4 have only a small number of non-liquefaction points helping to constrain the relationships. This is to be expected given the relative rarity of liquefaction cases in soils with higher fines contents as well the practice of performing fewer CPT soundings in areas outside the liquefied zones. Judgment may be necessary in applying the relationships for Soil Groups 3 and 4 until more case histories in these types of soils can be examined and possibly included in the database.

In summary, fines content influences the liquefaction resistance of soils. As a result, different empirical relationships are presented for the liquefaction potential of varying fines contents that are based on values of corrected CPT tip resistance. Because of the importance of fines content, the use of four soil groups instead of three, and the similarity in the soil descriptions, the new soil groups are labeled Groups 1-4 with the corresponding fines contents instead of as soil types as in Olson and Stark (1998)

New Liquefaction Potential Relationships

Figure 24 presents the new liquefaction potential relationships for the four fines content groups. The proposed liquefaction potential relationships in Figure 24 are obtained from Figure 20, Figure 21, Figure 22, and Figure 23 and constitute a liquefaction assessment chart that can be used to estimate the factor of safety against liquefaction for an earthquake magnitude of 7.5, a vertical effective overburden stress of less than or equal to 100 kPa, level ground conditions, and fines content ranging from zero to greater than 35%. Corrections described by Youd et al. (2001) should be used to adjust the soil capacity estimated from Figure 24 for other earthquake magnitudes, effective overburden stresses, and sloping ground conditions.

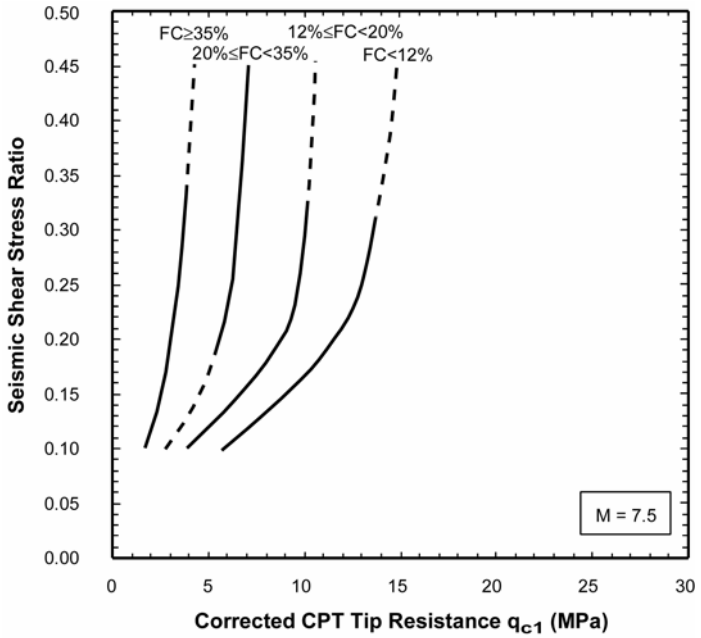

Figure 24. Relationship between Seismic Shear Stress Ratio triggering liquefaction and q_{c1} values for all four soil type groups and M=7.5 earthquakes.

The main disadvantage of the liquefaction relationships in Figure 24, and thus the use of the CPT in liquefaction assessments, is that an estimate of fines content is required. It is possible to estimate fines content from soil classification charts, e.g., Robertson and Wride (1998), based on CPT values of tip resistance and friction ratio. However, because of the uncertainties in estimating fines content from only CPT results (described subsequently), it is recommended that the CPT be used to delineate zones and/or seams of potentially liquefiable soils. In zones of potential liquefaction, a sample and blowcount(s) should be obtained to measure fines content, confirm soil stratigraphy, and verify the liquefaction potential. This combination of CPTs and one or more borings has been used in practice for many years, and thus should not significantly increase the cost of a site investigation (Stark and Olson 1995). Furthermore, the proposed CPT based liquefaction potential relationships will allow the use of CPT data directly, i.e., no conversion of tip resistance to an N-value, and should increase the effectiveness of

liquefaction assessments because of the continuous profile of tip resistance versus depth. This profile allows the natural variability of sandy deposits to be better characterized.

Comparison of Proposed and NCEER CPT-Based Liquefaction Potential Relationships

Figure 25 presents the CPT based liquefaction potential relationships derived from the NCEER Workshop on the Evaluation of Liquefaction Resistance of Soils (Youd et al. 2001).

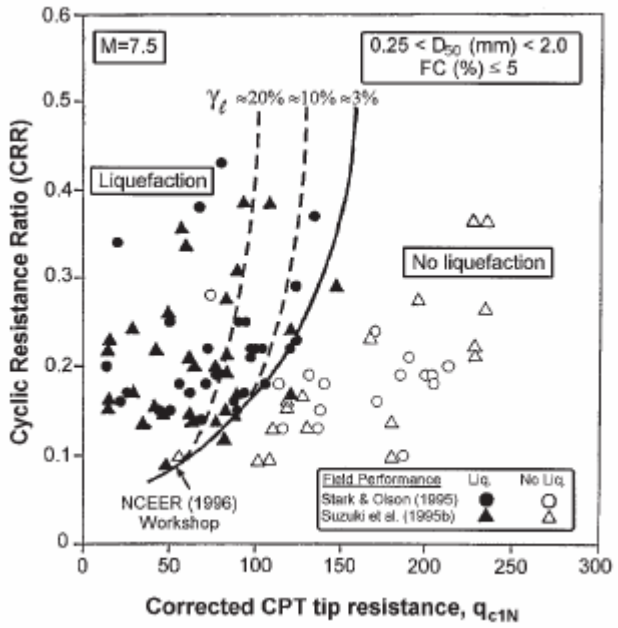

Figure 25. CPT-based liquefaction potential relationship for clean sand recommended by NCEER (1996) based on Robertson and Wride (1998)

The main difference between the NCEER liquefaction potential relationships and the relationships proposed in Figure 24 is the NCEER relationships use a fines content correction for the clean sand liquefaction relationship proposed by Robertson and Wride (1998) instead of using the measured fines content directly as shown in Figure 24. Instead of obtaining a soil sample and measuring fines content, Robertson and Wride (1998) present a procedure for determining soil type based on normalized CPT data that eliminates the need for a sample to measure fines content. The CPT friction ratio (measured sleeve friction, f_s, divided by measured cone tip resistance, q_c) generally increases with increasing fines content and soil plasticity. This allows a rough estimate of soil type and fines content to be determined from CPT data and not a sample. This is accomplished using a soil behavior chart such as the one reproduced from Robertson and Wride (1998) and shown in Figure 26.

The fines content correction used to modify the clean sand relationship in Figure 25 is also presented by Robertson and Wride (1998) and is a function of the soil classification

index, I_c (see Table 4). This soil classification index is a function of normalized cone resistance and friction ratio as illustrated in Figure 26.

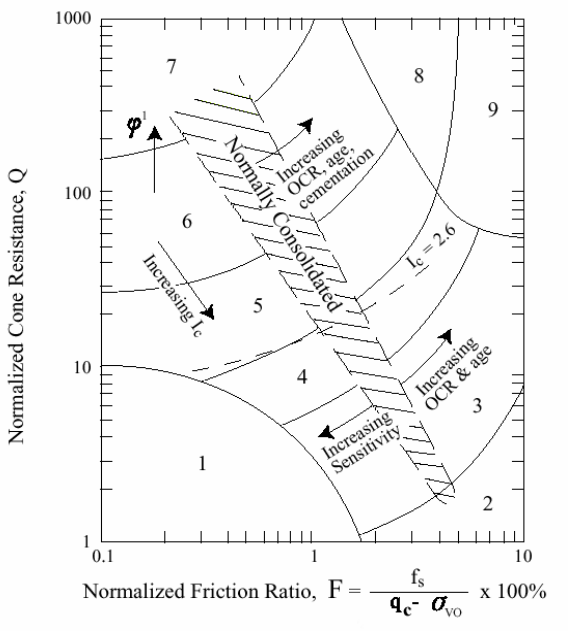

Figure 26. Normalized CPT soil behavior type chart from Robertson and Wride (1998). Soil types: 1. sensitive, fine grained, 2. peats, 3. silty clay to clay, 4. clayey silt to silty clay, 5. silty sand to sandy silt, 6. clean sand to silty sand, 7. gravelly and to dense sand, 8. very stiff sand to clayey sand, 9. very stiff, fine grained

The CPT relationship used to calculate I_c from tip resistance and sleeve friction from Robertson and Wride (1998) is

$$I_c = \left[(3.47 - \log Q)^2 + (\log F + 1.22)^2\right]^{0.5} \tag{12}$$

where

$$Q = \left(\frac{q_c - \sigma_{vo}}{P_{a2}}\right)\left(\frac{P_a}{\sigma'_{vo}}\right)^n \tag{13}$$

$$F = \frac{f_s}{q_c - \sigma_{v0}} \times 100\% \tag{14}$$

Q is the normalized dimensionless CPT penetration resistance, F is the normalized friction ratio, the exponent n is a function of soil type and is determined using the iterative procedure described below, σ_{vo} and σ'_{vo} are the total and effective overburden stresses, respectively, P_a is a reference pressure (1 atmosphere) in the same units as σ'_{vo} (i.e., P_a = 101 kPa if σ'_{vo} is in kPa), P_{a2} is a reference pressure in the same units as q_c and

σ_{vo} (i.e., P_{a2} = 0.101 MPa if q_c and σ_{vo} are in MPa) as described in Robertson and Wride (1998), and f_s is the sleeve friction. The normalization exponent, n, varies from 0.5 for sands to 1.0 for clays. In order to determine the correct value of n and then the soil classification index using the correct value of n, the following iterative procedure is used.

An initial value of n = 1.0 is used to calculate initial values of Q and I_c. If I_c is greater than 2.6 (indicating a clayey soil) then the point is plotted on the classification chart or used in the equation for the grain characteristic correction factor. If I_c is less than or equal to 2.6 (indicating a sandy soil) with n=1.0, then Q and I_c are recalculated using n = 0.5. If the new value of I_c is still less than or equal to 2.6, the soil is classified as sandy. This is in agreement with Figure 26 and the point is plotted on the classification chart or used in the grain characteristic correction equation, Equation (16). If the new value of I_c is greater than 2.6 with n=1.0 and less than 2.6 with n=0.5, then an intermediate value of n (0.75) should be used to calculate Q and I_c. The resulting value of I_c is used to plot the point on the classification chart or to obtain the grain characteristic correction factor. The final value of Q, using the appropriate value of n, is the normalized cone penetration resistance, q_{c1N}. Table 4 shows the relationship between calculated values of I_c and the soil behavior types shown in Figure 26.

Table 4. Boundaries of soil behavior types shown in Figure 26 (after Robertson and Wride (1998))

Soil Behavior Type Index, I_c	Zone	Soil Behavior Type
$I_c < 1.31$	7	Gravelly sand to dense sand
$1.31 < I_c < 2.05$	6	Sands: clean sand to silty sand
$2.05 < I_c < 2.60$	5	Sand mixtures: silty sand to sandy silt
$2.60 < I_c < 2.95$	4	Silt mixtures: clayey silt to silty clay
$2.95 < I_c < 3.60$	3	Clays: silty clay to clay
$I_c > 3.60$	2	Organic soils: peats

Robertson and Wride (1998) also propose a grain characteristic correction factor, K_c, to modify the normalized penetration resistance value to an equivalent clean sand penetration resistance, that is

$$(q_{c1N})_{cs} = K_c * q_{c1N} \tag{15}$$

The grain characteristic correction factor, or fines content correction, is defined as:

$$\begin{aligned} &\text{if } I_c \leq 1.64, \text{ then } K_c = 1.0. \\ &\text{if } I_c > 1.64, \text{ then } K_c = -0.403I_c^4 + 5.581I_c^3 - 21.63I_c^2 + 33.75I_c - 17.88 \end{aligned} \tag{16}$$

The resulting values of $(q_{c1N})_{cs}$ can be used with the clean sand relationship shown in Figure 25.

Figure 27 compares the liquefaction potential relationships proposed by Robertson and Wride (1998) with the relationships proposed in Figure 24. Although Robertson and Wride only present a relationship for clean sands, the appropriate grain characteristic

correction factor, Kc, was applied to the clean sand relationship to obtain liquefaction potential relationships for the fines content groups used in Figure 24. The appropriate values of K_c are summarized in Table 5.

Figure 27 shows that the proposed relationships and the those of Robertson and Wride (1998) are similar for fines contents less than 20%, while the proposed relationships are less conservative than the Robertson and Wride (1998) relationship at higher fines contents. This difference is attributed to the use of only the most critical CPT sounding or soundings for a given liquefaction case. The inclusion of extra soundings with higher q_{c1} values than the critical sounding or soundings in the database will tend to shift the relationships to the right, and thus the proposed relationships are to the left of the Robertson and Wride (1998) relationships.

Table 5. Values of soil type index, I_c, and grain characteristic correction factor, K_c, corresponding to fines contents for the proposed liquefaction potential relationships

Fines Content	Ic	Kc
0	1.26	1.00
12	1.96	1.26
20	2.23	1.74
35	2.59	3.28

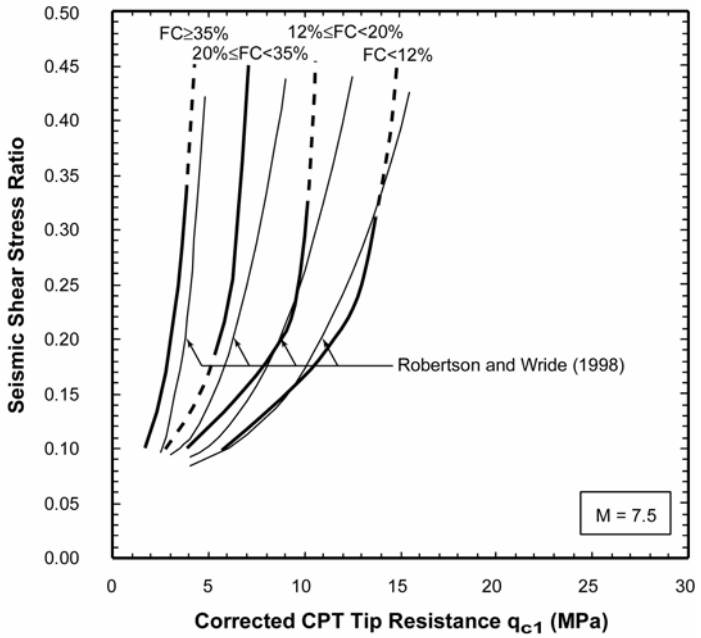

Figure 27. Comparison between proposed and Robertson and Wride (1998) liquefaction potential relationships

Comparison of Measured and NCEER Fines Contents

Robertson and Wride (1998) suggest a relationship between I_c and fines content using the boundaries in the classification chart in Figure 26 where

$$FC(\%) = 1.75 I_c^{3.25} - 3.7 \quad (17)$$

for $1.26 \leq I_c \leq 3.5$. For values of I_c less than 1.26 the fines content is zero and for values of I_c greater than 3.5 the fines content is 100%,

The liquefaction potential relationships proposed herein utilize fines content directly because of the discrepancy observed between measured fines content for the soils in the liquefaction case history database and the fines content derived from the soil classification index. Figure 28 shows the recommended relationship between fines content and I_c proposed by Robertson and Wride (1998) in Equation (17). The recommended relationship of Robertson and Wride (1998) is bounded by relationships for non-plastic (PI<5%) fines and for high plasticity fines (PI>20%). Thus, most of the data should fall between these bounds. Much of the data shown in Figure 28 does fall within these bounds but there is considerable scatter in measured fines contents below 35% (see dashed horizontal line). It appears that much of the fines content data plots near the non-plastic fines relationship, which is in agreement with the data being derived from liquefaction case histories. Thus, if I_c is to be used instead of measuring the fines content, a relationship possibly between the recommended and non-plastic fines relationships should be used for liquefaction assessment.

It appears that the equation for I_c presented by Robertson and Wride (1998) is derived for soil classification purposes and thus is used to represent a wide range of soil types and behavior instead of the narrow range of soils that are potentially liquefiable. Based on the database compiled herein, liquefaction potential is important for soils with a fines content less than or equal to 35%. Figure 28 shows there is no well-established trend in the measured fines content data for a fines content less than 35%. Thus, it was decided to use the measured fines content instead of I_c or K_c to develop the liquefaction potential relationships presented in Figure 24.

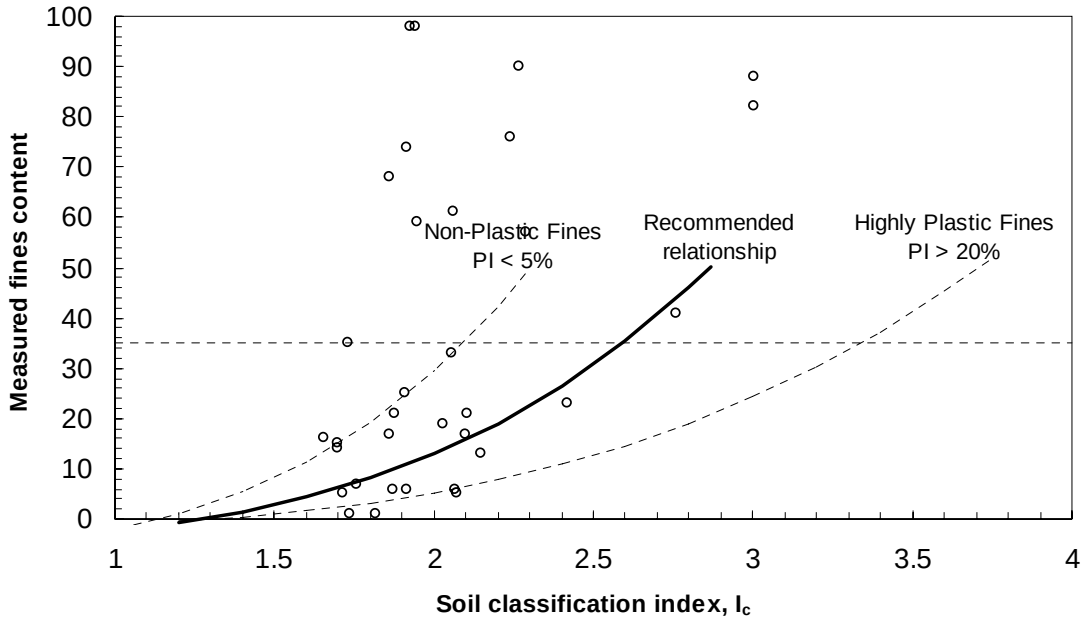

Figure 28. Comparison between measured fines contents and calculated fines contents using Robertson and Wride (1998) for cases in the updated liquefaction potential database

Because it was decided to use the measured fines content instead of I_c or K_c to develop the proposed liquefaction potential relationships, the main practical difference between the Robertson and Wride (1998) method and the proposed relationships is that the fines content of the potentially liquefiable layer or the paleoliquefaction layer must be measured. This requires the use of a soil boring after the potentially liquefiable or the paleoliquefaction layer has been identified and located via CPT soundings. The combination of CPTs and SPTs has been used in practice for many years, and thus should not significantly increase the cost of a site investigation especially after the CPT soundings have delineated the depth of interest. This combination still seems prudent given the uncertainty observed in the relationship between fines content and I_c shown in Figure 28 for fines content less than 35%. In addition, at most paleoliquefaction sites, a sample of the liquefied layer can be obtained without a boring because the liquefaction feature is exposed, e.g., in a river bank.

Determination of a_{max} at a Paleoliquefaction Site Using Proposed Liquefaction Potential Relationships

Marginal liquefaction sites provide the best estimate of ground shaking because the acceleration is just sufficient to initiate liquefaction. Sites of severe liquefaction and no liquefaction only provide lower and upper bound, respectively, estimates of a_{max} and M_W at a paleoliquefaction site.

The expression for the earthquake driving force is:

$$SSR_{driving} = \frac{0.65 a_{\max} \sigma_v r_d}{g \sigma'_v} * \frac{1}{K_\sigma K_\alpha MSF} \quad (18)$$

r_d = stress reduction coefficient to account for flexibility of the soil, recommended to be equal to 1-0.00765*z for z ≤ 9.15 meters and 1.74-0.0627*z for z > 9.15 meters to a maximum of 23 meters (recommended by Youd et al (2001)).

K_σ = correction for high overburden stresses, given by the expression

$$K_\sigma = \left(\frac{\sigma'_{vo}}{P_a} \right)^{(f-1)} \quad (19)$$

where f is a function of relative density, D_r. For D_r = 40 to 60%, f = 0.7 – 0.8. For D_r = 60 to 80%, f = 0.6 – 0.7 (recommended by Youd et al. (2001)).

K_α = correction for sloping ground, equal to unity when the slope angle is essentially 0 degrees.

MSF = magnitude scaling factor, recommended as $\frac{10^{2.24}}{M_w^{2.56}}$ for M_W>7.5 (Youd et al. 2001), where M_w is the moment magnitude of the earthquake.

For magnitudes less than 7.5, Youd et al. (2001) recommend a range of values shown in Figure 29. They recommend that judgment be used and the conservatism required for the specific project taken into account when selecting the MSF. Because the liquefaction evaluation procedure developed herein is to be used both for liquefaction assessment as well as back-analyses of paleoliquefaction sites, the average of the recommended range of MSF values presented in Figure 29 are used in developing the CPT liquefaction potential relationships. Thus, the values of MSF used in this study are equal to the average of $\frac{10^{2.24}}{M_w^{2.56}}$ and $\left(\frac{M_W}{7.5} \right)^{-3.3}$ for M_W<7.5 (Youd et al. 2001) which are shown in Table 6. These two expressions correspond to the upper and lower bounds, respectively, of the range of MSF values shown in Figure 29.

Table 6. Average MSF values from the range recommended by Youd et al. (2001)

M_W	MSF
6	1.93
6.5	1.50
7	1.22

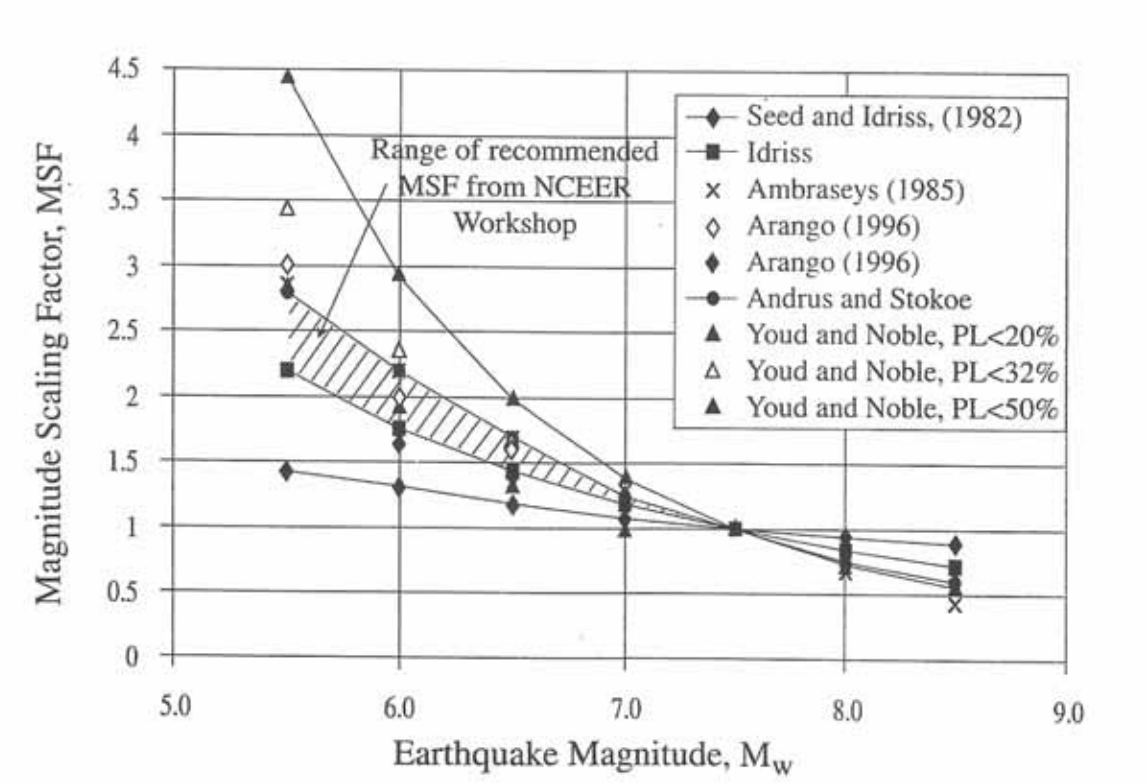

Figure 29. Magnitude scaling factors derived by various investigators (from Youd et al. 2001)

With a known value of SSR from Figure 24, Equation (18) can be rewritten as follows to solve for the maximum earthquake acceleration required to trigger liquefaction based on level ground case histories:

$$a_{\max} = \frac{g\sigma'_v}{0.65\sigma_v r_d} * SSR * K_\sigma K_\alpha MSF \qquad (20)$$

To facilitate interpretation of paleoliquefaction and liquefaction assessments, a spreadsheet was developed that performs the procedures outlined above and also applies any factors necessary to account for changes in the insitu condition since the time of the earthquake, such as soil aging and earthquake densification.

Because the proposed liquefaction relationships were developed primarily from case histories of penetration resistance testing conducted AFTER earthquake/liquefaction events, a correction for densification due to liquefaction is not applicable to this methodology for interpretation of paleoliquefaction features. Other required input data for interpretation of paleoliquefaction features are soil unit weight, depth of the water table, years elapsed since the earthquake under consideration, and a (trial) earthquake magnitude and maximum acceleration. The spreadsheet calculates the factor of safety against liquefaction, FS, versus depth for a cone sounding using the input described above and the following equation:

$$FS = \frac{SSR_{resisiting}}{SSR_{driving}} \tag{21}$$

Determination of a_{max} at Wolf River Liquefaction and No Liquefaction Sites Using Simplified Procedure

Among the Wolf River test sites where CPT soundings are available, the Wolf6 site is deemed the best example of marginal liquefaction. CPT sounding data for the Wolf6 site was obtained from the Internet address referenced earlier and imported into the liquefaction spreadsheet developed herein. Other input data used for the liquefaction analysis of Wolf6 are: total unit weight of soil (clay) = 17.2 kN/m^3, depth of clay cap = 3.25 m, total unit weight of soil (sand) = 21.7 kN/m^3, and depth to the ground water table = 3 m (at the time of the 1811 - 1812 earthquakes). Trial values of a_{max} and M_w are input to the spreadsheet to calculate the resulting factor of safety against liquefaction in the zone of observed marginal liquefaction using Equation (21). The values of a_{max} and M_W are varied until the critical layer in the profile exhibits a factor of safety of unity.

Because the factor of safety calculation depends on both the peak ground acceleration and the magnitude, the iteration process used to estimate a_{max} and M_W for a factor of safety of unity starts with an assumed value of M_W=7.5. When no effects of soil aging are taken into consideration, Wolf6 exhibits factors of safety of unity for an assumed event of M_w = 7.5 and a back-calculated a_{max} = 0.18 g. The factor of safety as a function of depth is plotted with the CPT data in Figure 30.

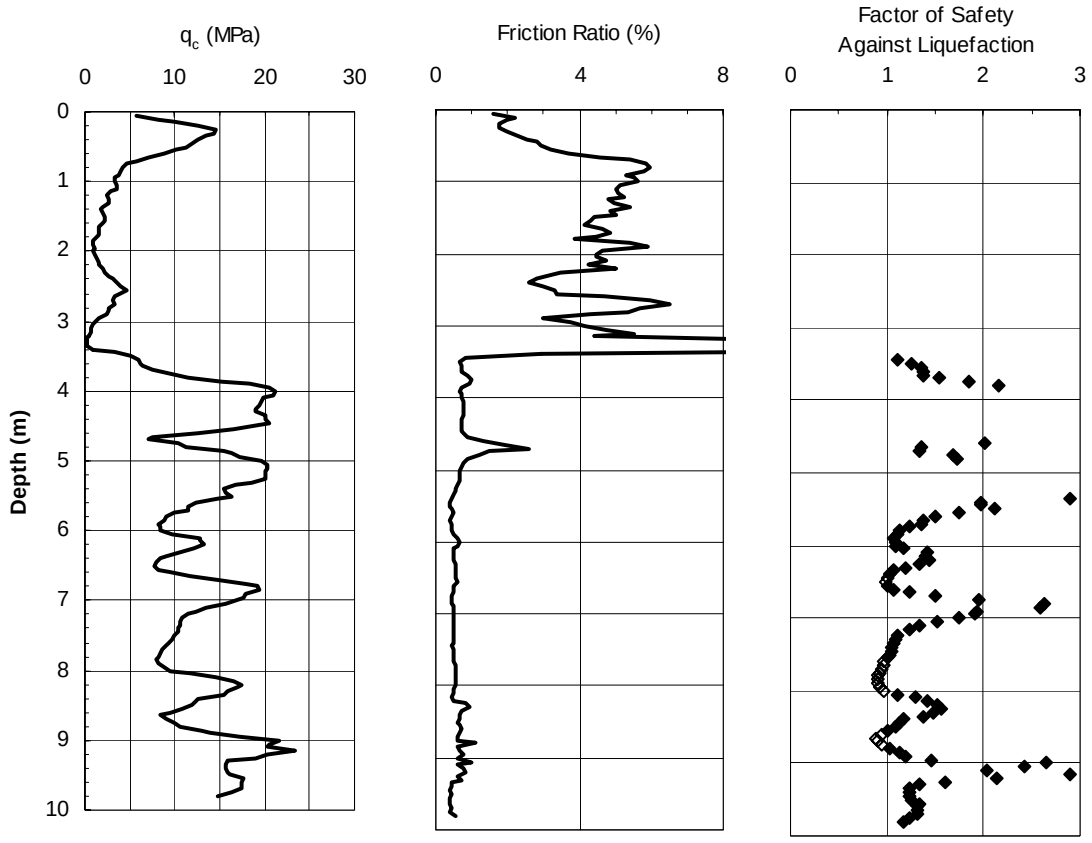

Figure 30. Wolf6 CPT data and calculated factors of safety for a_{max} = 0.18 g and M_W=7.5

The critical layer for liquefaction is at 7.5-8 meters of depth, with a layer only slightly less critical at 6-6.5 meters of depth. The higher q_c values and factors of safety exhibited at shallower depths are likely to be caused by densification that occurred as a result of the liquefaction or because of strength gains that occurred when the water table was lowered from approximately 3 meters at the time of the earthquakes to 6 meters today.

Table 7 presents the back-analysis results for the Wolf6 site and one of the Wolf River portable DCP sites, AA7, near the marginal liquefaction feature. The back-calculated a_{max} for the DCP site is larger than the a_{max} from the CPT measurement. This is caused by the DCP test not penetrating far enough below the water table to measure the penetration resistance in the zone where the CPT found the least resistance.

To account for changes in the strength of the soil since 1811-1812, varying increases in strength are used to illustrate the effect on the back-analysis. Figure 31 shows that the increase in soil strength since 1811-1812 is a significant factor in the back analysis of paleoliquefaction sites and has the potential to reduce the back-calculated acceleration significantly. An increase in q_c of only 20% since 1811-1812 results in a reduction in the back-calculated acceleration of 17%, i.e., 0.18 to 0.15, as shown in Figure 31.

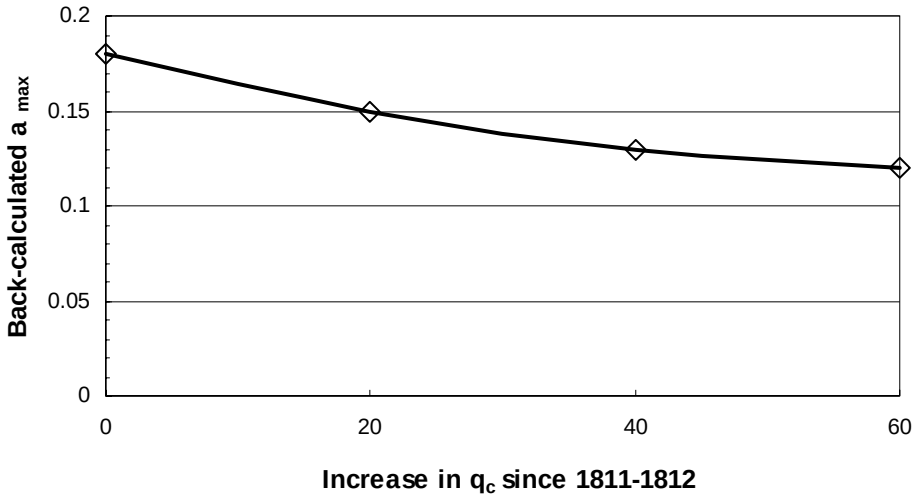

Figure 31. Effect of changes in soil strength on the acceleration required to cause liquefaction at Wolf6 assuming M_W=7.5

In summary, a back-analysis of the Wolf River marginal liquefaction site Wolf6 suggests that the shear stresses induced by a M_w = 7.5 earthquake with an a_{max} 0.18 g at the ground surface are required to create the observed marginal liquefaction features. The no liquefaction site at the Wolf River area, Wolf4, is analyzed below to confirm the values in Table 7 and to develop an upper bound of the a_{max} values.

In addition to Wolf6, a back-analysis of the Wolf4 CPT sounding (see Figure 32) is conducted. Wolf4 is located several hundred meters from any visible liquefaction feature and was subjected to the same ground motion that the other Wolf River sites experienced. Thus, the Wolf4 sounding corresponds to a site of no liquefaction and the a_{max} experienced at the Wolf4 site must be lower than the a_{max} necessary to trigger liquefaction at Wolf4. Therefore, Wolf4 provides an upper bound on the acceleration experienced in the Wolf River area.

Using the same procedure and parameters described above, a peak ground acceleration of 0.27 g and an assumed M_W=7.5 would have been necessary to trigger liquefaction at the Wolf4 sounding. Thus, the ground acceleration experienced at the Wolf River liquefaction site (disregarding soil ageing effects and assuming M_W=7.5) is probably below 0.27 g, which is the acceleration that would have been necessary to trigger liquefaction at Wolf4. This is in agreement with Wolf4 providing an upper bound for the analysis of the Wolf6 marginal liquefaction site where a_{max} must have been 0.18 as shown in Table 7.

The critical layer in Wolf4 is at 6-6.5 meters of depth. This layer is near a factor of safety of unity in the Wolf6 back analysis as well. The most critical layer in Wolf6 is at a factor of safety of 1.3-1.5 in the back-analysis of Wolf4 (see Figure 32). This is in agreement with the Wolf4 sounding providing an upper bound. The discrepancies in the identification of the critical layer in each sounding are probably because of the densification that occurred at the site following the liquefaction. The soils near the

marginal liquefaction features were changed more by the liquefaction than the soils further away.

Table 7. Back-calculated a_{max} at the Wolf River test site for M_W=7.5

	Aging Effects Not Considered
Test Site	a_{max}
Wolf6	0.18 g
AA7	0.24 g
Wolf4 (upper bound)	0.27 g

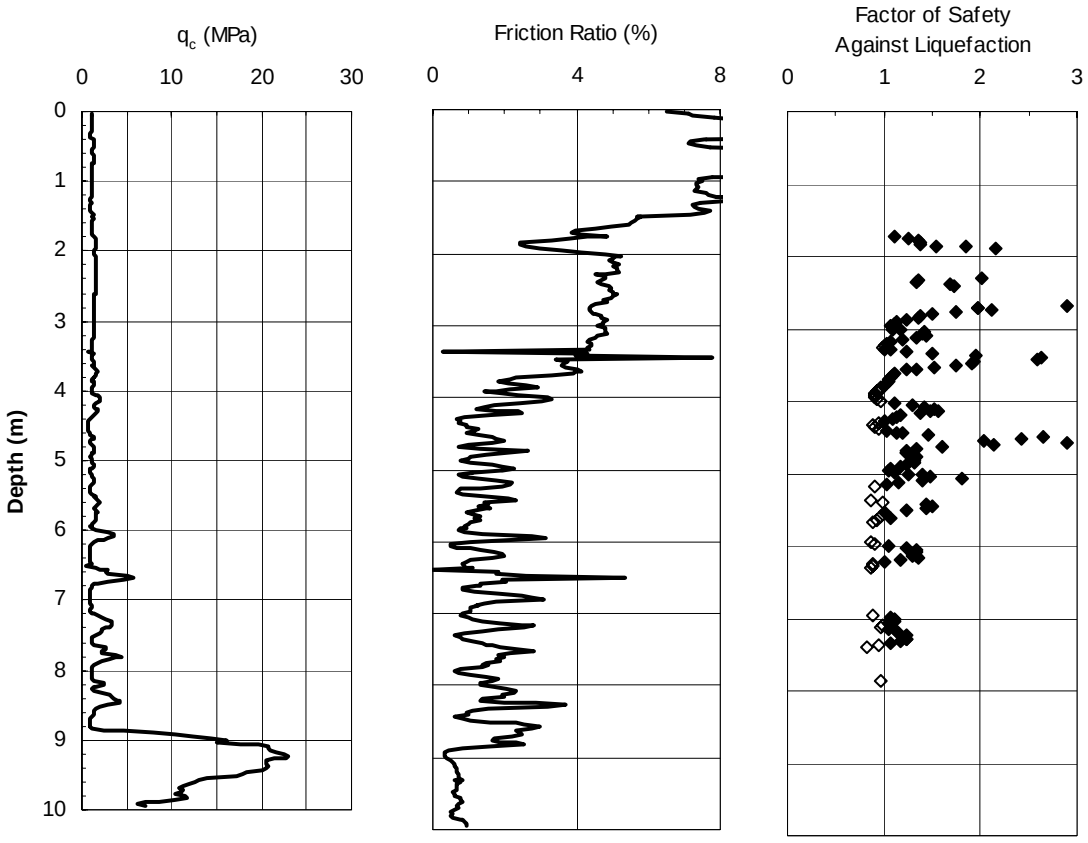

Figure 32. Wolf4 CPT data and calculated factors of safety for a_{max} = 0.27 g and M_W=7.5

Determination of a_{max} In the NMSZ Using Simplified Procedure

The Walker Farm site in Marked Tree, Arkansas contains two major liquefaction-induced sand dikes. A map of the Walker Farm test site is shown in Figure 12. Figure 12 shows that the CPT testing was performed in two linear arrays perpendicular to the main direction of the sand dikes. Soundings Mtree02 to Mtree08 were performed across the

sand dike on the south and soundings Mtree09 to Mtree14 were performed across the sand dike to the north. Based on this information, the Walker Farm site is classified as a severe liquefaction site and provides a lower bound on the estimation of a_{max} and M_W in the New Madrid Seismic Zone.

Using sounding Mtree11, located near the center of the northernmost line of soundings at the northernmost dike, an a_{max} of 0.17 g is necessary to trigger liquefaction if soil aging effects are not considered. The acceleration necessary to trigger liquefaction at the Walker Farm site is similar to that back-calculated at the Wolf6 site because of similarity in the age and depositional environments of the soils at both sites. The key difference between the two sites is their proximity to the New Madrid Fault system. The Walker Farm site is located only 65 km from the epicenter and should have experienced higher accelerations than the Wolf River site located 95 km from the epicenter. This is in agreement with the much higher severity of the liquefaction features observed at the Walker Farm site, despite both sites having similar triggering accelerations. The smaller distance from the epicenter at the Walker Farm site resulted in the triggering acceleration being significantly exceeded and therefore causing severe liquefaction instead of only marginal liquefaction. Thus, the Walker Farm site only provides a lower bound on a_{max}.

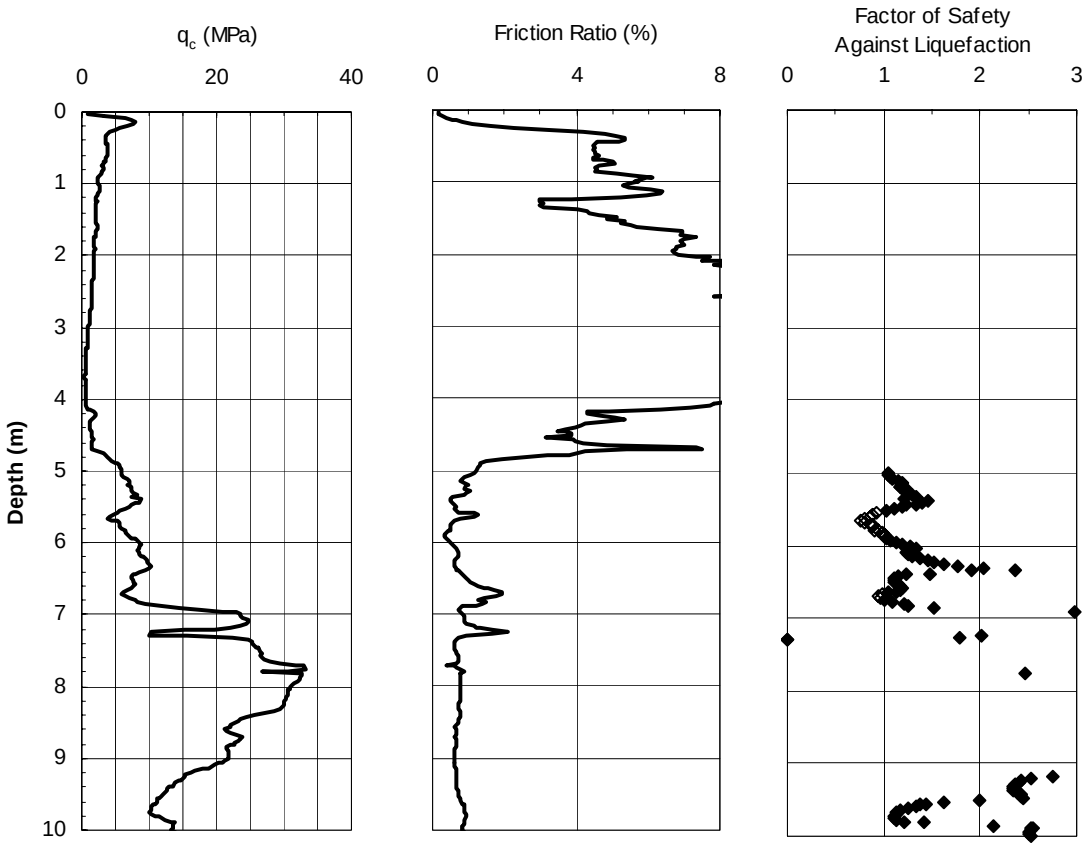

Figure 33. Mtree11 CPT data and calculated factors of safety for a_{max} = 0.18 g and M_W=7.5

In future research, a sounding outside of the area of liquefaction at the Walker Farm could provide an upper bound on the acceleration experienced at the site. Due to the severity of the liquefaction at the Walker Farm site, it is difficult to identify the extents of the liquefied soil deposit. Thus, it is not possible to determine whether other soundings not immediately adjacent to the liquefaction features are outside of the zone of liquefaction.

The Nodena Farm site in Wilson, AK also provides a lower bound on ground shaking in the region because severe liquefaction was triggered at the site. Of the four CPT soundings performed there, Wils02 penetrates seven meters into the sand layer. Using sounding Wils02, an acceleration of 0.21 g is back-calculated to cause liquefaction assuming a magnitude 7.5 earthquake with no corrections for soil aging. The Nodena Farms site is located 42 km from the Blytheville epicenter.

The q_{c1} values in the relevant layers at the Hillhouse Farms site are greater than 15 MPa and are thus too large to back-calculate a_{max} using the liquefaction potential relationships in Figure 25. This may be a result of the age of the soil deposit at the site.

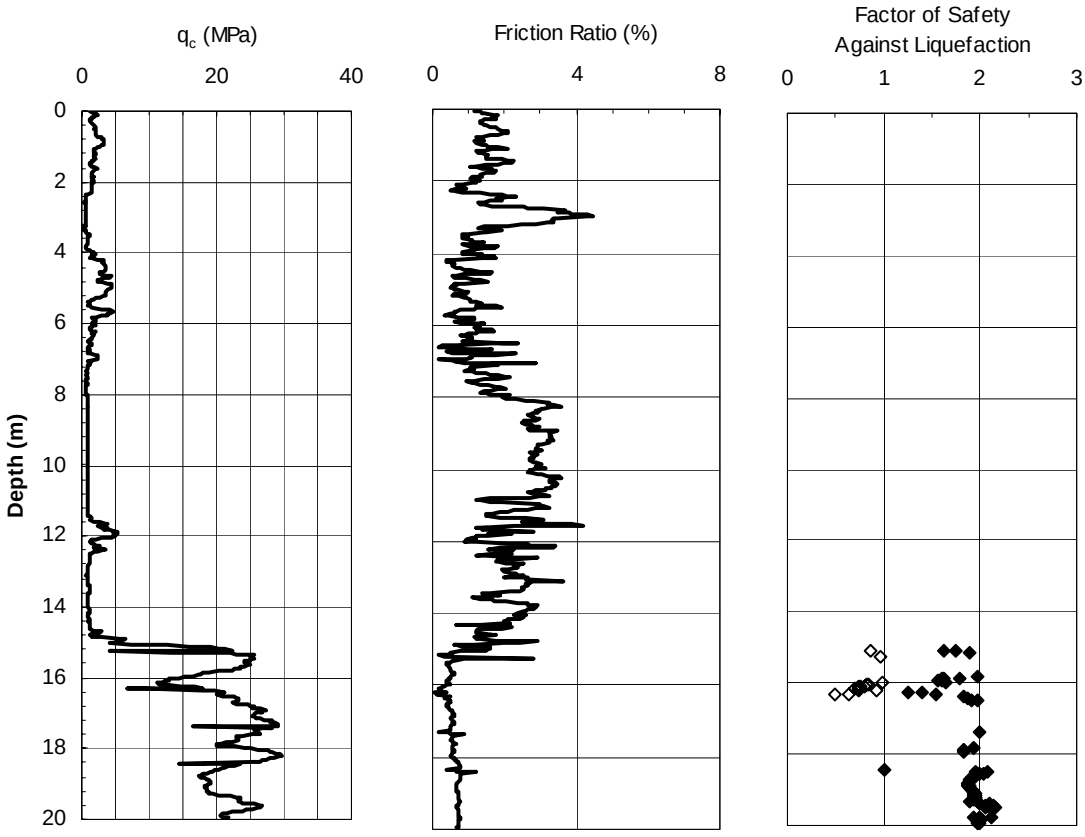

Figure 34. Wils02 CPT data and calculated factors of safety for a_{max} = 0.21 g and M_W=7.5

The Wilhelmina Cutoff site near Dexter, MO also provides a lower bound on ground shaking in the region because full liquefaction was triggered at the site. Using sounding Dex05, an acceleration of 0.20 g is back-calculated to cause liquefaction assuming a

magnitude 7.5 earthquake with no corrections for soil aging. The Wilhelmina Cutoff site is located 45 km from the Blytheville epicenter but only 30 km from the northernmost (New Madrid, MO) epicenter.

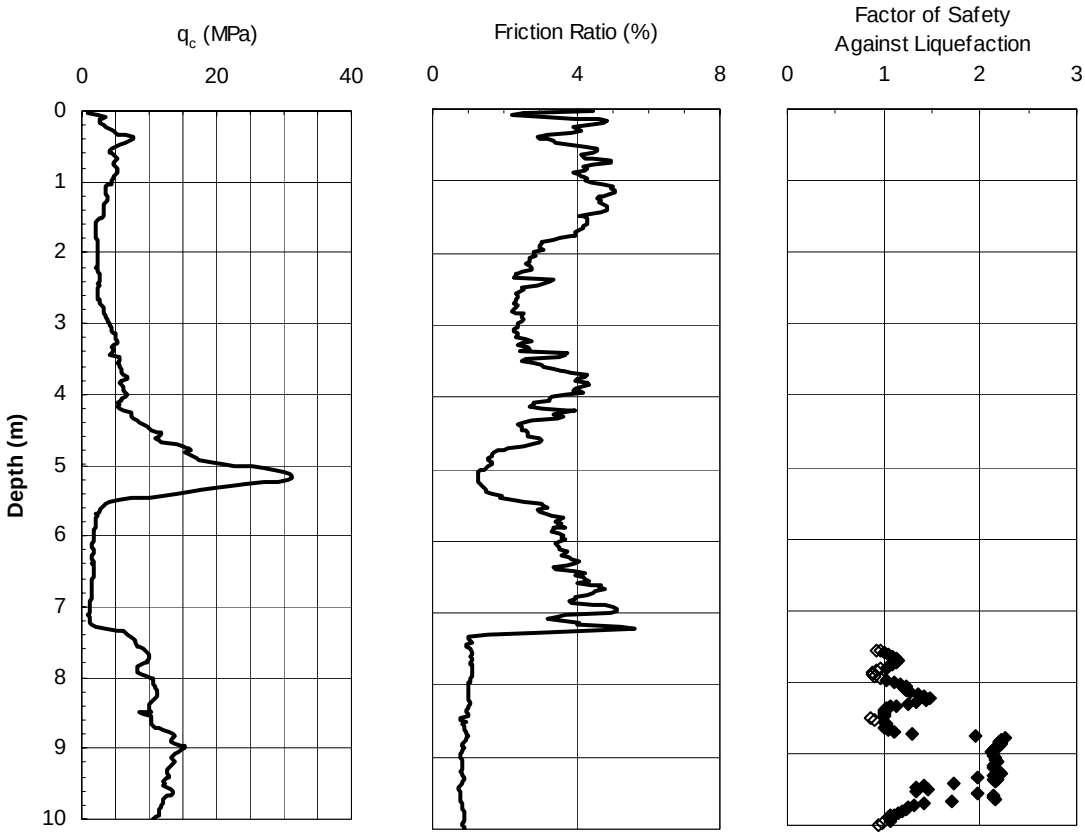

Figure 35. Dex05 CPT data and calculated factors of safety for a_{max} = 0.20 g and M_W=7.5

For the purposes of estimating earthquake magnitude from CPT back-analysis, marginal liquefaction sites provide the best estimate of ground shaking. Sites of severe liquefaction or no liquefaction can only provide lower and upper bounds, respectively, on the intensity of ground shaking. Because of the similarity in age and depositional environments of the liquefiable soils in the NMSZ, marginal liquefaction sites are rare in close proximity of the epicenter. Thus, to refine the estimates on earthquake magnitude and ground accelerations experienced in the NMSZ, additional sites of marginal liquefaction should be located and studied using CPT soundings conducted in the marginal liquefaction layer. In addition, it is recommended that CPT soundings be conducted both inside and well outside of liquefaction sites to obtain upper and lower bound estimates of a_{max} and M_W.

Table 8 presents a summary of the back-calculated values of a_{max} for the Wolf River and NMSZ sites. Table 8 shows that the marginal liquefaction site (Wolf6) experienced a lower acceleration than would have been required to trigger liquefaction at the nearby no liquefaction site (Wolf4). The sites located north of Memphis in the New Madrid Seismic Zone (Mtree11, Wils02, and Dex05) require similar accelerations similar to

Wolf6 trigger liquefaction. However, the NMSZ sites are full liquefaction sites and thus must have experienced larger accelerations than those back-calculated from the CPT data.

These accelerations are calculated without accounting for any increase in strength since the occurrence of the liquefaction due to soil aging, densification, etc. These accelerations should be considered to be overestimated values because the do not include any of the changes in strength discussed earlier. As illustrated in the back analysis for Wolf6, gains in strength result in a decrease in the back-calculated accelerations as shown in Figure 31. Thus, the actual accelerations required to trigger liquefaction at each of the sites are likely to be lower than the values calculated above.

Table 8. Summary of Back-calculated a_{max} Values Required to Trigger Liquefaction at the Wolf River and NMSZ Sites assuming M_W=7.5 with no soil aging correction

Test Site	Description	a_{max} Estimate	Without Soil Aging
Mtree11	Full Liquefaction	Lower Bound	0.18
Wils02	Full Liquefaction	Lower Bound	0.21
Dex05	Full Liquefaction	Lower Bound	0.20
Wolf6	Marginal Liquefaction	Best Estimate	0.18
Wolf4	No Liquefaction	Upper Bound	0.27

The back-calculated accelerations in Table 8 are those required to trigger liquefaction assuming a magnitude 7.5 earthquake. These accelerations are not necessarily those that were experienced at the liquefaction sites because the actual earthquake magnitude may be different than 7.5. Because a different assumed magnitude in the back-analysis results in a different back-calculated acceleration, there are many combinations of magnitude and peak ground acceleration that could trigger liquefaction at each of the paleoliquefaction sites. In order to determine what magnitude and accelerations were actually experienced at the sites, the results of the CPT liquefaction back-analyses must be in agreement with the results of the attenuation and site response analyses discussed subsequently.

USE OF ENERGY-BASED LIQUEFACTION EVALUATION PROCEDURE

Overview of Energy-Based Procedures for Liquefaction Assessment

The Simplified Procedure for liquefaction assessment described above was developed based on post-earthquake field observations of liquefaction and no liquefaction at the ground surface at sites in California and the Far East. The new database presented herein presents 115 case histories of liquefaction and no liquefaction at the ground surface that are used to develop the new liquefaction evaluation relationships presented in Figure 26. Thus, the Simplified Procedure provides an estimate of the a_{max} required to induce a paleoliquefaction feature at the ground surface. An energy-based liquefaction evaluation

method uses the amount of seismic energy that is transmitted to a potentially liquefiable layer to assess whether or not it will liquefy.

Because energy-based methodologies are under development at the present time, a consensus on the use of a particular energy method in practice has not developed. As a result, this section presents a brief review of the existing energy-based methods for liquefaction assessment and then describes the method developed herein for interpretation of paleoliquefaction sites in Memphis and in the New Madrid Seismic Zone using the cone penetrometer.

Pond (1996) presents an energy-based method based on the Gutenburg and Richter (1956) formulation that relates site specific penetration resistance, i.e., SPT blowcount, to earthquake magnitude via the Seismic Energy Intensity Function (SEIF). The expression for the SEIF is:

$$(N_1)_{60} = \left(\frac{10^{1.5M}/R^2}{1.445} \right)^{0.165} \tag{22}$$

where $(N_1)_{60}$ is the SPT blowcount normalized to an effective overburden stress of 1 tsf and a delivered SPT energy of 60% of the theoretical energy, M is the earthquake magnitude, and R is the hypocentral distance from the test site to the earthquake source. A conversion of Equation (22) for use with CPT results developed herein is:

$$q_{c1} = 1.92 \left(\frac{10^{1.5M}/R}{1.445} \right)^{0.165} \tag{23}$$

Equation (23) was converted to a cone penetration resistance using the SPT to CPT conversion presented by Stark and Olson (1995) using an average D_{50} for clean and silty sands of 0.25 mm. The conversion involves inclusion of the constant 1.92 to Equation (22) based on Stark and Olson (1995).

Kayen and Mitchell (1997) propose an Arias intensity approach for assessing the liquefaction potential of soil deposits during earthquakes. Arias intensity, calculated by integrating processed accelerograms records (time histories), can be used as a measure of the severity of the earthquake motion at a point on or below the ground surface. However, current research on site response analyses shows that actual time histories cannot be scaled up or down by more than 0.2 g without invalidating the site response analysis. Thus, the Arias Intensity method would have to rely directly on synthetic time histories because the recorded time histories in the New Madrid Seismic Zone need to be scaled by more than 0.2 g. The reliance on synthetic time histories limits the effectiveness of the Arias approach to paleoliquefaction analyses in the New Madrid Seismic Zone, though the same can be said for any type of liquefaction back-analysis in a region of low seismicity with a lack of useful time histories.

Green (2001) presents a mathematical expression for the energy imparted to a soil by an earthquake, termed the *Demand*. The *Demand* expression was developed by first quantifying the energy dissipated in a soil deposit during one earthquake loading cycle,

ΔW_1. The energy imparted to the soil for one full loading cycle is then multiplied by an equivalent number of loading cycles of the earthquake, N_{eqv}, to represent the entire energy of the earthquake, ΔW, as shown below.

$$Demand = \Delta W = N_{eqv} * \Delta W_1 \quad (24)$$

Thus, to characterize the energy of the earthquake the number of equivalent loading cycles for the earthquake must be estimated.

Green (2001) uses 126 case histories where the corrected, clean sand blow count value, $N_{1,60cs}$, at the depth of liquefaction is available. The value of $N_{1,60cs}$ for the liquefied soil is plotted versus the calculated value of *Demand* for the earthquake, as shown in Figure 36 below. Separating the resulting data points into cases of liquefaction and no liquefaction yields the trend line shown in Figure 36. This trend line is the *Capacity* relationship and corresponds to the *Capacity* of the soil that results in liquefaction for the applied earthquake *Demand*. Figure 36 presents the earthquake energy *Demand* in a normalized form, *NED*, which is described in the next section.

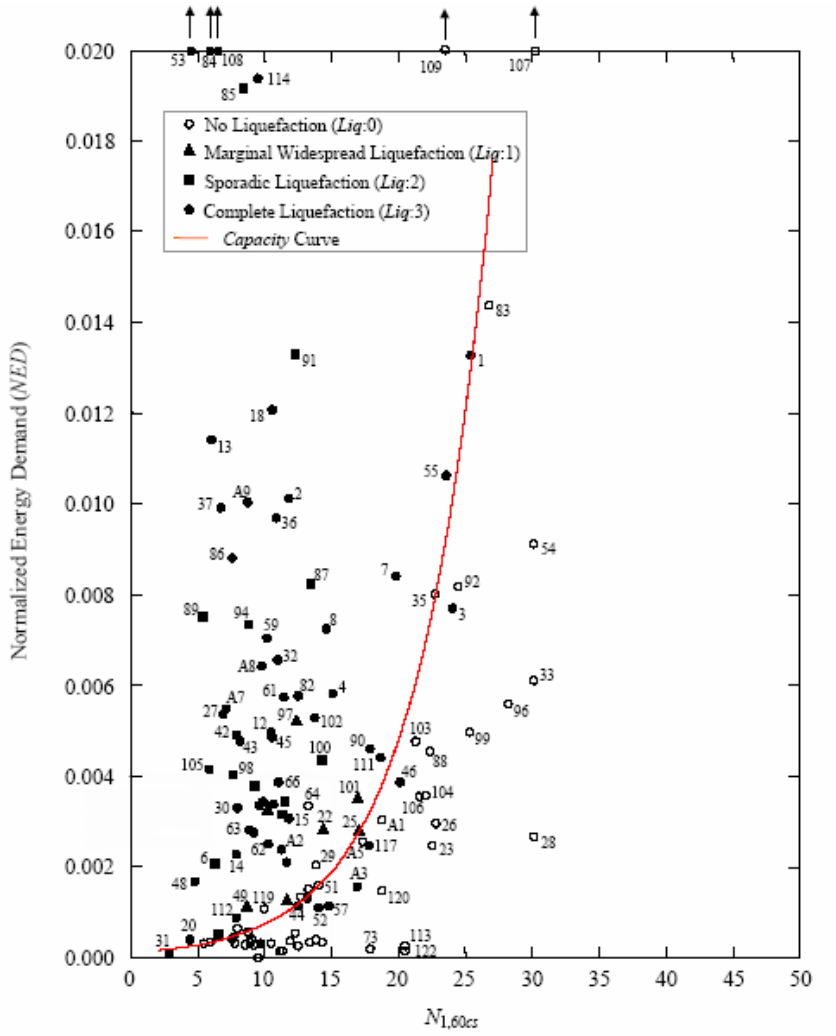

Figure 36. Case histories used to develop soil *Capacity* relationship in energy-based method (Green 2001)

The soil *Capacity* relationship in Figure 36 can be used for paleoliquefaction interpretation as described below. At a site of marginal liquefaction, (i.e. liquefaction just beginning to occur), the *Demand* of the earthquake and the *Capacity* of the soil are equal. If the resistance of the soil (given by $N_{1,60cs}$ or, as proposed herein, q_{c1}) at the time of the paleoearthquake is known, the *Demand* of the earthquake can be determined using the *Capacity* relationship. For example, if the value of $N_{1,60cs}$ is 20, the *NED* is approximately 0.005 at a site of marginal liquefaction.

In summary, the energy-based method proposed by Green (2001) appears applicable to the back-calculation of the *NED*, and thus earthquake magnitude and maximum acceleration, of historic earthquakes, such as the 1811-1812 New Madrid earthquakes. For this study, the Green (2001) method is adapted for use with cone penetration resistance values, q_c, instead of SPT blow count, *N*. Further details regarding the modifications to the Green (2001) method made during this study are given below.

Development of Mathematical Expression for Normalized Energy Demand

As discussed in Green (2001), the force-displacement response of an assemblage of particles can be described by a hysteresis loop. The area bounded by the hysteresis loop quantifies the energy dissipated in the system of particles. For a single cycle of loading, the energy dissipated in the system per unit volume is given by:

$$\Delta W_1 = \frac{2\pi D \tau_{avg}^{\ 2}}{G} \tag{25}$$

where ΔW_1 = dissipated energy per unit volume of material in one cycle of loading,
τ_{avg} = average applied shear stress,
D = damping ratio of the particles, and,
G = shear modulus.

The applied shear stress, τ, is calculated using the equation used in the Simplified Procedure, namely

$$\tau_{avg} = 0.65 \frac{a_{\max}}{g} \sigma_{vo} r_d \tag{26}$$

where a_{max} = peak acceleration at the ground surface of the site,
g = acceleration due to gravity,
σ_{vo} = total vertical overburden stress at depth, z, being considered, and
r_d = depth reduction factor, equal to 1-0.012*z, from Kayen (1992).

The damping ratio, *D*, and the shear modulus, *G*, are functions of the induced shear strain, γ, as shown in Figure 37. They model the decrease in *G* and increase in *D* with increasing shear strain.

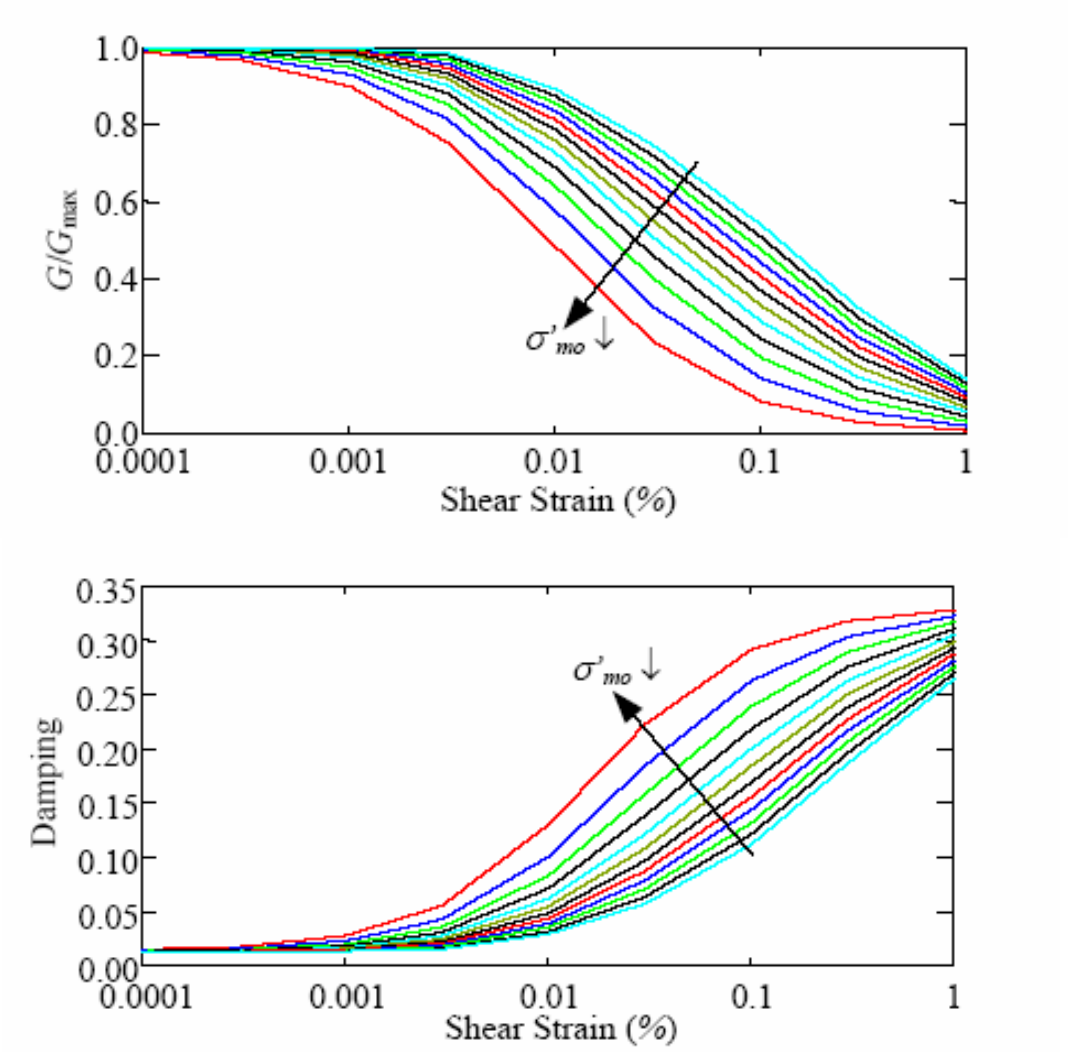

Figure 37. Shear modulus and damping degradation relationships from Ishibashi and Zhang (1993)

Determination of Soil Shear Modulus

Green (2001) uses the equation forms for the shear modulus, *G*, and damping *D*, degradation relationships presented by Ishibashi and Zhang (1993). The model of Ishibashi and Zhang is used herein to facilitate comparison of the resulting liquefaction potential relationship with that of Green (2001) in the initial development of the CPT-based relationships. Further research should investigate the effect that different equivalent linear soil models have on the results, especially with respect to the N_{eqv} relationship (see below). The shear modulus degradation relationship for a given soil can be expressed mathematically as:

$$\frac{G}{G_{\max}} = K(\gamma, I_p) \cdot (\sigma'_{mo})^{m'(\gamma, I_p)} \tag{27}$$

where $K(\gamma, I_p) = 0.5 \cdot \left\{1 + \tanh\left[\ln\left\langle\left(\frac{0.000102 + n(I_p)}{\gamma}\right)^{0.492}\right\rangle\right]\right\}$

$n(I_p)$	=	0.0	for $I_p = 0$	(sandy soils)
		$3.37 \times 10^{-6} I_p^{1.404}$	for $0 < I_p \leq 15$	(low plastic soils)
		$7.0 \times 10^{-7} I_p^{1.976}$	for $15 < I_p \leq 70$	(medium plastic soils)
		$2.7 \times 10^{-5} I_p^{1.115}$	for $70 < I_p$	(high plastic soils)

$$m'(\gamma, I_p) = 0.272 \cdot \left\{1 - \tanh\left[\ln\left\langle\left(\frac{0.000556}{\gamma}\right)^{0.4}\right\rangle\right]\right\} \cdot e^{-0.0145 I_p^{1.3}}$$

γ = shear strain,
I_p = plasticity index, and
σ'_{mo} = mean effective confining stress, $\frac{\sigma'_1 + \sigma'_2 + \sigma'_3}{3}$

To calculate the value of G using Equation (27), the value of $G_{\max}$ and γ must be known. The value of $G_{\max}$ is obtained from small-strain field or laboratory testing of shear wave velocity. The value of γ at a particular depth and soil type also must be estimated. The shear modulus G is related to the applied shear stress and the shear strain as shown below:

$$G = \frac{\tau_{avg}}{\gamma} \tag{28}$$

Dobry et al. (1982) present the following expression for determining the earthquake-induced shear strain at depth in a soil deposit using G and τ_{avg} and Equation (26):

$$\gamma = \frac{\tau_{avg}}{G} = \frac{0.65 \frac{a_{\max}}{g} \sigma_{vo} r_d}{G_{\max}\left(\frac{G}{G_{\max}}\right)_\gamma} \tag{29}$$

where G_{max} = small-strain shear modulus corresponding to $\gamma = 10^{-4}\%$,
(G/G_{max}) = ratio of shear moduli corresponding to γ and $\gamma = 10^{-4}\%$.

To utilize Equation (29), the final required parameter is G_{max}. As noted above, G_{max} can be estimated from insitu tests such as SPT or CPT. Green (2001) uses an expression from Seed et al. (1986) to relate SPT penetration resistance measured as a blow count, $N_{1,60}$, to G_{max}. The main focus of this study is the development of an energy based method that uses the CPT because of the many advantages of the CPT in characterizing sand deposits (Stark and Olson 1995). Figure 38 presents a correlation between G_{max} and q_c for uncemented quartz sands. The average relationship between normalized q_c and normalized G_{max} in Figure 38 can be expressed as follows:

$$G_{\max} = 1634\left(\frac{q_c}{\sqrt{\sigma'_v}}\right)^{-0.75}(q_c) \tag{30}$$

where q_c = penetration resistance in kPa,
σ'_v = effective vertical stress in kPa, and
G_{max} = small strain shear modulus in kPa.

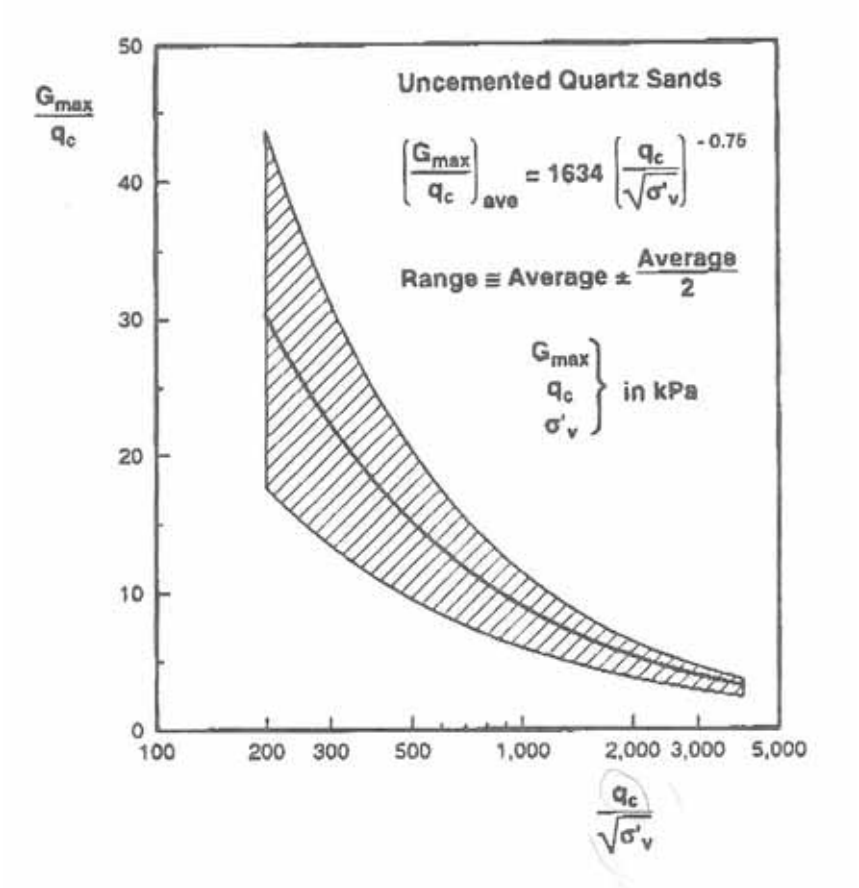

Figure 38. Correlation between G_{max} and q_c for uncemented, quartz sands showing average and range of values (Rix and Stokoe 1991).

Determination of Shear Strain for τ_{avg}

Green (2001) uses an iterative procedure to solve Equation (29) to determine the value of γ that corresponds to τ_{avg}. An initial value of G/G_{max} is assumed and the corresponding value of γ is computed. A new ratio of G/G_{max} corresponding to the γ from the previous iteration is used and a new value of γ is computed. The process is repeated until the assumed and computed ratios of G/G_{max} are within a tolerable error. For this study, an error tolerance of 1% is used. This process is illustrated in Figure 39 below.

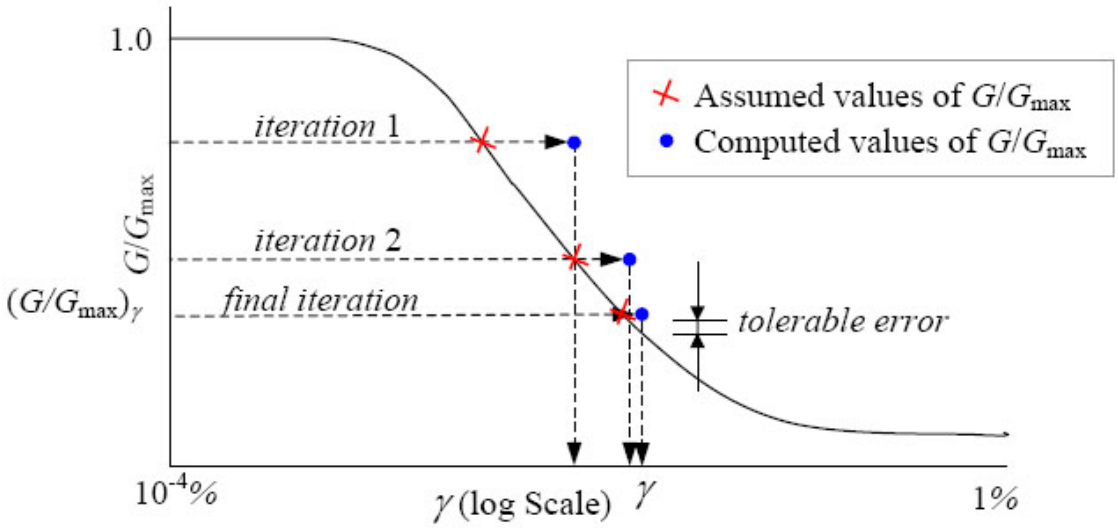

Figure 39. Iterative solution of Equation (29) to determine the effective shear-strain, γ, at a given depth in a soil profile (from Green 2001).

With the synchronized values of γ and G/G_{max} determined from the iterative procedure above, Green (2001) uses the following empirical relationship from Ishibashi and Zhang (1993) to determine the damping ratio, D, as a function of shear stress, γ:

$$D(\gamma, I_p) = \frac{0.333\left(1+e^{-0.0145 I_p^{1.3}}\right)}{2}\left\{0.586\left(\frac{G}{G_{max}}\right)^2_{(\gamma,Ip)} - 1.547\left(\frac{G}{G_{max}}\right)_{(\gamma,Ip)} + 1\right\} \quad (31)$$

Using the ratio of G/G_{max} for the applied γ, D from Equation (31), G_{max} from Equation (30), and τ_{avg} using Equation (26), the energy dissipated in the soil per unit volume during one cycle of earthquake loading can be estimated using Equation (32).

$$\Delta W_1 = \frac{2\pi D_\gamma}{G_{max}\cdot\left(\frac{G}{G_{max}}\right)_\gamma}\cdot\left[0.65\frac{a_{max}}{g}\sigma_{vo}r_d\right]^2 \quad (32)$$

Determination of Normalized Energy Demand (*NED*)

To estimate the total energy dissipated in the soil by the earthquake, it is necessary to multiply by an equivalent number of loading cycles that represents the entire earthquake loading:

$$\Delta W = \Delta W_1 \times N_{eqv} \quad (33)$$

where ΔW = dissipated energy per unit volume for the entire earthquake motion,

ΔW_1 = dissipated energy per unit volume for one equivalent cycle of earthquake motion, and

N_{eqv} = number of equivalent loading cycles in the earthquake motion.

To estimate the total energy of the earthquake, the equivalent number of loading cycles for the earthquake must be estimated. Green (2001) presents a correlation between the energy dissipated in the layers of a soil profile as determined from site response analysis to the energy dissipated in an equivalent cycle of loading multiplied by N_{eqv}. Green (2001) added an option to the site response computer program SHAKE91 (Idriss and Sun 1992) to compute the energy dissipated in each layer of a soil deposit subjected to an earthquake loading. The new version of the site response program is SHAKEVT, and it utilizes the equivalent linear method used by Idriss and Sun (1991). Using 24 earthquake motions and 12 soil profiles, SHAKEVT was used to compute the normalized energy demand, *NED*, for each layer in the 12 soil profiles. *NED* is defined as the dissipated energy per unit volume in the soil layer for the entire earthquake motion divided by the mean effective confining stress:

$$NED = \Delta W/\sigma'_{mo} \tag{34}$$

where σ'_{mo} = mean effective confining pressure, $\frac{\sigma'_1+\sigma'_2+\sigma'_3}{3}$

σ'_1 = vertical effective stress σ'_{vo} for conditions of level ground and a symmetric state of stress

σ'_2 = $k \cdot \sigma'_{vo}$

σ'_3 = $k \cdot \sigma'_{vo}$

k = coefficient of lateral earth pressure. For sands, $k = 1\text{-}\sin(\phi')$

ϕ' = effective stress friction angle.

Kulhawy and Mayne (1990) present the relationship for ϕ' based on cone tip resistance shown in Figure 40. The average trend line through the data in Figure 40 can be represented by the following equation:

$$\phi' = 17.6 + 11.0 \cdot \log\left[\frac{\frac{q_c}{P_a}}{\left(\frac{\sigma'_{vo}}{P_a}\right)^{0.5}}\right] \tag{35}$$

where P_a = 101.3 kPa

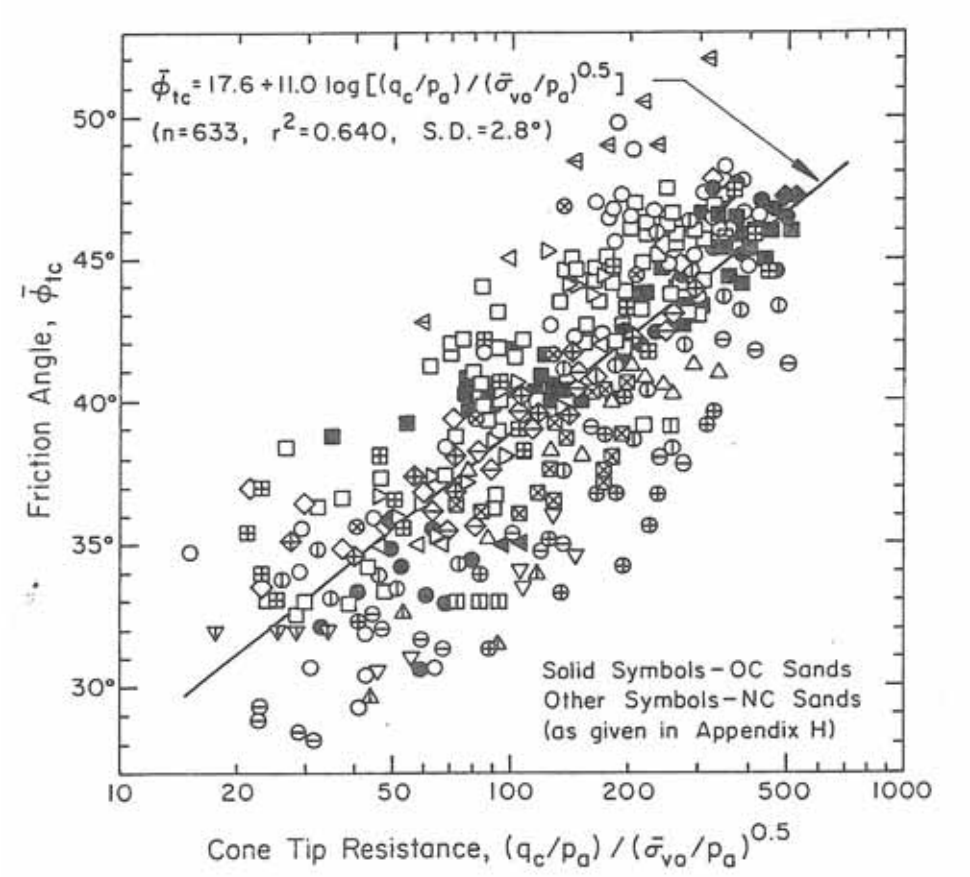

Figure 40. Trend of effective stress friction angle with normalized q_c (Kulhawy and Mayne 1990)

The value of equivalent number of cycles is obtained by dividing the normalized energy demand for the entire earthquake motion by the normalized energy demand for one cycle of the motion.

$$N_{eqv} = \frac{NED}{NED_1} \tag{36}$$

where NED_1 = $\Delta W_1/\sigma'_{mo}$ and ΔW_1 is estimated using Equation (32).

Using three-dimensional regression analyses to fit surfaces to the computed values of N_{eqv}, Green (2001) proposes the following equations for determining N_{eqv}. The relationship is plotted in Figure 41.

$$\boldsymbol{N_{eqv}} = \begin{cases} f(ED) & \text{for } f(ED) \le f(M) \\ f(M) & \text{for } f(ED) > f(M) \end{cases} \tag{37}$$

where

$$9.633M^2 - 110.453M + 325.172 \qquad for \qquad M \ge 5.7$$

$$f(M) = \begin{cases} 8.5 & for \quad M < 5.7 \end{cases}$$

$$f(ED) = \begin{cases} 0.011ED^2 - 0.012ED + 8.487 & for \quad ED \geq 0.55km \\ 8.5 & for \quad ED < 0.55km \end{cases}$$

M = Richter magnitude of earthquake
ED = epicentral distance from site to source

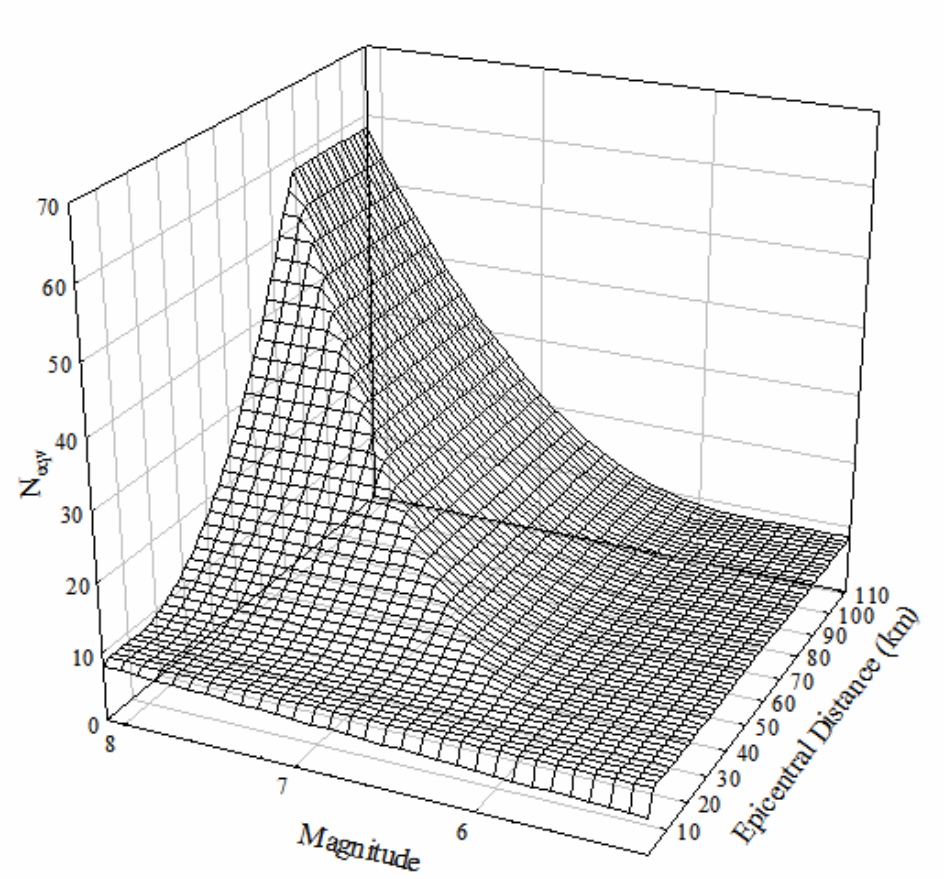

Figure 41. Relationship for N_{eqv} as a function of magnitude and epicentral distance

In summary, the normalized energy demand can be estimated using the procedure proposed by Green (2001) with two modifications to accommodate the use of the cone penetrometer. The two modifications presented herein for use of the cone penetrometer are the expressions for soil shear modulus in Equation (30) and effective stress friction angle in Equation (35). The resulting expression is shown below:

$$NED = \frac{\Delta W_1}{\sigma'_{mo}} \cdot N_{eqv} = \frac{2\pi D_\gamma}{\sigma'_{mo} \cdot G_{\max} \cdot \left(\frac{G}{G_{\max}} \right)_\gamma} \cdot \left[0.65 \frac{a_{\max}}{g} \sigma_{vo} r_d \right]^2 \cdot N_{eqv} \quad (38)$$

Development of Relationship between Cone Tip Resistance and Soil *Capacity*

Similar to the procedure used by Green (2001) to develop a relationship between SPT *N* value and soil *Capacity*, 90 earthquake liquefaction case histories were examined for this study. However, the main difference between the case histories is where Green (2001) uses SPT *N* values, this study will examine earthquake liquefaction case histories where cone penetration tip resistance is available. The main objective of this phase is to develop a correlation between normalized energy demand, *NED*, and tip resistance, which is analogous to the relationship in Figure 36. This new relationship is used to back-calculate values of magnitude and maximum acceleration for the historic earthquakes in Memphis and the New Madrid Seismic Zone.

Appendices B and C present the relevant information about the earthquake liquefaction case histories that are used to develop the CPT-based soil *Capacity* relationship.

For each of the earthquake liquefaction case histories listed in Appendix B, the normalized energy demand, that is, the entire energy dissipated by the earthquake at the depth of liquefaction, was calculated using the *Demand* equation described previously.

Liquefaction Potential of Sandy Soils Based on Normalized Energy Demand

Fines content is expected to be a factor in the energy-based liquefaction potential relationships in the same manner as the cyclic stress-based liquefaction potential relationships. The liquefaction resistance of soil is increased by the presence of fines that can reduce particle movement and pore pressure generation during shaking. Penetration resistance can also be reduced by the presence of fines causing an undrained shearing condition at the cone tip. To quantify the effect that fines content has on the *Capacity* curve, the database is sorted into groups based on fines content. Separate *Capacity* curves are developed for each of these groups. Field measurement of fines content can then be used to determine which relationship to use in the liquefaction or paleoliquefaction analysis.

Group 1 – Fines Contents less than 12%

Figure 42 presents a compilation of 27 liquefaction and 22 non-liquefaction field case histories involving soils with fines contents less than 12% where CPT, SPT, and fines content data are available. This soil group is referred to as Soil Group 1. From the field data, a boundary line is drawn between liquefied sites and non-liquefied sites. This boundary defines a relationship between the normalized energy demand and CPT q_{c1}-values for clean sand (fines content less than 12%). Figure 42 shows that the proposed liquefaction potential relationship is in good agreement with the field case history data.

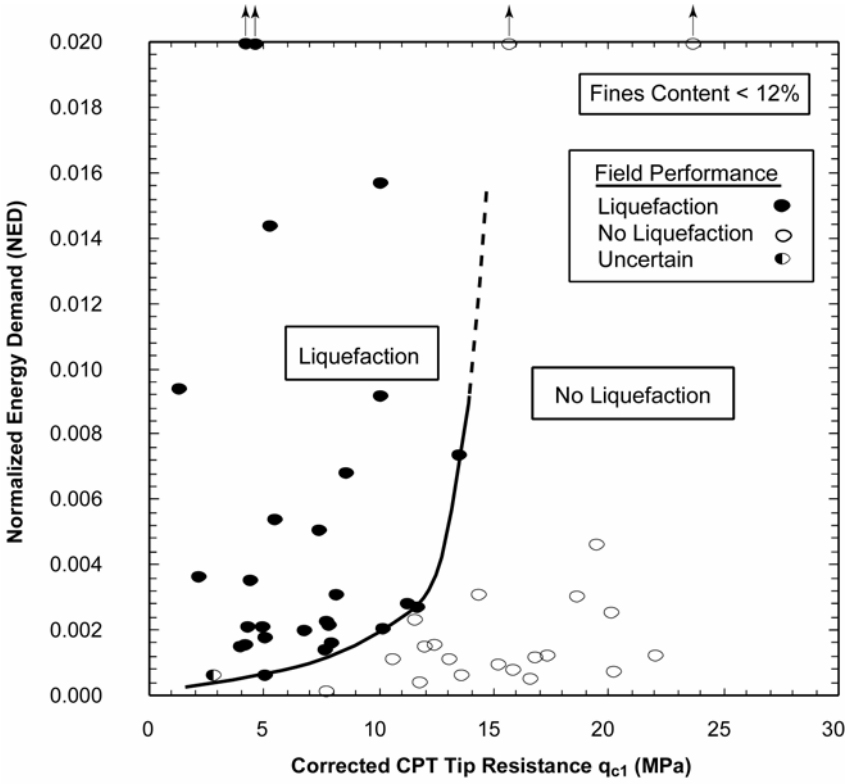

Figure 42. Relationship between normalized energy demand triggering liquefaction and q_{c1} values for Soil Group 1

Group 2 – Fines contents greater than or equal to 12% and less than 20%

Figure 43 presents a compilation of 16 liquefaction and 10 non-liquefaction field case histories involving sands with fines contents greater than or equal to 12% and less than 20% where CPT, SPT, and fines content data are available. This soil group is referred to as Soil Group 2. From the field data, a boundary line between liquefied sites and non-liquefied sites is established and defines a relationship between the normalized energy demand for liquefaction and CPT q_{c1} values. The relationship for Soil Group 2 plots to the left of the relationship for fines contents less than or equal to 12%.

Four of the case histories are derived from the 1999 Chi-Chi, Taiwan earthquake and are classified as "uncertain" by Juang et al. (2003) with respect to whether or not they are in liquefied areas.

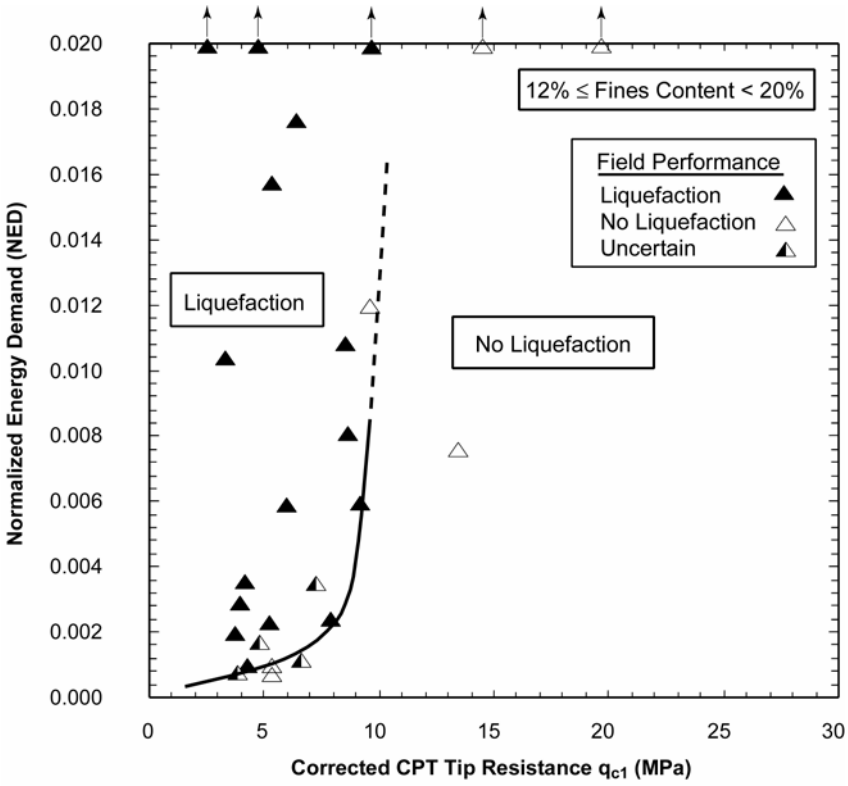

Figure 43. Relationship between normalized energy demand triggering liquefaction and q_{c1} values for Soil Group 2

Group 3 – Fines contents greater than or equal to 20% and less than 35%

Figure 44 presents a compilation of 7 liquefaction and 6 non-liquefaction field case histories involving sands with fines contents greater than or equal to 20% and less than 35% where CPT, SPT, and fines content data are available. From the field data, a boundary line between liquefied sites and non-liquefied sites is established in the same manner as the boundary for Soil Groups 1 and 2 and defines a relationship between the normalized energy demand for liquefaction and CPT q_{c1} values.

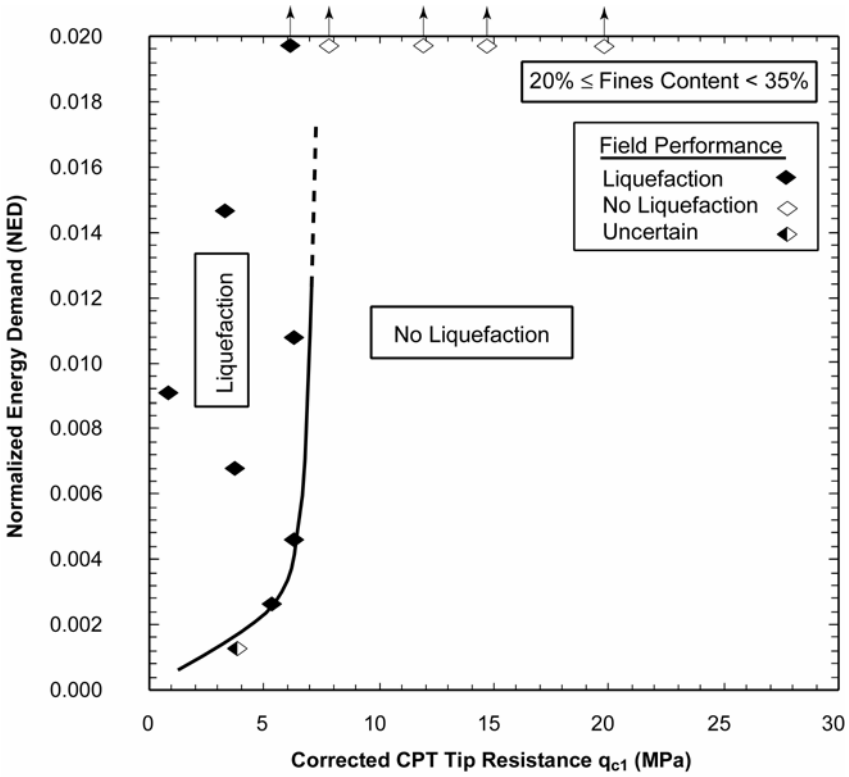

Figure 44. Relationship between normalized energy demand triggering liquefaction and q_{c1} values for Soil Group 3

Group 4 – Fines contents greater than or equal to 35%

Figure 45 presents a compilation of 19 liquefaction and 8 non-liquefaction field case histories involving sands with fines contents greater than 35% where CPT data are available. From the field data, a boundary line between liquefied sites and non-liquefied sites was established. In the same manner as the boundary for sands with other fines contents above, the boundary in Figure 45 defines a relationship between the normalized energy demand and CPT q_{c1}-values for appropriate sandy soils with fines contents greater than or equal to 35%.

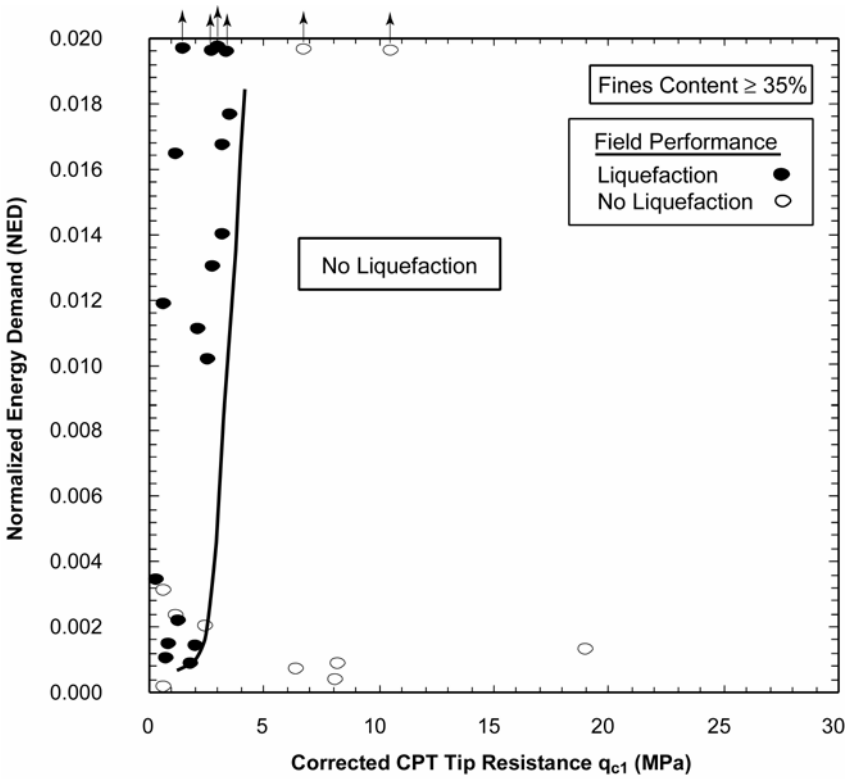

Figure 45. Relationship between normalized energy demand triggering liquefaction and q_{c1} values for Soil Group 4

Both the "liquefaction" and "no liquefaction" points at low values of q_{c1} have a large degree of uncertainty associated with the calculation of NED because of this small q_{c1}. The empirical relationships used to calculate G_{max} and ϕ' as described in the previous section were developed for cone penetration in primarily clean sands. Many of the q_{c1} values used in Soil Groups 3 and 4 are lower than or at the lower range of the data set used to develop these empirical relationships. Even for sandy soils containing a small amount of silts, the effect of inhibited drainage during penetration testing may result in the underestimation of soil properties using these empirical relationships.

New Liquefaction Potential Relationships

Figure 46 presents the new liquefaction potential relationships based on Normalized Energy Demand for the four fines content groups. The proposed liquefaction potential relationships in Figure 46 are obtained from Figure 42 through Figure 45 and constitute a liquefaction assessment chart that can be used to estimate the factor of safety against liquefaction for an earthquake a vertical effective overburden stress of less than or equal to 100 kPa and level ground conditions. As with the proposed liquefaction potential relationships for the Simplified Procedure, soil groups 3 and 4 are constrained by a relatively small number of points. In addition to the small number of points in these groups, there is more uncertainty associated with the empirical relationships used to calculated G_{max} and effective stress friction angle for these soils.

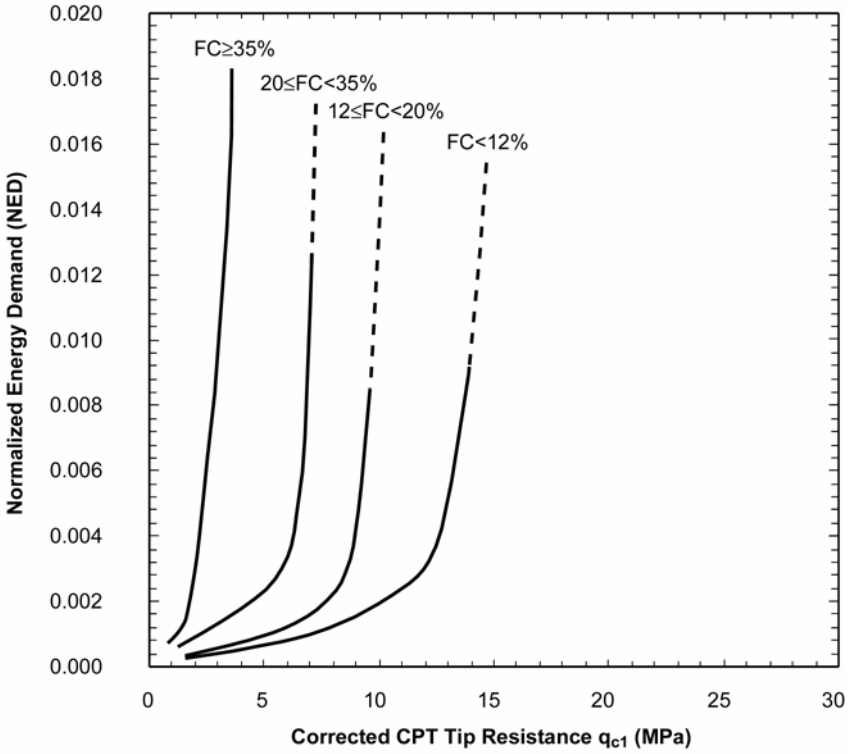

Figure 46. Relationship between Normalized Energy Demand triggering liquefaction and q_{c1} values for all four soil type groups

Comparison With SPT *Capacity* Curve

Because there are no existing energy-based *Capacity* relationships using CPT data, the proposed relationship is compared with the clean sand SPT-based *Capacity* relationship presented by Green (2001). To convert the SPT N values in Green (2001) to q_c values to make the comparison, the relationship between q_c/N_{60} ratio and median grain diameter, D_{50}, presented in Figure 47 from Stark and Olson (1995) is utilized. Because the ratio of q_c/N_{60} increases with D_{50}, an upper and lower bound q_c/N_{60} ratio based on the range of grain sizes for clean sands (Soil Group 1) for the SPT-based *Capacity* relationship can be determined. The resulting ratio can be used to calculate the upper and lower bounds of q_c for the N values used by Green (2001).

The minimum D_{50} corresponding to a clean sand from Olson and Stark (1998) is 0.2 mm. This corresponds to a q_c/N_{60} ratio of 0.5, which is used to convert the N value from Green (2001) to a q_c value. Figure 48 shows that the converted relationship from Green (2001) for D_{50}=0.2 mm plots above the proposed relationship. As a bound for coarser soils, Olson and Stark (1998) use 2.0 mm as the upper range of D_{50} for clean sands. Because the conversion in Stark and Olson (1995) only presents data up to a maximum D_{50} of 1 mm, the maximum q_c/N_{60} ratio of 0.8 corresponds to D_{50}=1 mm is used for coarser soils. As illustrated in Figure 48, the proposed relationship plots between the D_{50}=0.2 mm and 1 mm bounds for the converted SPT-based relationship from Green (2001). Thus the proposed q_c-based relationship that was developed independent of the SPT case histories used by Green (2001) is in agreement with the relationship proposed by Green (2001) after converting the N values to q_c values.

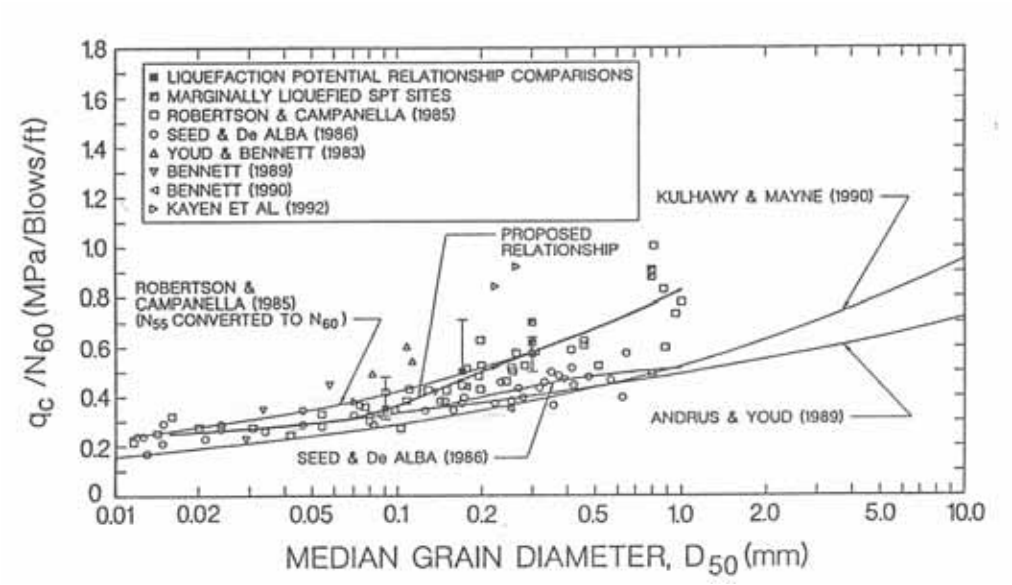

Figure 47. Conversion of SPT N-values to CPT q_c-values using median grain diameter (from Stark and Olson 1995)

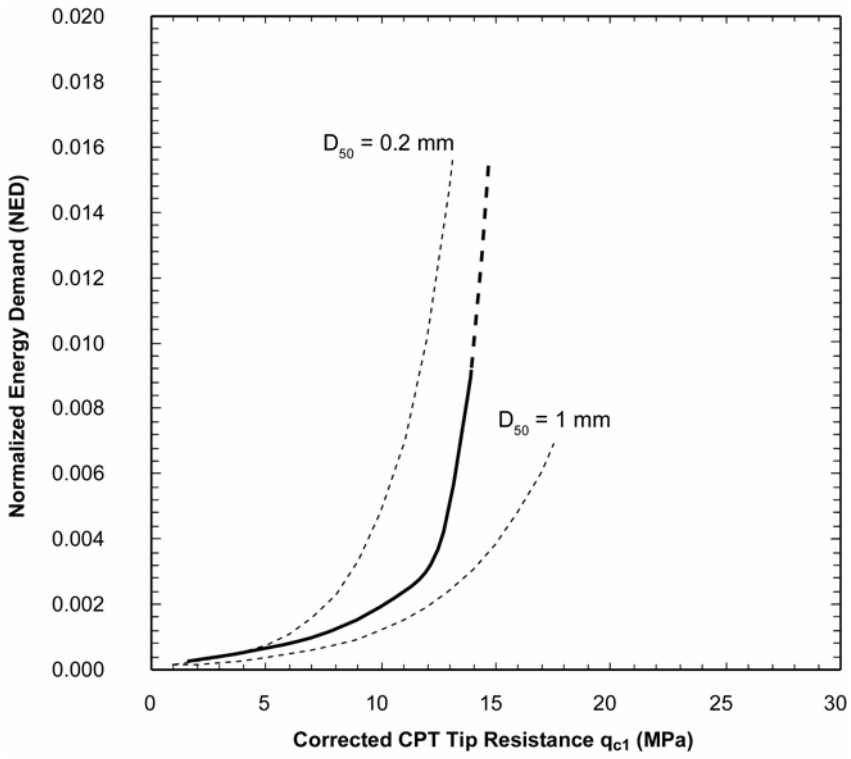

Figure 48. Comparison of CPT-based and SPT-based *Capacity* curves

Energy Back-Analysis at Wolf River

Because Wolf6 is a site of marginal liquefaction, it allows paleoliquefaction back-analyses to estimate the intensity of ground shaking experienced at the site. Similarly to the simplified procedure discussed earlier, normalized energy capacity and demand can be used to estimate the size of the earthquake required to trigger liquefaction at a given site.

The normalized energy demand (NED) placed on the soil by an earthquake is defined above as

$$\mathrm{NED} = \frac{\Delta W_1 N_{eqv}}{\sigma'_{m0}} \tag{39}$$

where ΔW_1 is the energy dissipated in the soil for one equivalent cycle of ground motion, N_{eqv} is the number of equivalent cycles caused by a given earthquake at the site, and σ'_{m0} is the mean effective confining pressure.

For a paleoliquefaction back-analysis, the normalized energy demand is estimated from an in-situ test, e.g., the CPT or SPT, and an empirical relationship representing normalized energy capacity from liquefaction case histories. At the initiation of liquefaction, the demand placed on the soil is equal to the capacity of the soil to resist liquefaction. Figure 36 and Figure 46 present empirical relationships for SPT- and CPT-based liquefaction case histories, respectively.

The energy dissipated in a single equivalent cycle of earthquake loading, ΔW_1, is a function of the soil properties and the peak ground acceleration, a_{max}. The number of equivalent cycles is a function of earthquake magnitude and epicentral distance. Like the Simplified Procedure, there is not a unique combination of acceleration and magnitude that yield the demand necessary to initiate liquefaction. Instead, there are many combinations of acceleration, magnitude, and epicentral distance that will yield the same demand.

The values of NED, acceleration, magnitude and epicentral distance are related through N_{eqv}. Figure 41 presents the relationship presented by Green (2001) for N_{eqv} as a function of magnitude and epicentral distance. Figure 41 shows the three-dimensional interrelationship between magnitude, epicentral distance, and N_{eqv}. To perform a back-analysis at a paleoliquefaction site, q_{c1} from the critical layer identified by the back-analysis using the Simplified Procedure above is calculated and then used to obtain the normalized energy capacity from the appropriate relationship in Figure 46. Because capacity and demand are equal at the initiation of liquefaction for marginal liquefaction sites, substituting the capacity and effective confining pressure at the critical depth into Equation (39) yields the following relationship between ΔW_1 and N_{eqv}:

$$\Delta W_1 N_{eqv} = \mathrm{NED} * \sigma'_{m0} \tag{40}$$

An iterative procedure developed by Green (2001) is used to estimate ΔW_1 using the equivalent linear soil model described above. Therefore, Equation (40) is solved by assuming a range of a_{max} values. For each a_{max} value, the iterative equivalent linear procedure (Green 2001) is used to calculate ΔW_1 for that acceleration. For each value of a_{max} and the corresponding ΔW_1, the number of cycles necessary to initiate liquefaction (N_{eqv}) and satisfy Equation (40) can be calculated.

For the paleoliquefaction analyses in this report, the epicentral distance is known and thus the iterative process is used to estimate the earthquake magnitude. When solving Equation (37), the appropriate epicentral distance is substituted in and used to calculate the magnitude yielding the value of N_{eqv} associated with each a_{max} value assumed at the beginning of the calculation. This procedure yields the magnitude necessary to initiate liquefaction at a particular paleoliquefaction site for the assumed epicentral distance and a_{max}.

The resulting relationship between a_{max} and M_W is valid for the input parameters used by Green (2001) for the development of the N_{eqv} relationship shown in Figure 41. One difference between the soil profiles analyzed by Green (2001) to develop N_{eqv} relationship and the soil profiles at paleoliquefaction sites in the NMSZ and the Wolf River area is the depth of the soil deposits. The soil profiles analyzed by Green (2001) have a depth of 30 meters, while the soil profiles in the NMSZ can be as deep as 1000 m (Romero and Rix 2001). In addition to the soil profiles, the time histories used by Green (2001) are all for Pacific Rim earthquakes, and thus may not accurately represent the relationship between magnitude, epicentral distance, and the number of equivalent cycles that applies to other regions. Due to the lack of time histories and the complex behavior of the deep soil deposits in the NMSZ, the development of an N_{eqv} relationship for the NMSZ (and other regions) is a topic that requires further study. The relationship developed by Green (2001) is used to develop the energy back-analysis methods herein.

The resulting relationship between a_{max} and magnitude in Figure 49 presents the combination of magnitude and acceleration for the assumed epicentral distance that results in sufficient number of equivalent cycles of ground motion to initiate liquefaction at the Wolf6 site, with no soil aging effects. As an upper bound on the ground motion experienced at the Wolf River area, the back-analysis for the Wolf4 is shown in Figure 50.

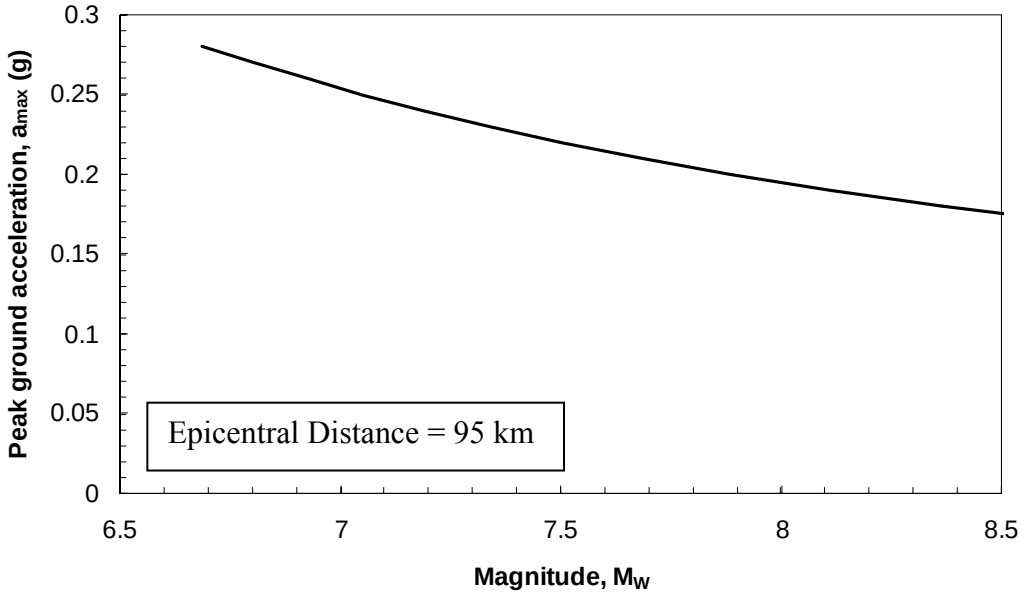

Figure 49. Relationship between magnitude and a_{max} necessary to initiate liquefaction at Wolf6 disregarding soil aging effects

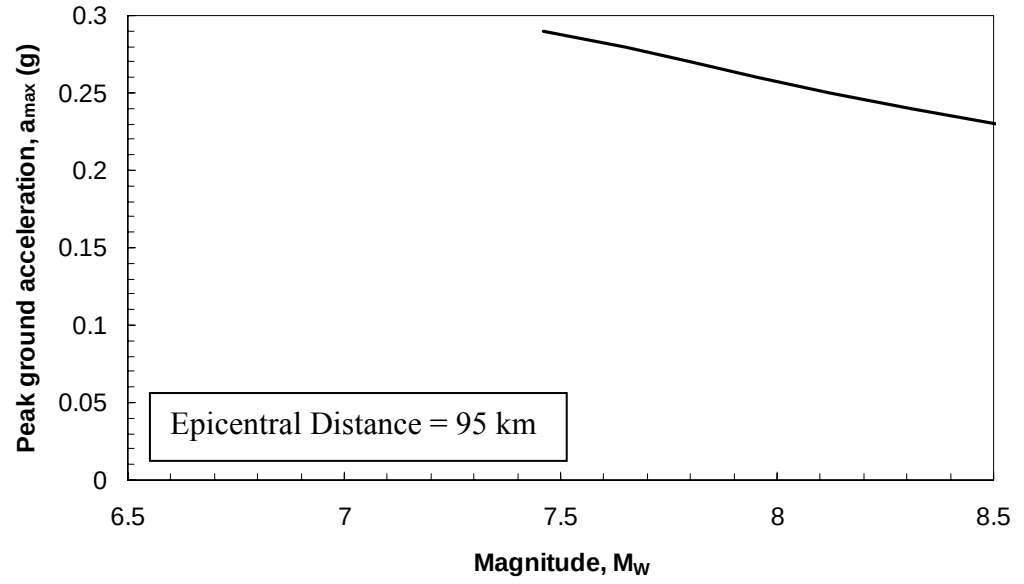

Figure 50. Relationship between magnitude and a_{max} necessary to initiate liquefaction at Wolf4 disregarding soil aging effects

Energy Back-Analysis at NMSZ Sites

Sites of full liquefaction, e.g., Mtree11, Wils02, Dex05 are locations where the capacity of the soil to resist liquefaction is significantly exceeded and large liquefaction features resulted. Because the magnitudes and accelerations back-calculated at these sites are

only those sufficient to trigger liquefaction, they only provide a lower bound on the magnitude and acceleration experienced at the sites.

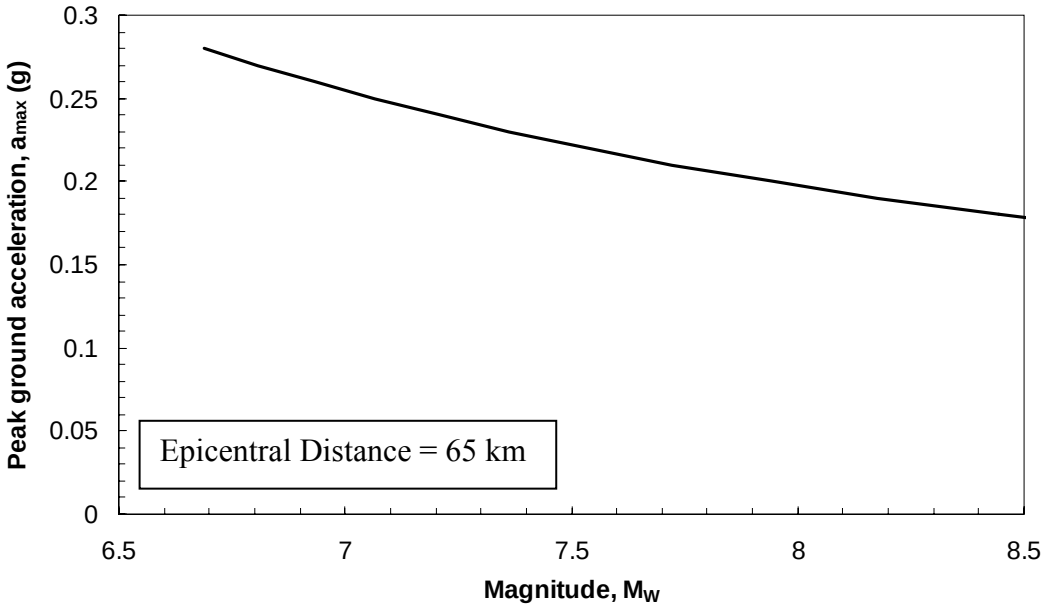

Figure 51. Relationship between magnitude and a_{max} necessary to initiate liquefaction at Mtree11 disregarding soil aging effects

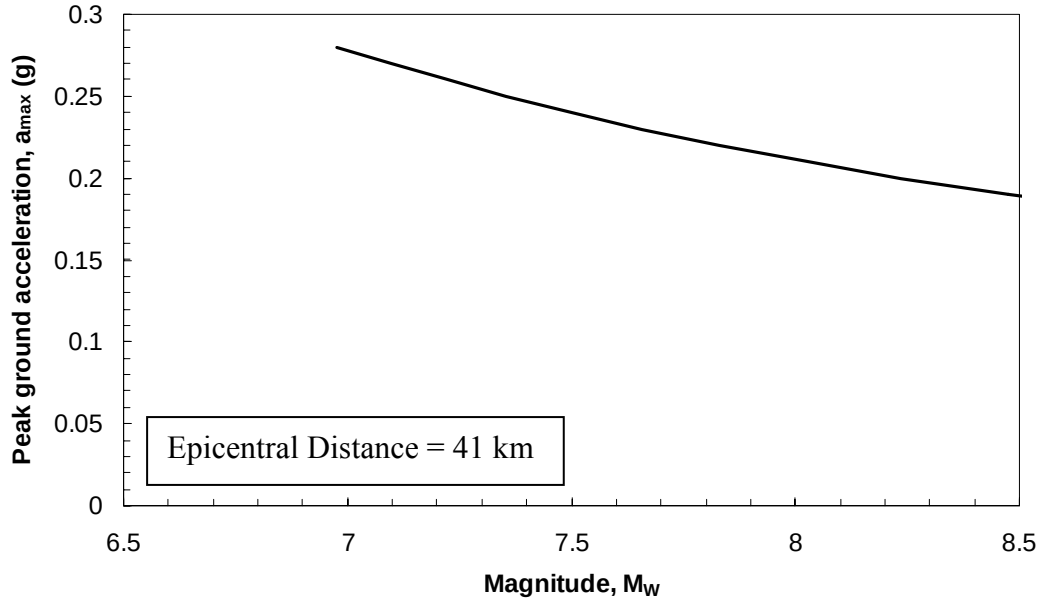

Figure 52. Relationship between magnitude and a_{max} necessary to initiate liquefaction at Wils02 disregarding soil aging effects

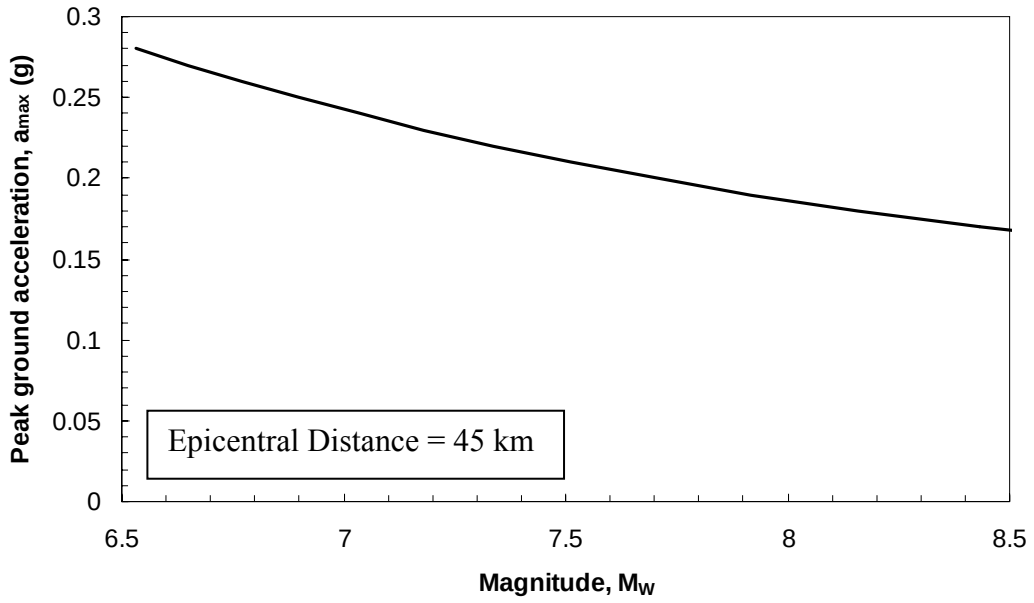

Figure 53. Relationship between magnitude and a_{max} necessary to initiate liquefaction at Dex05 disregarding soil aging effects

Table 9 presents a summary of the accelerations and magnitudes back calculated to trigger liquefaction at the paleoliquefaction sites using the energy-based method proposed herein. In order to facilitate comparison with each other and with the results of the Simplified Procedure, accelerations corresponding to M_W=7.5 for the Energy Procedure are presented in Table 9. As with the Simplified Procedure, these back-calculated accelerations are overestimates because no corrections are made for soil aging effects.

Table 9. Summary of back-calculated a_{max} values required to trigger liquefaction at the Wolf River and NMSZ sites assuming M_W=7.5 with no soil aging correction

Test Site	Description	a_{max} Estimate	Simplified Procedure	Energy Procedure
Mtree11	Full Liquefaction	Lower Bound	0.18	0.23
Wils02	Full Liquefaction	Lower Bound	0.21	0.23
Dex05	Full Liquefaction	Lower Bound	0.20	0.22
Wolf6	Marginal Liquefaction	Best Estimate	0.18	0.26
Wolf4	No Liquefaction	Upper Bound	0.27	0.28

DETERMINING MAGNITUDE OF HISTORIC EARTHQUAKES

From a paleoliquefaction site, the a_{max} or range of a_{max} required for triggering liquefaction at a selected magnitude can be estimated as described above. The back-analysis procedures described above yields a relationship between a_{max} and M necessary to cause

liquefaction at a given site. To determine which combination of magnitude and a_{max} actually occurred at a given paleoliquefaction site, a ground motion attenuation and site response analysis must be conducted. This analysis models the seismic waves that radiate from the earthquake source and propagate through the bedrock to the paleoliquefaction site. A site response analysis models the vertical propagation of the seismic waves from the bedrock through the soil column under the site. This procedure yields a relationship between a_{max} and M for a given earthquake scenario at the paleoliquefaction site. The combination of a_{max} and M where the results of the back-analysis and the results of the ground motion and site response analyses are equal represents the earthquake that was necessary to cause liquefaction at that paleoliquefaction site.

As illustrated schematically in Figure 74, seismic waves originate at a fault rupture. The waves radiate away from the rupture or earthquake source through the bedrock and eventually reach the bedrock beneath the paleoliquefaction site. At the paleoliquefaction site, the seismic waves propagate upwards through the softer sediments. The amplitude and frequency content of the seismic waves change (are amplified or attenuated) as they travel vertically through the various soils between the bedrock and the ground surface.

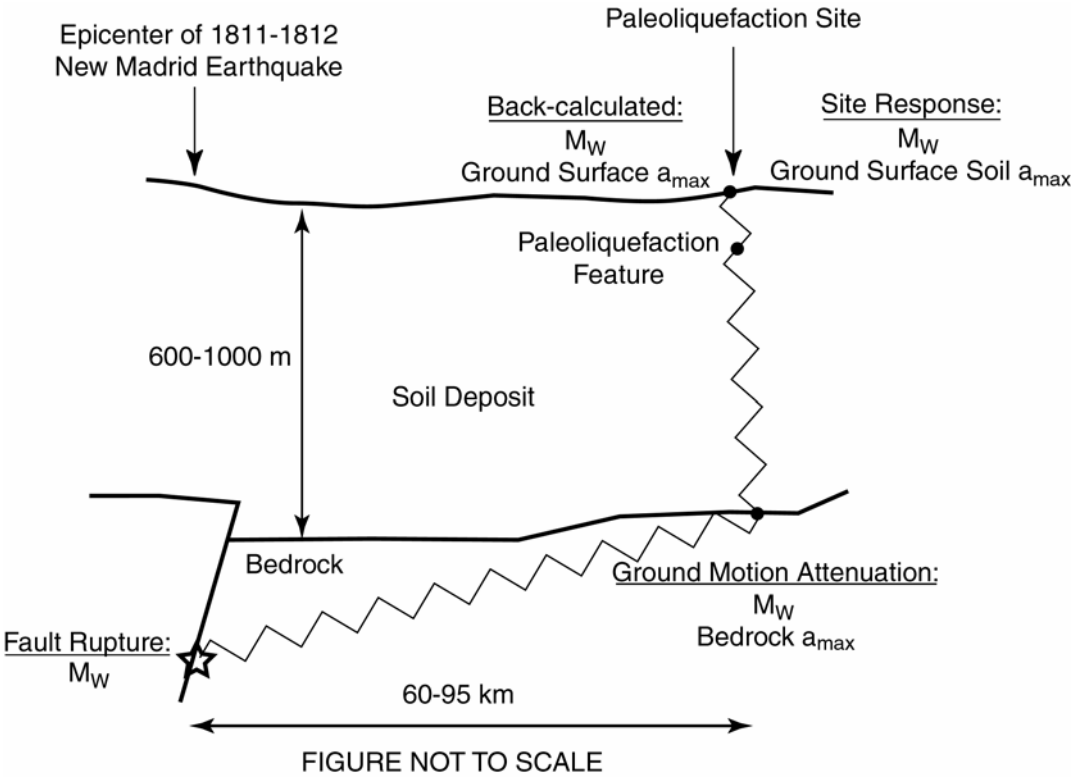

Figure 54. Schematic of paleoliquefaction back analysis

To estimate the peak ground acceleration at a specific site resulting from an earthquake of a given magnitude, a ground motion attenuation and site response analysis must be conducted. The three main steps in the attenuation and site response analyses are: (1) the

earthquake source must be modeled, (2) the path that the seismic waves travel from the source to the site must be characterized, and (3) and the effect of the soil deposits on the site response analysis above the bedrock must be assessed.

Ground Motion Attenuation and Site Response Model

Because of the lack of earthquake records for large earthquake magnitudes originating in the NMSZ, it is common to use synthetic earthquake records in attenuation and site response analyses. These synthetic earthquake records are developed from semi-empirical source, path, and site models and used to study the seismic behavior of sites in the NMSZ.

The Fourier amplitude spectrum of an earthquake motion is calculated using the model parameters described below. If synthetic time histories are required for analysis, the Fourier spectrum is applied to a randomly-generated signal of band-limited, finite-duration white noise (Boore 2003). If time histories are not required, peak ground motion parameters (peak ground acceleration, velocity, or displacement and spectral accelerations, velocities, or displacements) can be estimated from the Fourier amplitude spectrum using random vibration theory. The calculations involved in applying random vibration theory have the advantage of not requiring the computationally-intensive step of converting the earthquake motion from the frequency domain to the time domain. A thorough discussion of the background of random vibration theory and its application to seismology is given by Boore (2003). The computer program SMSIM (**S**tochastic **M**odel **SIM**ulation), developed by Boore (1996), performs the calculations necessary to calculate peak ground acceleration using random vibration theory, the Fourier amplitude spectrum, and the input parameters described below.

The main components of the Fourier amplitude spectrum for any given earthquake are (a) the Fourier amplitude spectrum of the earthquake at the source, (b) the effect of the bedrock material properties and bedrock quality on this spectrum, (c) the effect of the site characteristics on the spectrum. A brief description of the parameters used in this study is given below. A more detailed description of the models utilized is given in Appendix E, as well as in Boore (2003) and Romero and Rix (2001).

The US National Seismic Hazard maps utilize as one of their source models for the Central and Eastern US earthquakes a 150-bar stress drop (Frankel et al. 1996 and 2002) to account for the possibility of earthquakes with larger stress drops, like those measured for the magnitude 5.9 Saguenay, Quebec (1988) earthquake with a stress drop of 655 bars and the magnitude 4.7 New Madrid, MO (1989) earthquake with a stress drop of 229 bars (Toro et al. 1997). The analysis presented below also uses 150-bar Brune source model to calculate the source spectrum of the ground motion. For this study, the bedrock mass density and shear wave velocity, 2.8 g/cm^3 and 3.52 km/s respectively, from Catchings (1999), also utilized by Romero and Rix (2001), are used.

Atkinson and Boore (1995) propose a two-corner source model where the values of the two corner frequencies depend on earthquake magnitude. The empirical Atkinson and Boore (1995) model better characterizes the frequency content of intraplate earthquakes

in the range of one to 10 Hz. The empirical earthquake data used to relate the locations of the two corner frequencies have magnitudes ranging from four to seven. Because the magnitudes relevant to the calculations in this study are larger than four to seven, the Brune model is assumed for the source spectrum with a stress drop of 150 bars instead of the empirical two-corner frequency model from Atkinson and Boore (1995).

The source to site attenuation term consists of an anelastic (or inelastic) attenuation term and a geometric spreading term. The anelastic diminution is the reduction in amplitude and frequency due to intrinsic losses as the seismic waves travel through the bedrock, characterized using a rock quality factor, *Q(f)*, as a function of frequency. The rock quality factor used herein is recommended by Atkinson and Boore (1995) for eastern North America:

$$Q(f) = 680 f^{0.36} \tag{41}$$

The geometric spreading term, $D_g(R)$, is the reduction in amplitude as the seismic waves travel further from the source. It is a function of hypocentral distance and is characterized by Atkinson and Boore (1995) as follows:

$$\begin{aligned} D_g(R) &= \frac{1}{R} && \text{for R<70 km} \\ D_g(R) &= \frac{1}{70} && \text{for } 70 \le \text{R} \le 130 \text{ km} \\ D_g(R) &= \frac{1}{70}\left(\frac{130}{R}\right)^{0.5} && \text{for R} \ge 130 \text{ km} \end{aligned} \tag{42}$$

The low-pass filter has a significant effect on the calculated value of a_{max} and is required to reduce the high frequency energy from the frequency spectrum calculated using the above source and path models. This reduction in amplitude of the higher frequencies could be an effect of the source or the site as discussed by Boore (2003) and Atkinson and Boore (1998). Atkinson and Boore (1995) recommend the f_{max} filter proposed by Hanks (1982). This filter removes frequencies above the specified cutoff frequency. The f_{max} filter is a fairly abrupt cutoff.

Another type of low pass filter, usually called a κ filter, is proposed by Anderson and Hough (1984). The *k* filter reduces the high-frequency energy by

$$P(f) = \exp(-\pi \kappa f) \tag{43}$$

where κ is the slope of the Fourier spectrum at high frequencies. Anderson and Hough (1984) propose that κ is a function of the site geology. Herrmann and Akinci (2000) recommend κ of 0.048 for soil sites in the Mississippi embayment, while Frankel et al. (1996 and 2002) use a κ of 0.01 for firm rock sites in Eastern North America in developing the US National Seismic Hazard Maps. The value of κ=0.01 from Frankel et al. (1996 and 2002) is based on measurements made in a firm rock profile in South Carolina. EPRI (1993) recommends κ=0.006 for hard rock profiles and κ=0.048 for soil

profiles. Romero and Rix (2001) use κ=0.02 for their NEHRP BC rock boundary analyses, κ=0.006 for their NEHRP Rock A (hard rock) analyses, and κ=0.048 for their soil site analyses.

The value of κ appears to increase with epicentral distance (Anderson and Hough 1984), but because the increase is small and dependent on the site properties it is often disregarded. Thus, the value of κ is usually assumed to be independent of epicentral distance and is assumed constant herein.

The earthquake source and path models only take into account the focal depth of the fault rupture by the relationship between hypocentral and epicentral distance. A focal depth of 8 km (Romero and Rix 2001) is used in this study.

The stochastic simulations of the earthquake source and path for this study are calculated for a hard rock (NEHRP Rock A) profile. Therefore, a value of κ=0.006 from EPRI (1993) is used in order to be consistent with the definition of a hard rock profile (Rock A) in Romero and Rix (2001). Figure 77 shows the variation of a_{max} for the hard rock profile as a function of distance and magnitude developed herein as calculated using SMSIM and the input parameters described above.

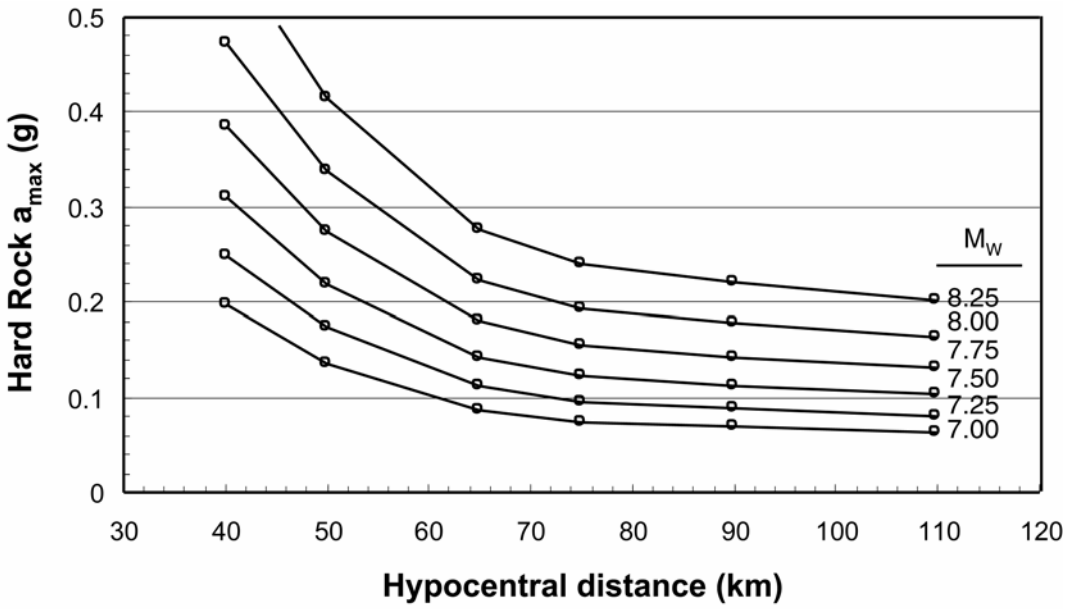

Figure 55. Variation of a_{max} with distance for varying magnitudes calculated using SMSIM for the Hard Rock profile used by Romero and Rix (2001)

Site Response Analysis

A one-dimensional site response analysis is used to analyze the vertical propagation of horizontal shear waves through a horizontally layered soil deposit above the bedrock (see Figure 54). This analysis is necessary to determine how the seismic waves will be affected (attenuated or amplified) as they travel vertically through the soft, nonlinear soil deposits in the upper Missippi embayment.

Romero and Rix (2001) describe a detailed study on dynamic soil properties and site response in the upper Mississippi embayment. They present extensive data on soil shear wave velocity, V_s, measured using seismic cone penetration tests (SCPT), seismic refraction surveys, and crosshole wave travel tests in a variety of locations in and around Memphis. Using this data, Romero and Rix present representative soil profiles for use in their site response analyses. They performed statistical analyses to quantify the variability in the material properties for the soil profiles. Based on the statistical study, Romero and Rix (2001) randomized the soil profiles and dynamic material properties. In addition to material properties, Romero and Rix (2001) studied the effects that the various seismological parameters described in the previous section have on the site response and ground motions. They discuss in detail the various effects that the input parameters have on the Fourier amplitude spectra and response spectra of the ground motions. For paleoliquefaction and liquefaction analyses, the main parameter of interest is the peak ground acceleration, a_{max}, and thus it is the parameter studied in the site response analyses.

The soil profiles developed and studied by Romero and Rix (2001) can be divided into two groups based on their age: Holocene deposits and Pleistocene deposits. Holocene deposits are the most recent, generally being found in the modern alluvial plains of rivers in the region. Pleistocene deposits are older and are generally found in the terrace zones between rivers in Tennessee. Figure 56 and Figure 57 show the distribution of the surficial deposits in the upper Mississippi embayment and in the Memphis area, respectively.

From the V_s data collected, Romero and Rix (2001) developed generic regional profiles and site-specific soil profiles. Two generic profiles for the NMSZ area are presented by Romero and Rix (2001) and correspond to an uplands profile and a lowlands profile. The uplands profile consists mainly of older Pleistocene deposits that tend to be stiffer and more variable than the Holocene soils. The lowlands profile corresponds to the Mississippi River floodplain in Arkansas and Tennessee as well as the alluvial plains of the regional tributary rivers in Tennessee, making it most relevant to the Wolf River paleoliquefaction site as well as the paleoliquefaction sites in the NMSZ. The lowlands profile consists of younger Holocene deposits. In general, the soils in the lowlands deposits are more coarse-grained than the uplands profile.

A number of site-specific profiles were developed for Holocene-aged soils by Romero and Rix (2001). Two of these profiles are used in their site-response analyses. The first site-specific profile (referred to as H-WR) was compiled from shear wave velocity measurements in the Wolf River alluvial plain. The second profile was compiled from measurements taken in the Tennessee portion of the Mississippi River flood plain and is referred to as H-TN. The average shear wave velocity in the upper 30 meters of each of these profiles is on the order of 200-250 m/s (Romero and Rix 2001).

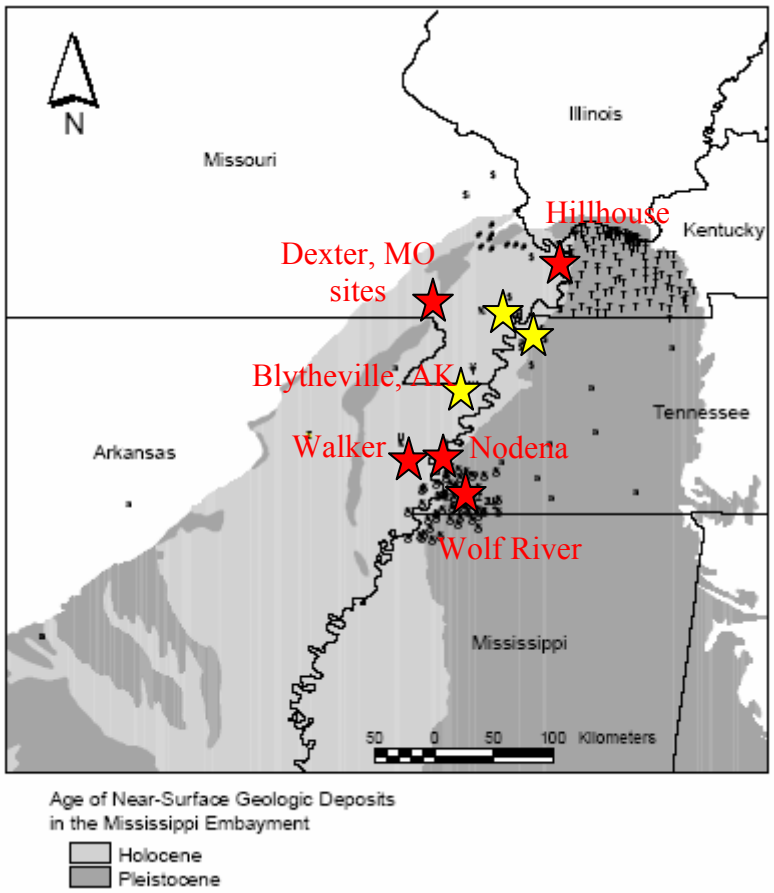

Figure 56. Map showing distribution and age of surface deposits in the upper Mississippi embayment (from Romero and Rix 2001), the locations of the paleoliquefaction sites examined in this study, and the epicenters listed in Table 1

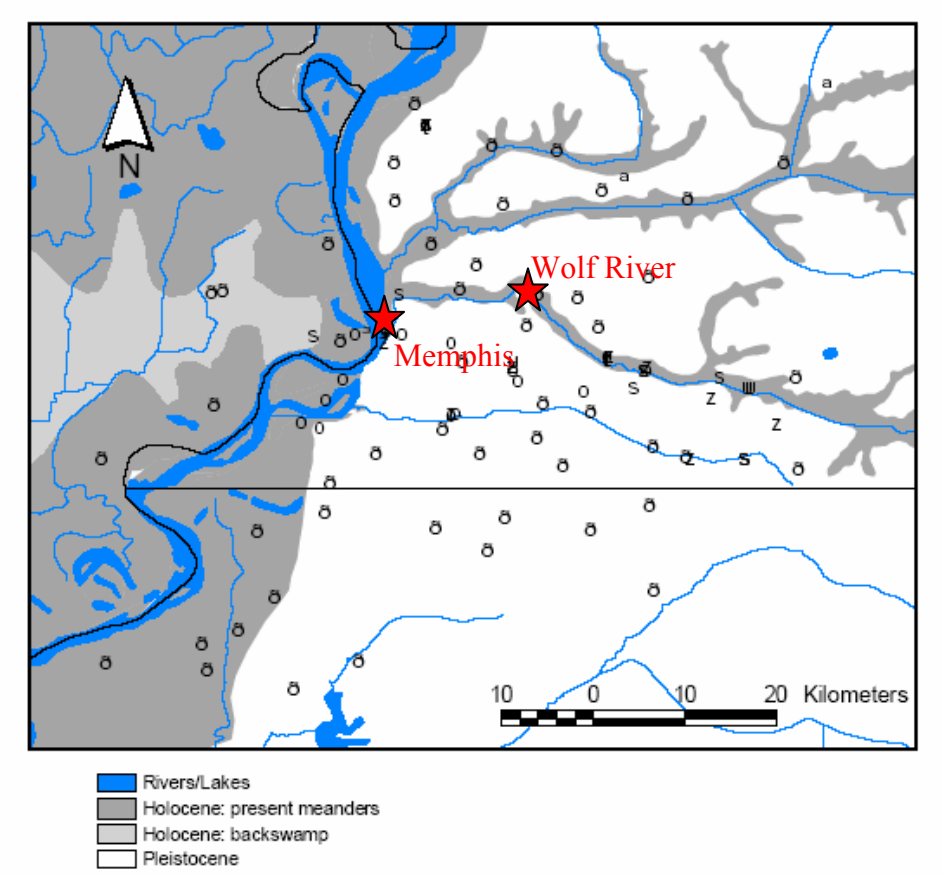

Figure 57. Map showing age of surficial deposits in and around Memphis (from Romero and Rix 2001) and the location of the Wolf River paleoliquefaction site

The site response analyses performed by Romero and Rix (2001) were conducted using SMSIM (Boore 1996) to generate ground motions and RASCALS (Silva and Lee 1987), to perform the site response analysis. RASCALS performs one-dimensional site response analyses in the frequency domain using an equivalent linear soil model. Equivalent linear material properties from EPRI (1993) are used to model the soil behavior. Equivalent linear modulus reduction and damping relationships from EPRI (1993) are used to a depth of 150 m. The damping in the remainder of the soil column was captured through the use of the parameter κ=0.048 (for soil sites) in the low pass filter term of the ground motion model. The EPRI material properties are only defined to a depth of 305 m. Below that depth, EPRI (1993) does not present any material property data. Thus, the dynamic material properties used for the materials below a depth of 305 m correspond to the lowest (most linear) shear modulus degradation relationship available (at a depth of 305 m) and the damping is accounted for using a value of κ=0.048 in the low-pass filter (Romero and Rix 2001).

The location of the Wolf River marginal liquefaction site and the NMSZ liquefaction sites are plotted on a map in Figure 58 showing contours of embayment depth. The southernmost paleoliquefaction sites considered herein are located between embayment

depths of 600 and 900 meters, while the northernmost near Dexter, MO is located near 300 m.

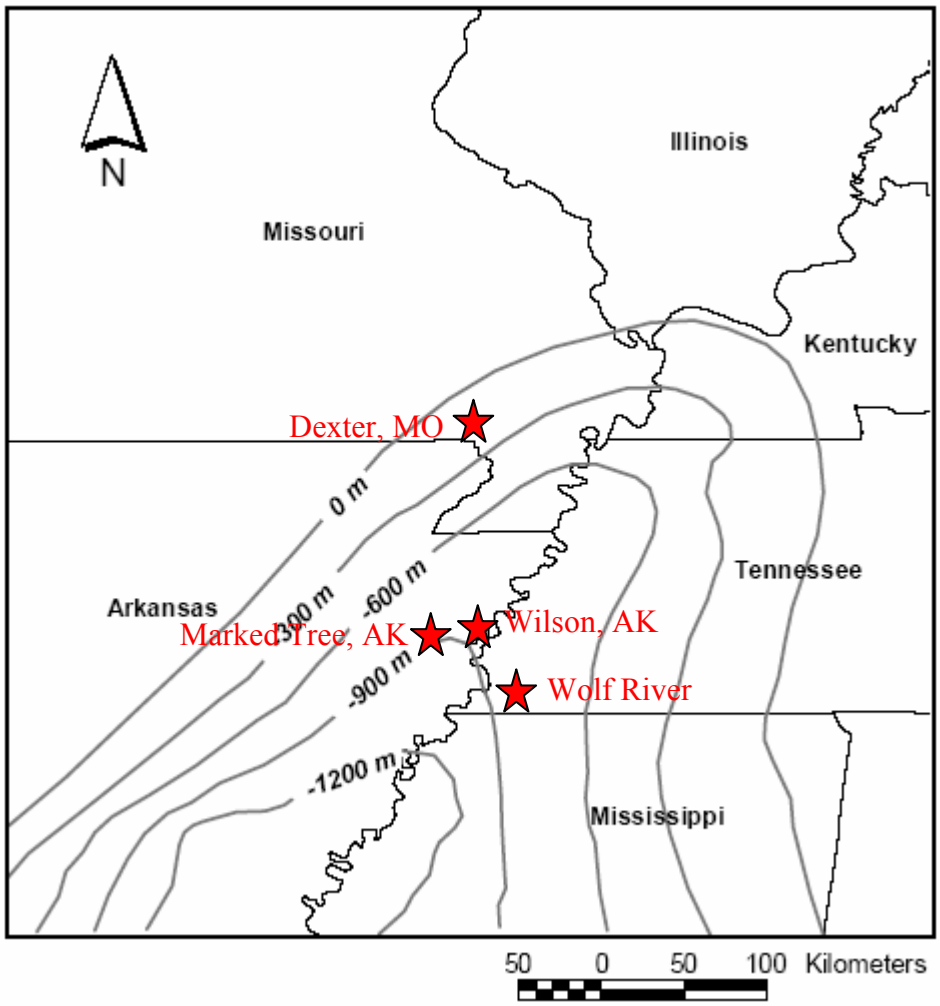

Figure 58. Map showing the depth of the upper Mississippi Embayment (from Romero and Rix 2001) and the locations of the paleoliquefaction sites examined in this study

Paleoliquefaction Site Amplification Factors

Table 10 presents median peak ground accelerations (PGAs) calculated by Romero and Rix (2001) for the soil profiles and seismological parameters relevant to this study and described previously. The last column presents the amplification factors calculated by dividing the median PGA for a soil profile by the median PGA for the hard rock profile of the same hypocentral distance, magnitude, and stress drop. Similar to the soil amplification factors proposed by EPRI (1993), soil amplification factors for the upper Mississippi embayment as a function of the hard rock a_{max} are used in the paleoliquefaction back analysis. Representing the soil amplification as a function of the hard rock a_{max} allows the nonlinearity of the dynamic soil properties to be characterized in the selection of an amplification factor. The dynamic behavior of the soil deposits in the upper Mississippi embayment is such that at larger shear strains, it exhibits lower stiffness and higher damping as a result of the larger strains. The magnitude of the hard

rock a_{max} is an indicator of the strain level in the soil column and therefore also indicates the degree of nonlinearity and damping that can be expected in the soil response.

Figure 59 presents the site amplification factors calculate in Table 10 plotted as a function of the hard rock PGA used to calculate each amplification factor. Scenarios from Romero and Rix (2001) included in Table 10 are: embayment depths of 100m, 600m, and 1000m, moment magnitudes of 5.5, 6.5, 7.5, and 8; stress drops of 110 bars and 150 bars; and the soil profiles representative of the lowlands, the H-TN, and the H-WR soil profiles. The relationship between the logarithm of hard rock PGA and the soil amplification factor is nearly linear.

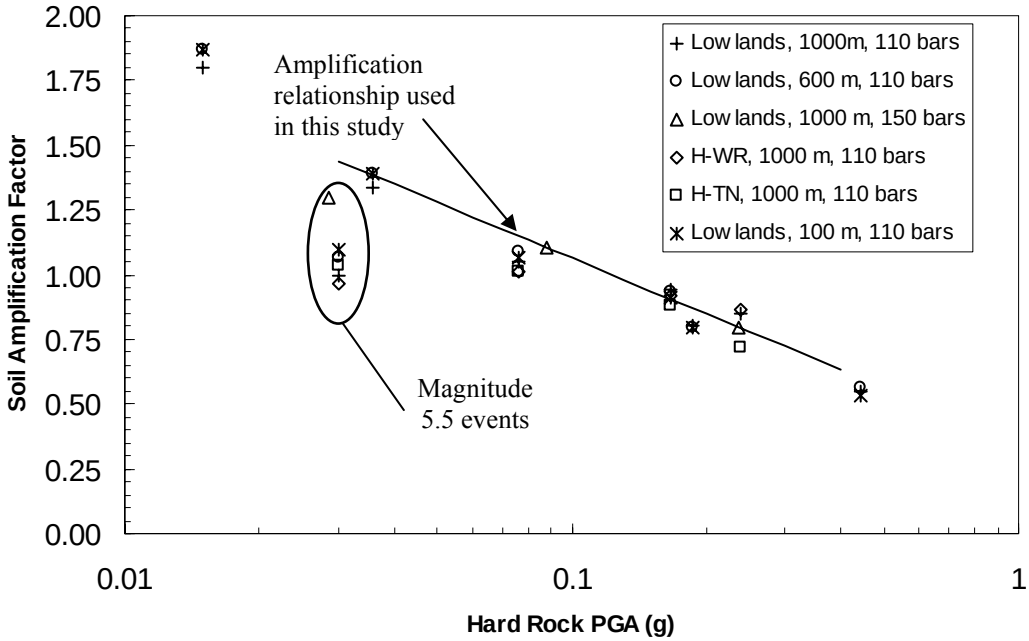

Figure 59. Relationship between hard rock PGA and soil amplification factor using data from Romero and Rix (2001)

The site amplification factors that plot at or above the trend line in Figure 59 correspond to magnitudes 7.5 or 8, or a stress drop of 150 bars. The amplification factors plotting towards below the trend line are for magnitude 6.5 earthquakes and a stress drop of 110 bars. The amplification factors for magnitude 5.5 earthquakes plot well below the rest of the data. As will be shown below, magnitudes in the 7-8 range are more relevant for this study than those in the 5.5-6.5 range and the relevant rock accelerations are in the range of 0.10 - 0.20 g. Thus, the relationship used to calculate amplification factors from hard rock values of a_{max} is drawn through the upper range of the data plotted in Figure 59. A flowchart illustrating the steps taken in calculating soil accelerations, rock accelerations, and the soil amplification factor is shown in Figure 61.

Figure 60 shows the variation of PGA with distance and magnitude calculated for the three Holocene soil profiles soil profile. These relationships are developed using the hard rock accelerations calculated and presented in Figure 77 and multiplying these accelerations by the appropriate soil amplification factor from Figure 59. These

relationships represent the PGA experienced by a Holocene soil profile located at various hypocentral distances for earthquakes with magnitudes greater than 7.

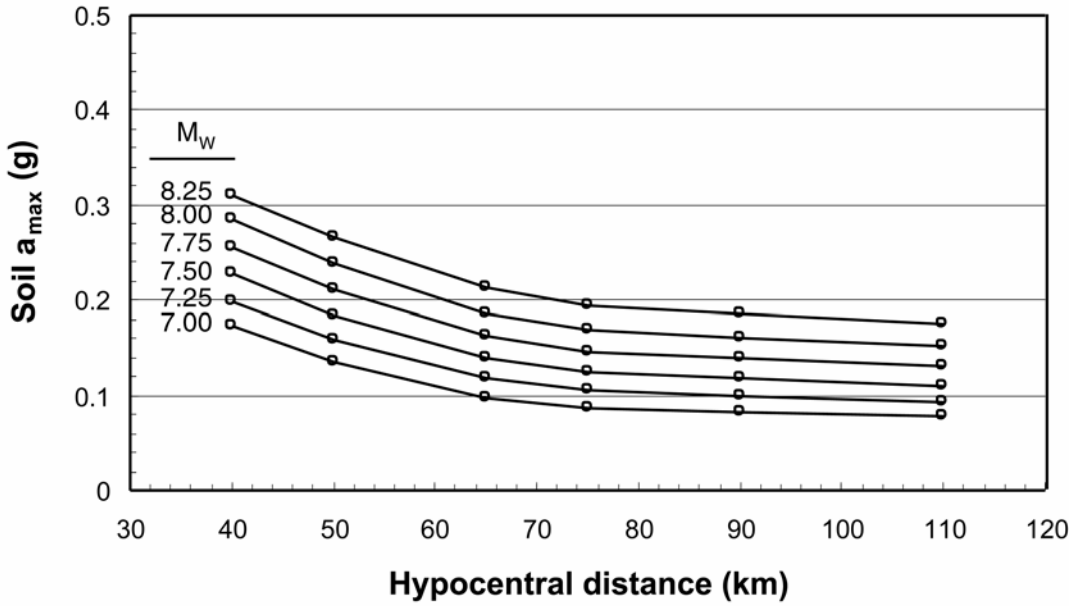

Figure 60. Variation of soil PGA with hypocentral distance using amplification factors calculated from Romero and Rix (2001) site response analyses

Table 10. Median accelerations for scenarios studied by Romero and Rix (2001)

Profile	Depth (m)	$\Delta\sigma$ (bars)	M_W	Hypocentral Distance (km)	Median PGA (g)	Amplification Factor**
Hard Rock (A)	0	110	5.5	50	0.030	-
			7.5	50	0.167	-
			8	50	0.238	-
			6.5	10	0.444	-
			6.5	25	0.186	-
			6.5	50	0.076	-
			6.5	100	0.036	-
			6.5	200	0.015	-
Hard Rock (A)	0	150	5.5	50	0.027*	-
			6.5	50	0.088*	-
			7.5	50	0.236*	-
Lowlands	100	110	5.5	50	0.033	1.10
			7.5	50	0.152	0.91
			8	50	0.238	0.54
			6.5	10	0.148	0.80
			6.5	25	0.081	1.07
			6.5	50	0.05	1.39
			6.5	100	0.028	1.87
			6.5	200	0.033	1.10
Lowlands	600	110	5.5	50	0.032	1.07
			7.5	50	0.156	0.93
			6.5	10	0.249	0.56
			6.5	25	0.148	0.80
			6.5	50	0.083	1.09
			6.5	100	0.050	1.39
			6.5	200	0.028	1.87
Lowlands	1000	110	5.5	50	0.030	1.00
			7.5	50	0.157	0.94
			8	50	0.203	0.85
			6.5	10	0.245	0.55
			6.5	25	0.149	0.80
			6.5	50	0.080	1.05
			6.5	100	0.048	1.33
			6.5	200	0.027	1.80
Lowlands	1000	150	5.5	50	0.037	1.29
			6.5	50	0.097	1.11
			7.5	50	0.188	0.80
H-WR	1000	110	5.5	50	0.029	0.97
			6.5	50	0.077	1.01
			7.5	50	0.154	0.92
			8.0	50	0.205	0.86
H-TN	1000	110	5.5	50	0.031	1.03
			6.5	50	0.077	1.01
			7.5	50	0.167	0.88
			8.0	50	0.238	0.72

* Values calculated using the source, path, and hard rock site model of Romero and Rix (2001).

** Median PGA divided by the Hard Rock (A) median PGA.

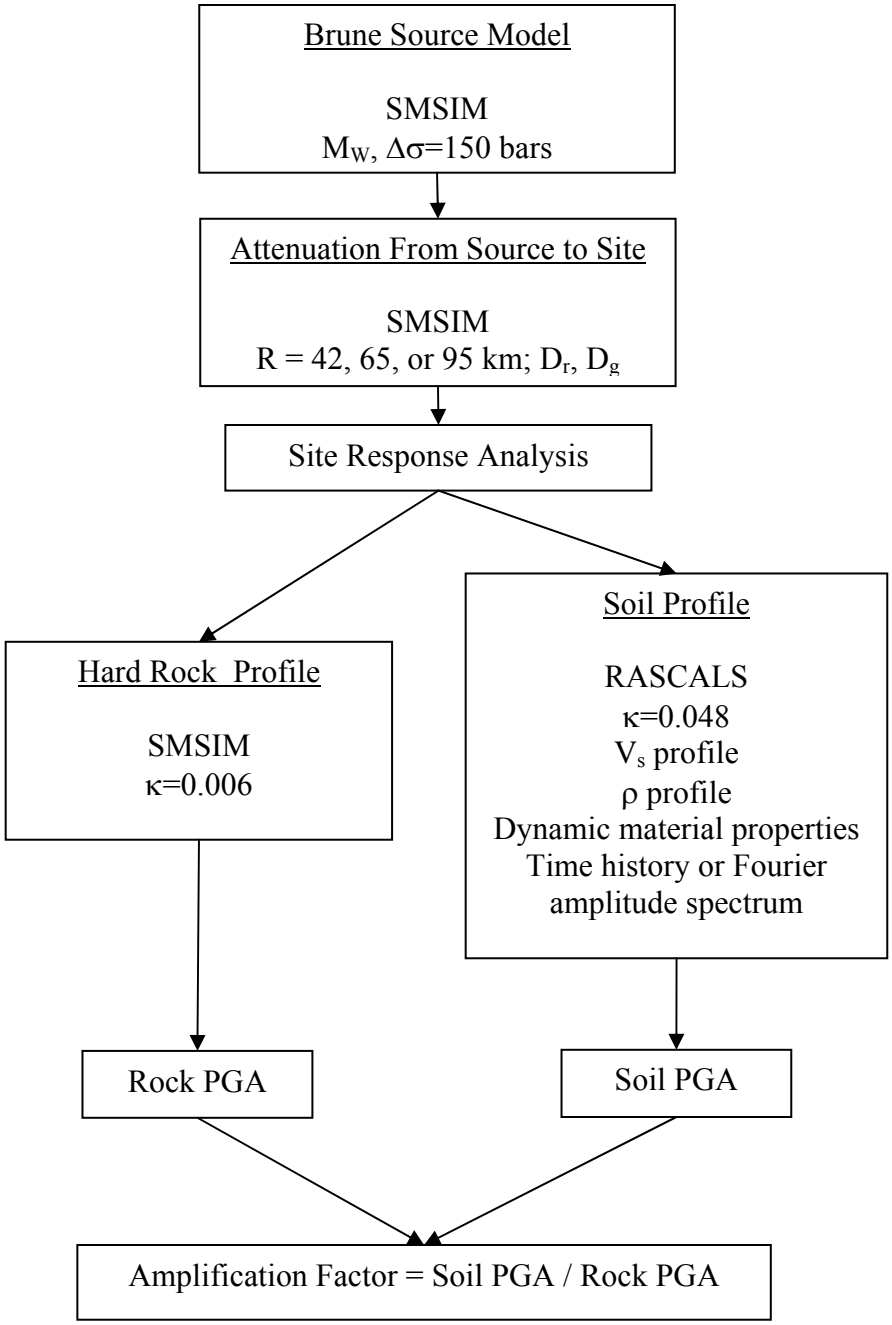

Figure 61. Flowchart showing steps in calculation of amplification factors for analysis of paleoliquefaction sites

Magnitude Back-Calculated at Wolf River

Because the earthquake Magnitude Scaling Factor (MSF) is the only parameter used to adjust the seismic stress ratio from the simplified procedure for varying magnitudes, it can be used with the results of the attenuation and site response analyses directly. Figure 62 presents the relationship between peak ground acceleration and magnitude necessary to cause liquefaction at Wolf6 (solid line). This relationship was obtained by multiplying the acceleration back-calculated for M_W=7.5 by the appropriate magnitude scaling factors.

To determine which combination of magnitude and acceleration occurred to cause the liquefaction feature at Wolf6, the results of the attenuation and site response analyses at an epicentral distance of 95 km are plotted in Figure 62 (broken line). The magnitude and acceleration where the results of the paleoliquefaction back-analysis and the results of the attenuation and site response analyses are equal represents the magnitude and resulting peak ground acceleration that occurred to cause the marginal liquefaction at Wolf6.

An a_{max} of 0.18 g was back-calculated previously at Wolf6 assuming a magnitude of 7.5 and no soil aging. Figure 62 suggests that a magnitude larger than 7.5 is necessary to yield a peak ground acceleration of 0.18 g at a hypocentral distance of 95 km, thus the assumed magnitude of 7.5 is incorrect. Figure 62 shows that a magnitude 7.9 earthquake yielding a peak ground acceleration of 0.15 g is in agreement with the attenuation and site response analyses and sufficient to cause marginal liquefaction at Wolf6.

The effect that the strength gain in a soil deposit with time might have is illustrated during the simplified procedure back-analysis. An increase of 20% in q_c was found to result in a reduction of the back-calculated acceleration from 0.18 g to 0.15 g for Wolf 6, assuming a magnitude of 7.5. Comparing these results with the accelerations calculated using site response and attenuation models as above yields a magnitude 7.7 earthquake and a peak ground acceleration of 0.14 as being necessary to cause liquefaction at Wolf6. The reduction in the back-calculated magnitude from 7.9 without aging to 7.7 with only a small gain in strength due to aging illustrates that soil aging can have a significant effect on the interpretation and back-analysis of ground shaking at paleoliquefaction sites.

As with the Simplified Procedure, the results from the back-analysis using the Energy Procedure can be compared with the results of the attenuation and site response analyses to determine what magnitude earthquake was necessary to cause liquefaction at a site. Figure 64 and Figure 65 show the back-analysis results for Wolf4 using the Simplified Procedure and the Energy Procedure, respectively. Using the Simplified Procedure a magnitude of 8.4 and acceleration of 0.20 g are back-calculated to cause liquefaction while a magnitude of approximately 8.6 and acceleration o 0.23 g are back-calculated using the Energy Procedure.

For an upper bound on magnitude based on measurements at the Wolf River site at Wolf4, the back-calculated a_{max} of 0.27 g assuming a magnitude 7.5 earthquake with no soil aging is examined. Plotting the acceleration and MSF relationship with the results of the attenuation and site response analyses as in Figure 64 shows a magnitude of 8.4 and a

peak ground acceleration of 0.20 g is necessary to cause liquefaction at Wolf4 without considering soil aging. Using the Energy Procedure a magnitude of approximately 8.6 and an acceleration of 0.23 g is necessary to cause liquefaction at Wolf4 disregarding soil aging. Because Wolf4 is a no liquefaction site, these results are upper bounds on the ground shaking experienced at Wolf4.

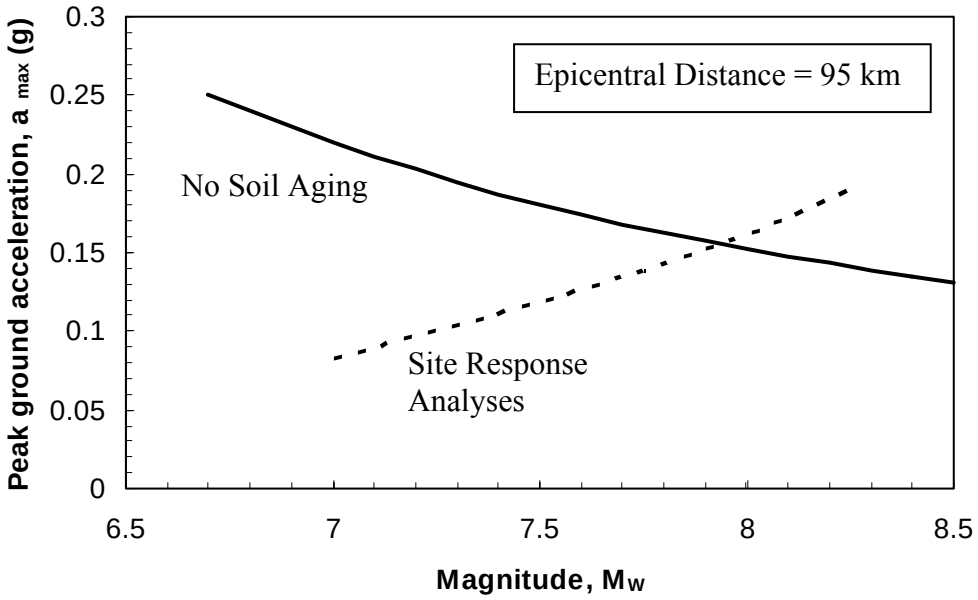

Figure 62. Relationship between peak ground acceleration and magnitude necessary to cause liquefaction at Wolf6 using the simplified procedure and disregarding soil aging (solid line) and peak ground acceleration and magnitude calculated from attenuation and site response analyses (broken line)

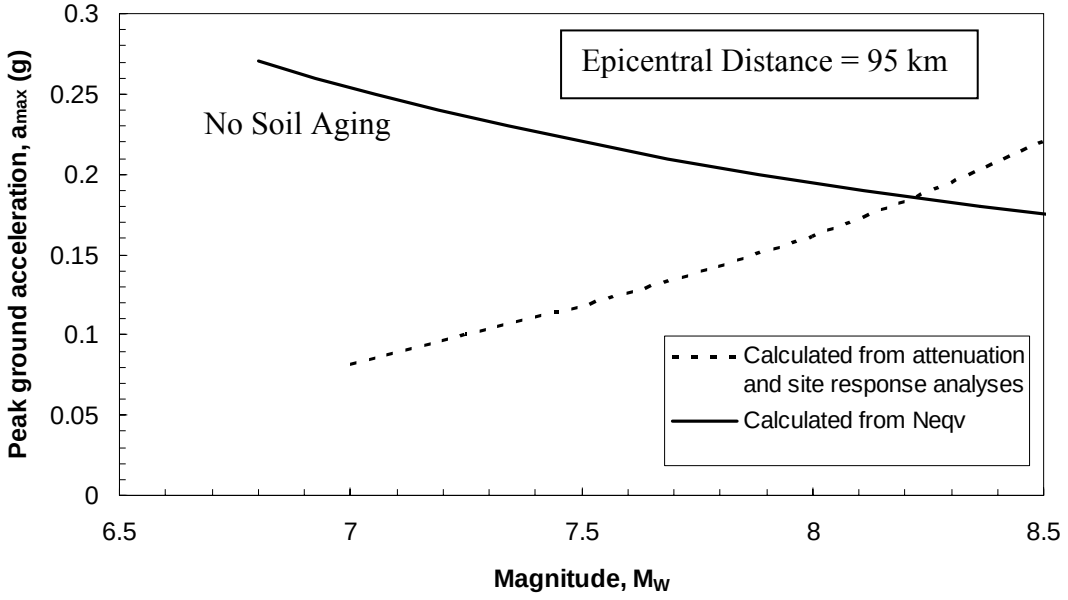

Figure 63. Relationship between peak ground acceleration and magnitude necessary to cause liquefaction at Wolf6 using the Energy Procedure and disregarding soil aging (solid line) and peak ground acceleration and magnitude calculated from attenuation and site response analyses (broken line)

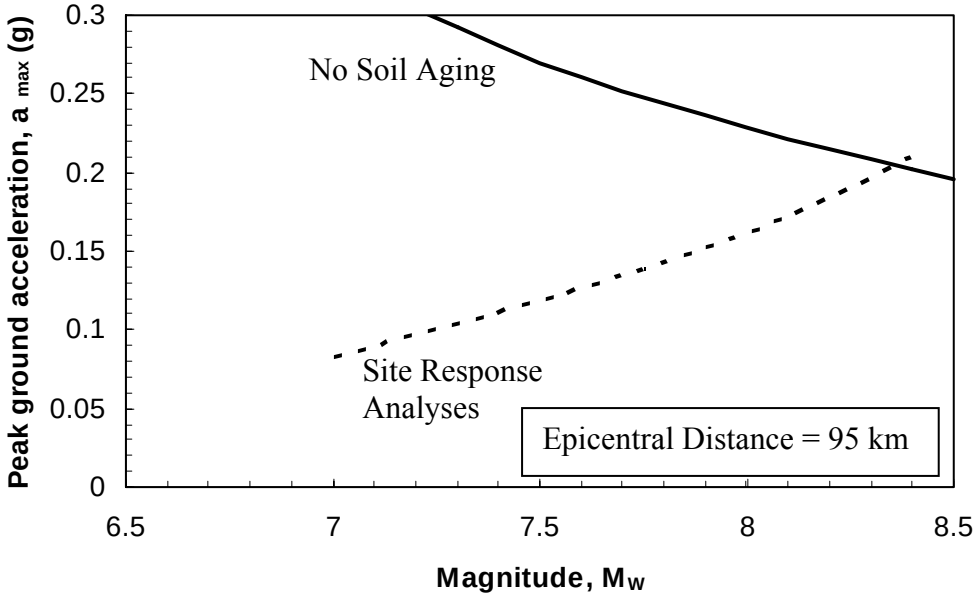

Figure 64. Relationship between peak ground acceleration and necessary to cause liquefaction at Wolf4 using the simplified procedure and disregarding soil aging (solid line) and peak ground acceleration and magnitude calculated from attenuation and site response analyses (broken line)

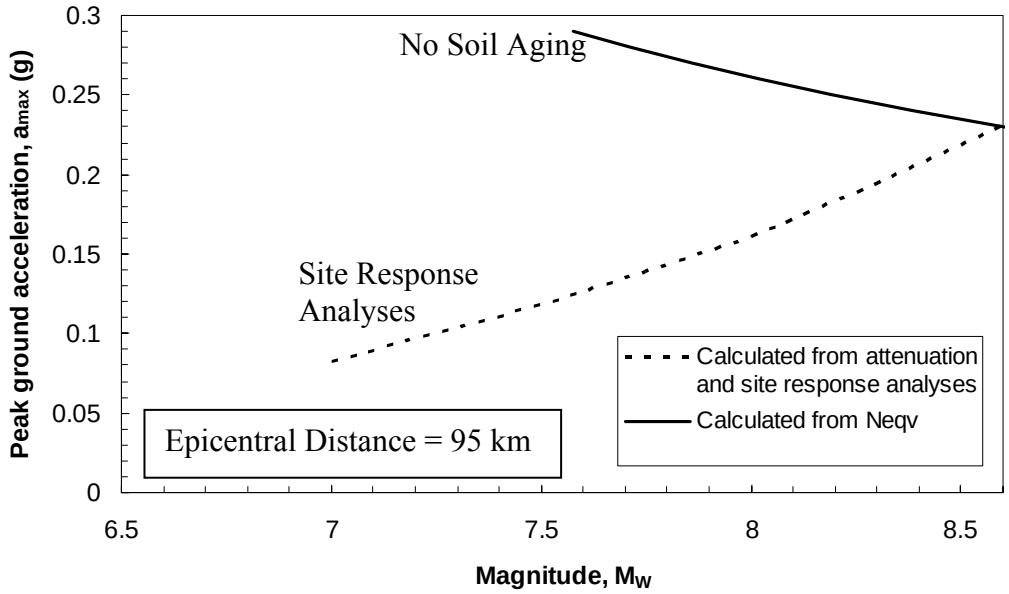

Figure 65. Relationship between peak ground acceleration and magnitude necessary to cause liquefaction at Wolf4 using the Energy Procedure and disregarding soil aging (solid line) and peak ground acceleration and magnitude calculated from attenuation and site response analyses (broken line)

Magnitude Back-Calculated in NMSZ

For the Walker Farm site in Marked Tree, AK, a hypocentral distance of 65 km and the triggering acceleration of 0.18 g correspond to an assumed magnitude of 7.5. Plotting the accelerations adjusted using the magnitude scaling factors and the results of the attenuation and site response analyses as performed for the Wolf River sites above suggests a magnitude of 7.8 and a peak ground acceleration of 0.16 are necessary to cause liquefaction at Mtree11 using the Simplified Procedure, while the Energy Procedure yields a magnitude of 8.1 and an acceleration of 0.19 g (see Figure 66 and Figure 67). Because the Walker Farm site is a site of severe liquefaction, the back-calculated a_{max} and magnitude for the initiation of liquefaction is a lower bound on the ground motion experienced at the site to cause the severe liquefaction features.

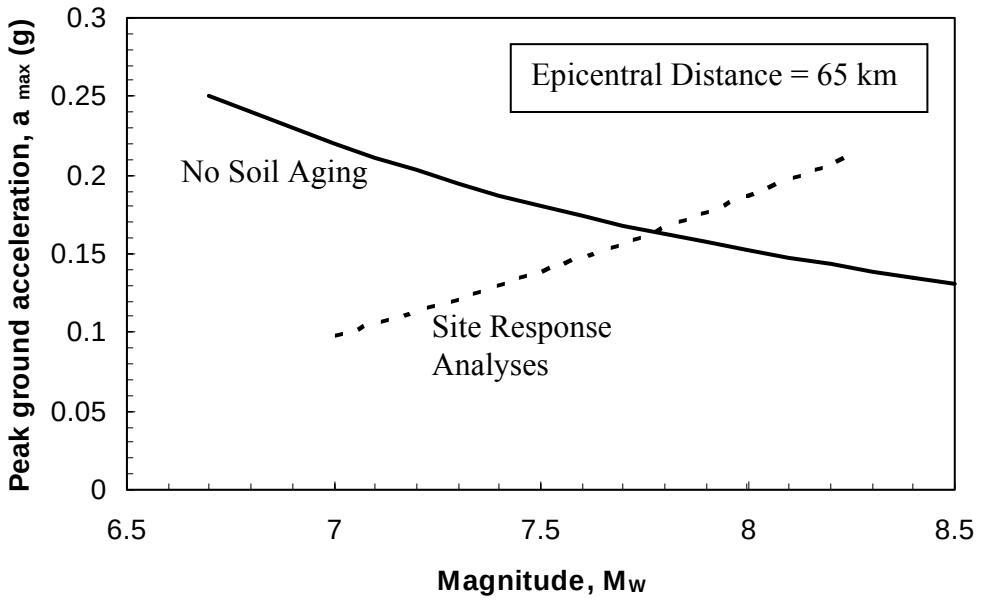

Figure 66. Relationship between peak ground acceleration and magnitude necessary to cause liquefaction at Mtree11 using the Simplified Procedure and disregarding soil aging (solid line) and peak ground acceleration and magnitude calculated from attenuation and site response analyses (broken line)

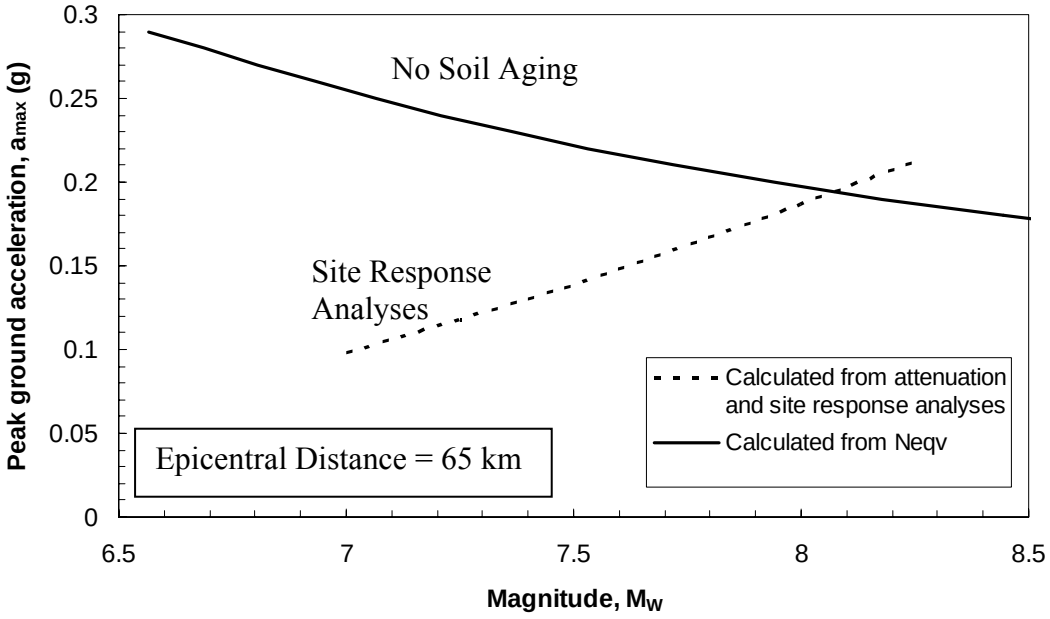

Figure 67. Relationship between peak ground acceleration and magnitude necessary to cause liquefaction at Mtree11 using the Energy Procedure and disregarding soil aging (solid line) and peak ground acceleration and magnitude calculated from attenuation and site response analyses (broken line)

For the Nodena Farm site in Wilson, AK, at an epicentral distance of 42 km, the triggering acceleration of 0.21 g corresponds to an assumed magnitude of 7.5 using the Simplified Procedure. Using the Simplified Procedure and the results of the attenuation and site response analyses, a magnitude of 7.4 and acceleration of 0.22 g is necessary to cause liquefaction at Wils02. A magnitude of 7.6 and an acceleration of 0.24 are necessary to cause liquefaction at Wils02 using the Energy Procedure. Because this site is a site of severe liquefaction, the back-calculated a_{max} and magnitude for the initiation of liquefaction is a lower bound on the ground motion experienced at the site.

The Dexter, MO site is located further north than the sites examined previously. It is located 45 km from the Blytheville epicenter, but only 30 km from the northernmost (Sikeston, MO) epicenter. The accelerations back-calculated earlier for this site are similar to those at the other NMSZ sites. Because of the proximity of the epicenters, the magnitude required to cause liquefaction at that site cannot be calculated as reliably as the other sites. The same uncertainty exists for the Hillhouse Farms site located further to the northwest (see Figure 56).

Table 11 presents a summary of the earthquake magnitudes back-calculated to trigger liquefaction at the paleoliquefaction sites examined in this study. Currently, the Simplified Procedure probably provides a better estimate of the ground shaking at liquefaction sites than the energy-based method developed herein. The regional attenuation behavior used in developing N_{eqv} from Green (2001) is a factor in the back-analysis that requires further study. The magnitude scaling factors used in the simplified procedure also were not developed for the NMSZ, but have received more scrutiny in other regions since their initial development. Despite the larger magnitudes estimated using the Energy Procedure, the relative magnitudes are still in agreement with the observations at each site, i.e., the no liquefaction site yields the largest back-calculated magnitude while the sites of full liquefaction yield the lowest. As a result, it is anticipated that the Energy Procedure will yield better estimates of earthquake magnitudes than the Simplified Procedure after the effects of deeper soil profiles and regional attenuation relationships on N_{eqv} are clarified in subsequent research.

Table 11. Summary of back-calculated a_{max} and M_W values required to trigger liquefaction at paleoliquefaction sites

Test Site	Description	Ground Motion Estimate	Simplified Procedure		Energy Procedure	
			a_{max}	M_W	a_{max}	M_W
Mtree11	Full Liquefaction	Lower Bound	0.16	7.8	0.19	8.1
Wils02	Full Liquefaction	Lower Bound	0.22	7.4	0.24	7.6
Wolf6	Marginal Liquefaction	Best Estimate	0.15	7.9	0.18	8.2
Wolf4	No Liquefaction	Upper Bound	0.20	8.4	0.30	8.6

The back-analysis of the marginal liquefaction site, Wolf6, provides the best estimate of earthquake magnitude. Using the Simplified Procedure and disregarding soil aging, a magnitude of 7.9 is back-calculated to have triggered the observed liquefaction (see Table 11). The effect of soil aging on the back-analysis can be significant as illustrated earlier in reducing the back-calculated magnitude from 7.9 to 7.7 assuming a 20% gain in strength since 1811-1812. All of the accelerations and magnitudes in Table 11 should be treated as overestimates because of the uncertainty in the change in q_c with time and soil aging.

In addition to soil aging, the depth of the ground water surface in 1811 or earlier in the NMSZ and the Wolf River are conservatively estimated to be 3 m. There is evidence to suggest that the ground water surface may have shallower than 3 m (Penick 1976), especially in the NMSZ. Penick (1976) suggests the ground water surface was at or near the ground surface in 1811-1812. A shallower ground water surface results in lower back-calculated magnitudes for the full liquefaction sites in the NMSZ (Wils02 and Mtree11) in Table 11 because of the reduced effective stresses.

Given the uncertainties in the back-analysis of the paleoliquefaction sites shown in Table 11, it is likely that the magnitude back-calculated to have caused the paleoliquefaction features is lower than the 7.9 value shown in Table 11 for Wolf6 and lower than the upper bounds estimated for Wolf4 in Table 11. The lower bounds calculated for older paleoliquefaction sites in the NMSZ are in agreement with these results as well.

SUMMARY

Liquefaction features preserved in the geologic record can provide important evidence regarding the magnitude of earthquakes that occurred before the advent of scientific measuring instruments. This study presents a methodology for analyzing cone penetration data measured at sites of full, marginal, and no liquefaction to determine the characteristics of the earthquake shaking that caused the observed liquefaction features.

Marginal liquefaction features represent the threshold where the earthquake driving forces are essentially equal to the soil resisting strength. At the Wolf River test site near Memphis, marginal liquefaction features are exposed in river banks that allow locations to be identified for penetration testing to estimate the resistance to liquefaction of the soil.

To accurately analyze a site of paleoliquefaction, it is necessary to determine the in situ condition of the soil just prior to the earthquake event that caused the liquefaction (Olson, Obermeier, and Stark 2001). A number of factors that contribute to changes in soil strength over time are examined and some are found to be significant. Recommendations are presented herein for quantifying soil strength changes due to aging and changes in the water table since the occurrence of the earthquakes. The soil aging adjustment has a high degree of uncertainty and is the main uncertainty in the magnitudes back-calculated for each site.

The CPT liquefaction case history database used by Olson and Stark (1998) is updated herein to add data from recent earthquakes as well as to quantify the criteria used for

including and excluding case histories from the database. The resulting database is used to develop new stress-based liquefaction potential relationships that can be used to perform back analyses on sites of paleoliquefaction and for liquefaction assessment.

The Simplified Procedure is used to determine the value of maximum acceleration that caused marginal liquefaction using penetration resistance data measured at each site. At the Wolf River marginal liquefaction test site, the back-calculated value of a_{max} ranges from 0.15 to 0.20 with no soil aging effects taken into consideration. At sites of full liquefaction north and west of Memphis in the New Madrid Seismic Zone, back-calculated accelerations without soil aging range from 0.16 to 0.21. These accelerations are lower bounds on the earthquake shaking that caused the severe liquefaction features at the sites.

To correlate the back-calculated accelerations for a paleoliquefaction site to the earthquake that had to occur to induce the liquefaction, the earthquake source, path, and site effects are modeled. The seismological and geotechnical parameters chosen in this analysis can also have a significant effect on the back-calculated magnitudes and accelerations. The effect of NMSZ soil profiles are taken into account through the use of site amplification factors developed from site response analyses performed by Romero and Rix (2001) for a range of seismological and geotechnical scenarios in the upper Mississippi embayment. The magnitudes necessary to cause liquefaction at the sites in this study range from 7.4 to 8.4 disregarding soil aging effects based on the Simplified Liquefaction Evaluation Procedure.

Because the sites in the NMSZ are dated to events older than the 1811-1812 earthquakes, they should be treated as lower bounds on historical seismicity for the region in general, not for the 1811-1812 earthquakes. Also because of the increased age of the soils at these sites, the effect of any adjustments made for soil aging will be larger at these sites than at younger sites dated to 1811-1812.

Energy-based approaches to paleoliquefaction assessment may be more appropriate than the Simplified Procedure. A method of estimating liquefaction potential based on the energy dissipated in the soil during ground shaking derived from Green (2001) is presented using the updated CPT liquefaction database and applied to paleoliquefaction sites. This method allows site-specific soil behavior to be quantified in both the capacity of the soil to resist liquefaction and the demand placed on the soil by an earthquake. Using this method, magnitudes necessary to cause liquefaction at the sites examined range from 7.6 to 8.6, disregarding soil aging. These magnitudes are higher than the magnitudes back-calculated using the Simplified Procedure because of the regional attenuation and soil profiles used by Green (2001) in developing the N_{eqv} parameter for the Energy Method.

RECOMMENDATIONS FOR FUTURE RESEARCH

Several issues identified during this study deserve further research to accurately quantify their effect on paleoliquefaction back-analyses in the New Madrid Seismic Zone.

First, a better understanding of soil aging effects on penetration testing and liquefaction resistance is critically needed. The soil aging effects in paleoliquefaction back-analyses could be studied by examining modern liquefaction cases where cone penetration testing is conducted at intervals years or decades after the liquefaction occurred. The new aging adjustments should then be used to re-interpret the paleoliquefaction sites considered herein.

Second, the effect that bedrock attenuation and the deep soil deposits in the Mississippi embayment have on the magnitude scaling factors in the Simplified Procedure and N_{eqv} in the energy-based method should be quantified. In particular, a new relationship for N_{eqv} should be developed for the NMSZ, which is a topic of future research of the authors. Green (2004) is currently developing a new N_{eqv} relationship for the Central and Eastern United States that may assist the back-analysis of paleoliquefaction sites. However, the new relationship for N_{eqv} may still need to be revised to reflect the influence of deep soil profiles and soil constitutive behavior in the NMSZ. The back-calculated earthquake magnitudes can be reevaluated when the new relationship for N_{eqv} becomes available from Green (2004) and/or the ongoing studies of the authors.

Third, more liquefaction sites dated to the 1811-1812 earthquakes should be identified and studied. Marginal liquefaction or severe liquefaction sites at the greatest distances from the epicenters in the southern part of the NMSZ should be chosen when possible as these provide better estimates of ground motion than sites near the epicenters.

APPENDIX A

GRAIN SIZE DISTRIBUTION CURVES FOR WOLF RIVER LIQUEFACTION SITES

WOLF RIVER TEST SITES AA1, AA3, AA7, & CPT6

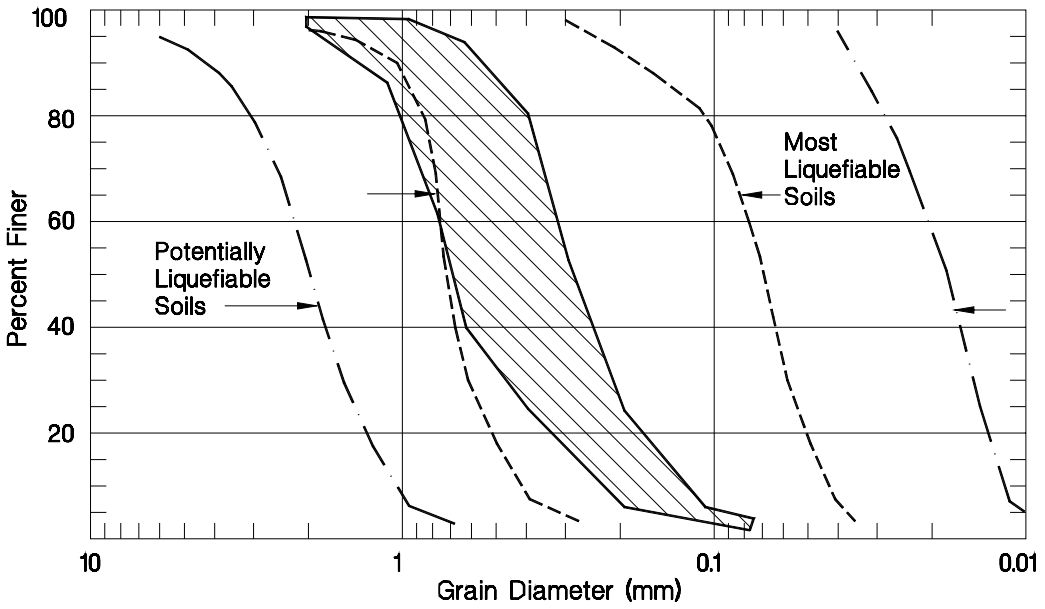

Figure A1. Grain size distribution curves for samples taken at Wolf River test site AA1

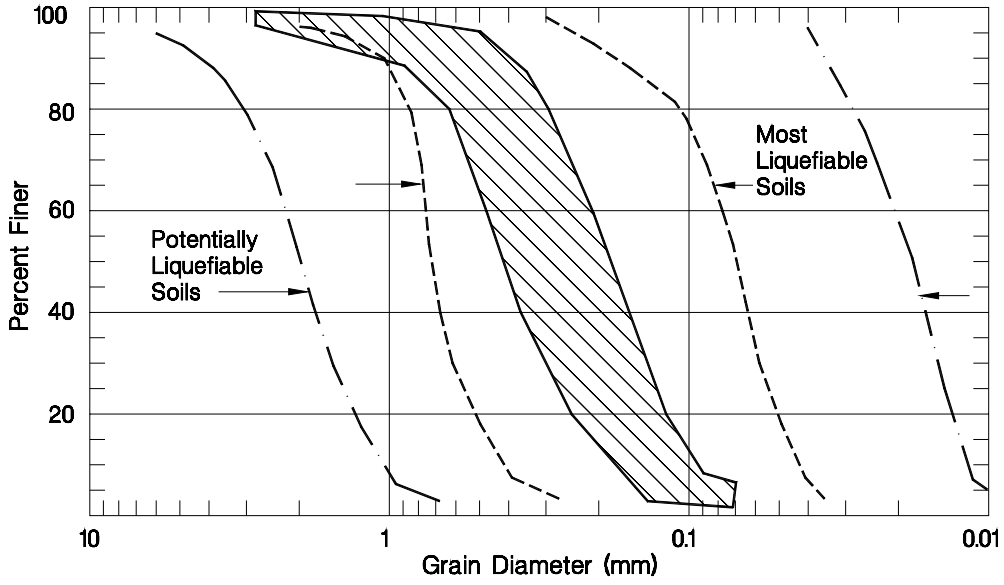

Figure A2. Grain size distribution curves for samples taken at Wolf River test site AA3

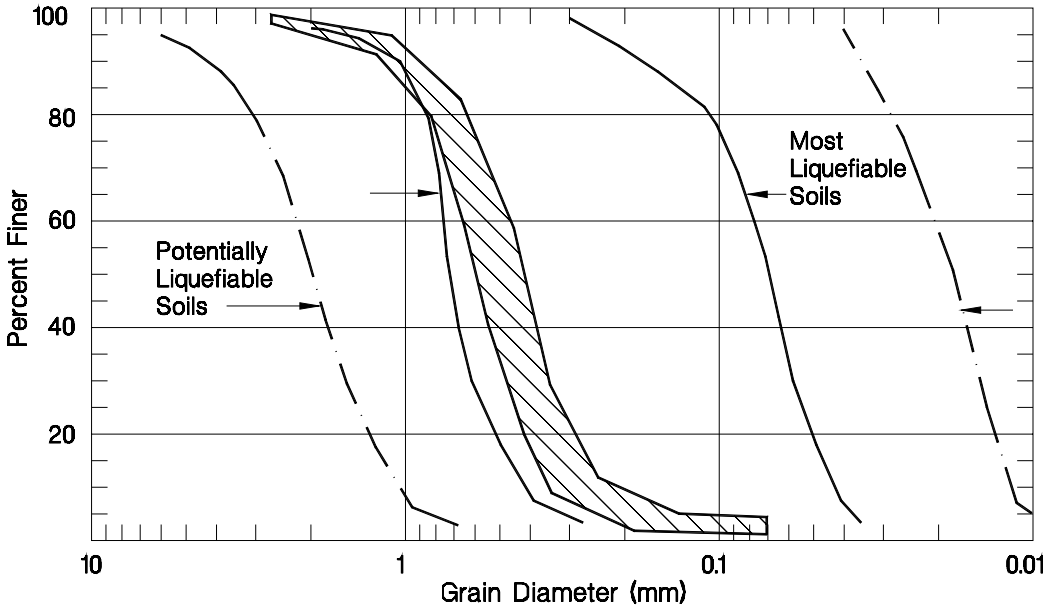

Figure A3. Grain size distribution curves for samples taken at Wolf River test site AA7

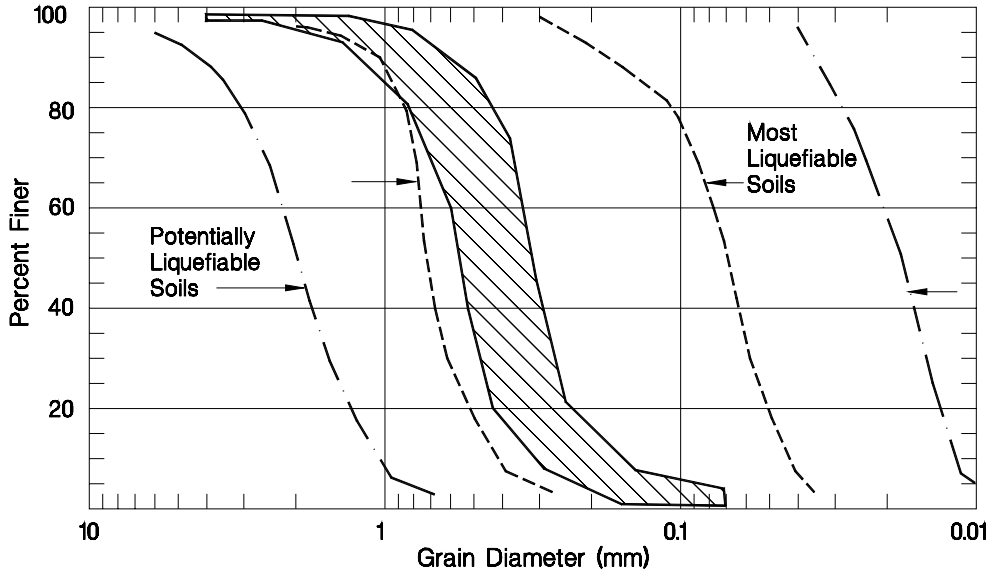

Figure A4. Grain size distribution curves for samples taken at Wolf River test site CPT6

APPENDIX B

LIQUEFACTION CASES UTILIZED IN DATABASE FOR CPT LIQUEFACTION POTENTIAL RELATIONSHIPS

Case No.	Year	Earthquake	Site	Boring	Magnitude	Epicentral Distance (km)	Reference
1	1964	Niigata	Kwagishi-Cho Building		7.5	56	Shibata and Teparaksa (1988)
2	1964	Niigata	South Bank		7.5	56	
3	1971	San Fernando Valley	Juvenile Hall	2-B1	6.4	12	Bennett (1989)
4	1971	San Fernando Valley	Juvenile Hall	4-B2	6.4	12	
5	1971	San Fernando Valley	Juvenile Hall	6-B1	6.4	12	
6	1971	San Fernando Valley	Juvenile Hall	10-B1	6.4	12	
7	1971	San Fernando Valley	Juvenile Hall	11-B1	6.4	12	
8	1975	Haicheng	chemical fiber		7.3	30	Arulanadan et al. (1986)
9	1975	Haicheng	Construction Building		7.3	30	
10	1975	Haicheng	Fishery and shipbuilding		7.3	30	
11	1975	Haicheng	Glass Fiber		7.3	30	
12	1975	Haicheng	Paper Mill		7.3	30	
13	1979	Imperial Valley	Heber Road	S2	6.6	8	Bennett et al. (1984) Youd and Bennett (1983)
14	1979	Imperial Valley	Kornbloom Road	K4	6.6	56	
15	1979	Imperial Valley	Radio Tower	R4	6.6	42	
16	1979	Imperial Valley	River Park	Unit C	6.6	38	
17	1979	Imperial Valley	Vail Canal	V2	6.6	51	
18	1981	Westmorland	Kornbloom Road	K4	6	4	
19	1981	Westmorland	Radio Tower	R4	6	12	
20	1981	Westmorland	Vail Canal	V2	6	6	
21	1988	Sanguenay	Ferland, Quebec		5.9	26	Tuttle el. al. (1990)
22	1989	Loma Prieta	Bay Farm Island	BFI-Dike	7.1	56	Bennett (1990) Boulanger et al. (1997) Mitchell et al. (1994)
23	1989	Loma Prieta	Clint Miller Farms	CMF 3	7.1	12	
24	1989	Loma Prieta	Clint Miller Farms	CMF 5	7.1	12	
25	1989	Loma Prieta	Clint Miller Farms	CMF 8	7.1	12	
26	1989	Loma Prieta	Clint Miller Farms	CMF 10	7.1	12	
27	1989	Loma Prieta	Farris	FAR 58	7.1	13	
28	1989	Loma Prieta	Granite Construction	GRA 123	7.1	12	
29	1989	Loma Prieta	Jefferson Ranch	JFF 32	7.1	29	

Case No.	Year	Earthquake	Site	Boring	Magnitude	Epicentral Distance (km)	Reference
30	1989	Loma Prieta	Jefferson Ranch	JFF 34	7.1	29	Bennett and Tinsley (1995)
31	1989	Loma Prieta	Kett	KET 74	7.1	11	
32	1989	Loma Prieta	Leonardini	LEN 37	7.1	31	
33	1989	Loma Prieta	Leonardini	LEN 39	7.1	31	
34	1989	Loma Prieta	Leonardini	LEN 51	7.1	28	
35	1989	Loma Prieta	Leonardini	LEN 52a	7.1	29	
36	1989	Loma Prieta	Leonardini	LEN 53	7.1	31	
37	1989	Loma Prieta	Marina District	MAR1	7.1	100	
38	1989	Loma Prieta	Marina District	MAR2	7.1	100	
39	1989	Loma Prieta	Marina District	MAR3	7.1	100	
40	1989	Loma Prieta	Marina District	MAR4	7.1	100	
41	1989	Loma Prieta	Marina District	MAR5	7.1	100	
42	1989	Loma Prieta	Marinovich	MRR 65	7.1	14	
43	1989	Loma Prieta	Marinovich	MRR 67	7.1	14	
44	1989	Loma Prieta	McGowan	MCG 138	7.1	14	
45	1989	Loma Prieta	Model Airport	AIR 18	7.1	14	
46	1989	Loma Prieta	Model Airport	AIR 21	7.1	14	
47	1989	Loma Prieta	Moss Landing, General Fish	CPT-5	7.1	30	
48	1989	Loma Prieta	Moss Landing, General Fish	CPT-6	7.1	30	
49	1989	Loma Prieta	Moss Landing, Harbor Office	UC-13	7.1	30	
50	1989	Loma Prieta	Moss Landing, Harbor Office	UC-20	7.1	30	
51	1989	Loma Prieta	Moss Landing, Marine Lab	C2	7.1	30	
52	1989	Loma Prieta	Moss Landing, Marine Lab	C3	7.1	30	
53	1989	Loma Prieta	Moss Landing, MBARI No. 3	RC-5	7.1	30	
54	1989	Loma Prieta	Moss Landing, MBARI No. 3	RC-6	7.1	30	
55	1989	Loma Prieta	Moss Landing, MBARI No. 3	RC-7	7.1	30	
56	1989	Loma Prieta	Moss Landing, MBARI No. 4	CPT-1	7.1	30	
57	1989	Loma Prieta	Moss Landing, MBARI No. 4	CPT-2	7.1	30	
58	1989	Loma Prieta	Moss Landing, MBARI No. 4	CPT-3	7.1	30	
59	1989	Loma Prieta	Moss Landing, MBARI No. 4	CPT-4	7.1	30	

Case No.	Year	Earthquake	Site	Boring	Magnitude	Epicentral Distance (km)	Reference
60	1989	Loma Prieta	Moss Landing, MBARI Technology	RD-9	7.1	30	
61	1989	Loma Prieta	Moss Landing, Sandholt Road	RC-1	7.1	30	
62	1989	Loma Prieta	Moss Landing, Sandholt Road	UC-2	7.1	30	
63	1989	Loma Prieta	Moss Landing, Sandholt Road	RC-4	7.1	30	
64	1989	Loma Prieta	Moss Landing, Sandholt Road	UC-6	7.1	30	
65	1989	Loma Prieta	Moss Landing, State Beach	UC-15	7.1	30	
66	1989	Loma Prieta	Moss Landing, State Beach	UC-17	7.1	30	
67	1989	Loma Prieta	Moss Landing, State Beach	UC-18	7.1	30	
68	1989	Loma Prieta	Moss Landing, Woodward Marine	UC-9	7.1	30	
69	1989	Loma Prieta	Moss Landing, Woodward Marine	UC-11	7.1	30	
70	1989	Loma Prieta	Moss Landing, Woodward Marine	15-A	7.1	30	
71	1989	Loma Prieta	Port of Oakland	POO7-3	7.1	69	
72	1989	Loma Prieta	Port of Oakland	POO7-4	7.1	69	
73	1989	Loma Prieta	Port of Richmond	POR2	7.1	88	
74	1989	Loma Prieta	Radovich	RAD 98	7.1	14	
75	1989	Loma Prieta	Salinas River Bridge	SRB 117	7.1	41	
76	1989	Loma Prieta	Scattini	SCA 23	7.1	25	
77	1989	Loma Prieta	Scattini	SCA 28	7.1	25	
78	1989	Loma Prieta	Sea Mist	SEA 31	7.1	27	
79	1989	Loma Prieta	SF-Oakland Bay Bridge	SFOBB1	7.1	72	
80	1989	Loma Prieta	SF-Oakland Bay Bridge	SFOBB2	7.1	72	
81	1989	Loma Prieta	Silliman	SIL 68	7.1	14	
82	1989	Loma Prieta	SPRR Bridge	SP 48	7.1	13	
83	1994	Northridge	Balboa Boulevard	BAL10	6.8	8	Bennett et al. (1998)
84	1994	Northridge	Malden Street	MAL14	6.8	1	
85	1994	Northridge	Wynn Avenue	WYNN5a	6.8	1	
86	1999	Chi-Chi	Nantou	NT-C15	7.6	12	Juang (2002)
87	1999	Chi-Chi	Nantou	NT-C7	7.6	12	Juang et al. (2003)
88	1999	Chi-Chi	Yuanlin	YL-C2	7.6	28	
89	1999	Chi-Chi	Yuanlin	YL-C19	7.6	22	

Case No.	Year	Earthquake	Site	Boring	Magnitude	Epicentral Distance (km)	Reference
90	1999	Chi-Chi	Yuanlin	YL-C22	7.6	24	
91	1999	Chi-Chi	Yuanlin	YL-C45	7.6	23	
92	1999	Chi-Chi	Yuanlin	YL-C15	7.6	23	
93	1999	Chi-Chi	Yuanlin	YL-C6	7.6	22	
94	1999	Chi-Chi	Yuanlin	YL-C16	7.6	23	
95	1999	Chi-Chi	Yuanlin	YL-C21	7.6	21	
96	1999	Chi-Chi	Yuanlin	YL-C22	7.6	21	
97	1999	Kocaeli	Adapazari	CPT 1-11	7.4	60	Bray et al. (2000)
98	1999	Kocaeli	Adapazari	CPT 1-6	7.4	60	
99	1999	Kocaeli	Adapazari	CPT 1-25	7.4	60	Youd et al. (2000)
100	1999	Kocaeli	Adapazari	CPT 1-33	7.4	60	
101	1999	Kocaeli	Adapazari	CPT 1-42	7.4	60	
102	1999	Kocaeli	Adapazari	CPT 2-3	7.4	60	
103	1999	Kocaeli	Adapazari	CPT 2-10	7.4	60	
104	1999	Kocaeli	Adapazari	CPT 3-3	7.4	60	
105	1999	Kocaeli	Adapazari	CPT 3-6	7.4	60	
106	1999	Kocaeli	Building Site B	CPT-B1	7.4	60	
107	1999	Kocaeli	Building Site C	CPT-C3	7.4	60	
108	1999	Kocaeli	Building Site D	CPT-D1	7.4	60	
109	1999	Kocaeli	Building Site E	CPT-E1	7.4	60	
110	1999	Kocaeli	Building Site F	CPT-F1	7.4	60	
111	1999	Kocaeli	Building Site G	CPT-G3	7.4	60	
112	1999	Kocaeli	Building Site H	CPT-H2	7.4	60	
113	1999	Kocaeli	Building Site I	CPT-I1	7.4	60	
114	1999	Kocaeli	Building Site J	CPT-J2	7.4	60	
115	1999	Kocaeli	Building Site L	CPT-L1	7.4	60	

APPENDIX C

DATABASE FOR CPT LIQUEFACTION POTENTIAL RELATIONSHIPS

Case No.	Liq?	Depth (m)	Ground Water Depth (m)	Vertical Total Stress (kPa)	Vertical Effective Stress (kPa)	Fines Content (%)	q_c (MPa)	q_{c1} (MPa)	a_{max} (g)	$SSR_{M=7.5}$	NED
1	y	4.60	1.1	82.8	48.5	5	1.6	2.2	0.16	0.171	0.0036
2	n	4.50	0.5	81.0	41.8	5	7.9	11.7	0.16	0.195	0.0023
3	y	9.00	6.5	162.0	137.5	50	3.9	3.3	0.50	0.224	0.0139
4	y	7.20	6.7	129.6	124.7	64	2.5	2.2	0.50	0.200	0.0110
5	y	4.60	4.3	82.8	79.9	74	1.1	1.3	0.50	0.204	0.0164
6	y	5.80	4.7	104.4	93.6	65	2.8	2.9	0.50	0.217	0.0129
7	y	6.30	5.9	113.4	109.5	61	2.8	2.7	0.50	0.201	0.0101
8	y	7.50	1.5	135.0	76.1	61	1.2	1.4	0.15	0.151	0.0021
9	y	7.00	1.5	126.0	72.0	83	0.4	0.5	0.15	0.149	0.0034
10	y	3.50	1.5	63.0	43.4	90	1.3	1.9	0.15	0.127	0.0008
11	y	3.00	1.5	54.0	39.3	42	0.5	0.8	0.15	0.121	0.0010
12	y	4.00	1.5	72.0	47.5	72	0.7	0.9	0.15	0.132	0.0014
13	y	4.00	2.1	72.0	53.4	18	1.8	2.4	0.60	0.350	0.0844
14	n	4.00	2.5	72.0	57.3	82	0.6	0.8	0.08	0.044	0.0001
15	n	2.70	2.0	48.6	41.7	98	5.5	8.2	0.18	0.092	0.0003
16	n	5.00	0.2	90.0	42.9	15	4.9	7.2	0.20	0.180	0.0035
17	n	4.30	3.5	77.4	69.6	6	6.5	7.9	0.13	0.062	0.0001
18	y	4.00	2.5	72.0	57.3	88	0.6	0.8	0.37	0.152	0.0118
19	n	2.50	2.0	45.0	40.1	98	5.5	8.3	0.29	0.108	0.0008
20	y	4.30	3.5	77.4	69.6	6	6.5	7.9	0.37	0.134	0.0023
21	y	4.50	1.8	81.0	54.5	15	2.8	3.7	0.25	0.115	0.0020
22	n	3.00	2.0	54.0	44.2	20	26.0	37.9	0.30	0.198	0.0017
23	y	7.00	5.7	126.0	113.2	22	3.5	3.3	0.53	0.308	0.0147
24	y	6.50	4.7	117.0	99.3	16	8.5	8.6	0.53	0.328	0.0108
25	y	5.75	4.9	103.5	95.2	17	8.4	8.7	0.53	0.304	0.0081
26	n	7.75	3.0	139.5	92.9	20	7.5	7.9	0.53	0.414	0.0292
27	y	6.00	4.8	108.0	96.2	2	9.9	10.2	0.54	0.319	0.0091
28	y	6.00	5.0	108.0	98.2	11	8.5	8.6	0.50	0.289	0.0068
29	y	3.25	1.8	58.5	44.3	5	3.1	4.5	0.28	0.201	0.0035

Case No.	Liq?	Depth (m)	Ground Water Depth (m)	Vertical Total Stress (kPa)	Vertical Effective Stress (kPa)	Fines Content (%)	q_c (MPa)	q_{c1} (MPa)	a_{max} (g)	$SSR_{M=7.5}$	NED
30	n	2.25	1.7	40.5	35.1	2	7.6	11.9	0.21	0.129	0.0004
31	y	2.75	1.5	49.5	37.2	15	6.4	9.9	0.69	0.498	0.0472
32	n	3.50	2.5	63.0	53.2	13	3.9	5.3	0.21	0.137	0.0010
33	y	3.50	1.9	63.0	47.3	11	3.0	4.3	0.21	0.154	0.0015
34	y	4.25	1.8	76.5	52.5	8	3.8	5.2	0.21	0.167	0.0018
35	n	3.25	2.7	58.5	53.1	12	3.9	5.3	0.21	0.127	0.0007
36	y	4.75	2.1	85.5	59.5	7	6.2	8.0	0.21	0.164	0.0016
37	n	5.80	2.3	104.4	70.1	5	16.8	20.2	0.24	0.189	0.0025
38	n	3.40	2.7	61.2	54.3	3	9.8	13.1	0.24	0.146	0.0011
39	n	6.90	2.7	124.2	83.0	4	13.0	14.5	0.24	0.188	0.0030
40	y	6.10	2.9	109.8	78.4	21	0.8	0.9	0.24	0.177	0.0091
41	y	6.40	2.4	115.2	76.0	3	1.2	1.4	0.24	0.192	0.0094
42	y	7.25	5.6	130.5	114.3	12	6.9	6.4	0.59	0.351	0.0177
43	n	6.25	6.2	112.5	112.0	15	14.2	13.4	0.59	0.311	0.0076
44	n	7.75	1.8	139.5	81.1	18	8.5	9.6	0.38	0.339	0.0120
45	y	4.25	2.4	76.5	58.4	10	5.7	7.5	0.38	0.267	0.0051
46	y	4.00	2.4	72.0	56.3	5	4.2	5.6	0.38	0.261	0.0054
47	y	2.10	1.5	37.8	31.9	4	2.5	4.0	0.25	0.161	0.0015
48	n	2.60	1.7	46.8	38.0	4	10.0	15.3	0.25	0.167	0.0009
49	y	4.10	1.9	73.8	52.2	15	5.8	7.9	0.25	0.189	0.0024
50	y	4.70	3.0	84.6	67.9	10	4.1	5.0	0.25	0.166	0.0021
51	y	9.80	2.2	176.4	101.8	27	3.8	3.8	0.25	0.219	0.0068
52	y	4.40	1.5	79.2	50.8	3	8.2	11.3	0.25	0.209	0.0028
53	n	3.50	1.8	63.0	46.3	1	15.5	22.2	0.25	0.183	0.0012
54	n	4.10	2.6	73.8	59.1	1	13.0	16.9	0.25	0.167	0.0011
55	n	4.70	3.7	84.6	74.8	1	9.2	10.8	0.25	0.151	0.0011
56	n	3.40	1.9	61.2	46.5	4	8.5	12.2	0.25	0.177	0.0015
57	n	2.50	1.8	45.0	38.1	4	10.4	15.9	0.25	0.160	0.0008
58	n	4.10	2.3	73.8	56.1	4	9.4	12.5	0.25	0.176	0.0015
59	n	1.90	1.5	34.2	30.3	4	8.4	13.8	0.25	0.154	0.0006

Case No.	Liq?	Depth (m)	Ground Water Depth (m)	Vertical Total Stress (kPa)	Vertical Effective Stress (kPa)	Fines Content (%)	q_c (MPa)	q_{c1} (MPa)	a_{max} (g)	$SSR_{M=7.5}$	NED
60	n	3.50	2.0	63.0	48.3	4	12.4	17.5	0.25	0.176	0.0012
61	y	1.40	1.4	25.2	25.2	4	3.0	5.1	0.25	0.137	0.0006
62	n	1.90	1.7	34.2	32.2	4	10.4	16.7	0.25	0.145	0.0005
63	y	5.00	1.8	90.0	58.6	1	9.0	11.8	0.25	0.204	0.0027
64	n	6.50	1.7	117.0	69.9	1	15.5	18.7	0.25	0.220	0.0030
65	y	3.00	1.8	54.0	42.2	1	3.0	4.4	0.25	0.173	0.0021
66	y	4.40	2.6	79.2	61.5	1	5.4	6.9	0.25	0.172	0.0020
67	n	4.00	3.4	72.0	66.1	1	16.4	20.3	0.25	0.146	0.0007
68	y	2.90	1.2	52.2	35.5	5	6.6	10.3	0.25	0.199	0.0020
69	y	2.20	1.0	39.6	27.8	15	3.1	5.2	0.25	0.194	0.0023
70	y	2.90	1.3	52.2	36.5	3	5.1	7.9	0.25	0.194	0.0021
71	y	4.00	3.0	72.0	62.2	5	6.5	8.3	0.29	0.180	0.0031
72	n	7.00	3.0	126.0	86.8	0	18.0	19.6	0.29	0.221	0.0046
73	y	5.00	2.5	90.0	65.5	57	1.7	2.1	0.16	0.117	0.0014
74	y	5.50	3.5	99.0	79.4	5	9.0	10.2	0.56	0.368	0.0156
75	n	7.50	6.4	135.0	124.2	10	3.3	2.9	0.16	0.090	0.0006
76	n	2.00	1.5	36.0	31.1	39	4.0	6.5	0.23	0.145	0.0006
77	y	2.75	1.2	49.6	34.3	2	4.9	7.7	0.23	0.180	0.0014
78	y	4.25	0.8	76.5	42.7	16	2.8	4.1	0.21	0.206	0.0036
79	y	5.50	3.0	99.0	74.5	13	5.1	6.0	0.29	0.204	0.0059
80	y	6.50	3.0	117.0	82.7	16	8.2	9.1	0.29	0.216	0.0060
81	y	6.25	3.5	112.5	85.5	15	4.3	4.7	0.57	0.392	0.0338
82	y	6.25	5.3	112.5	103.2	13	3.3	3.3	0.49	0.281	0.0104
83	y	8.50	7.2	153.0	140.2	23	7.3	6.0	0.84	0.418	0.0619
84	y	9.50	3.9	171.0	116.1	41	1.5	1.4	0.51	0.337	0.0649
85	y	6.50	4.3	117.0	95.4	6	13.2	13.6	0.51	0.290	0.0074
86	y	8.50	3.4	153.0	103.0	6	5.4	5.3	0.43	0.400	0.0143
87	y	6.00	5.0	108.0	98.2	25	6.2	6.3	0.43	0.302	0.0046
88	y	14.00	0.6	252.0	120.5	21	5.9	5.3	0.19	0.214	0.0026
89	y	11.00	0.8	198.0	97.9	13	3.9	4.0	0.19	0.227	0.0029

Case No.	Liq?	Depth (m)	Ground Water Depth (m)	Vertical Total Stress (kPa)	Vertical Effective Stress (kPa)	Fines Content (%)	q_c (MPa)	q_{c1} (MPa)	a_{max} (g)	$SSR_{M=7.5}$	NED
90	n	13.00	2.3	234.0	129.0	17	5.5	4.8	0.19	0.192	0.0017
91	n	4.00	2.3	72.0	55.3	19	2.9	3.9	0.19	0.161	0.0008
92	n	6.00	0.9	108.0	58.0	55	14.6	19.2	0.19	0.227	0.0012
93	n	6.00	1.8	108.0	66.8	90	2.1	2.6	0.19	0.197	0.0020
94	n	6.00	2.5	108.0	73.7	33	3.3	3.9	0.19	0.179	0.0013
95	n	7.50	2.5	135.0	86.0	14	6.1	6.7	0.19	0.189	0.0012
96	y	3.00	1.1	54.0	35.4	17	2.7	4.2	0.19	0.191	0.0010
97	n	6.60	2.4	118.8	77.6	20	10.4	12.0	0.40	0.363	0.0281
98	n	7.20	0.4	129.6	62.6	13	11.5	14.6	0.40	0.489	0.0767
99	n	7.00	2.6	126.0	82.8	17	17.7	19.7	0.40	0.360	0.0212
100	n	8.00	0.7	144.0	72.4	9	13.3	15.8	0.40	0.467	0.0627
101	n	8.00	0.6	144.0	71.4	9	19.9	23.8	0.40	0.473	0.0520
102	n	9.30	0.9	167.4	85.0	20	13.3	14.6	0.40	0.456	0.0610
103	n	8.00	0.8	144.0	73.4	20	16.8	19.8	0.40	0.461	0.0521
104	n	5.20	0.5	93.6	47.5	35	7.3	10.4	0.40	0.473	0.0770
105	n	5.80	1.2	104.4	59.3	35	5.2	6.8	0.40	0.421	0.0649
106	y	3.75	3.3	67.5	63.1	21	5.0	6.3	0.40	0.260	0.0108
107	y	6.25	1.0	112.5	61.0	5	3.7	4.7	0.40	0.439	0.1005
108	y	2.25	1.7	40.5	35.1	59	2.1	3.3	0.40	0.283	0.0167
109	y	1.75	0.3	31.5	17.3	2	2.2	4.1	0.40	0.450	0.0747
110	y	2.25	1.6	40.5	34.1	68	2.3	3.6	0.40	0.292	0.0176
111	y	2.00	0.7	36.0	23.2	69	1.7	3.0	0.40	0.381	0.0504
112	y	2.50	1.7	45.0	37.2	15	3.4	5.3	0.40	0.297	0.0158
113	y	3.00	0.8	54.0	31.9	61	2.0	3.2	0.40	0.413	0.0826
114	y	2.75	0.4	49.5	26.4	76	1.6	2.6	0.40	0.458	0.1526
115	y	2.50	0.7	45.0	27.3	74	1.7	2.9	0.40	0.404	0.0734

APPENDIX D

DENSIFICATION CAUSED BY LIQUEFACTION

Change in N Value

The Niigata earthquake of June 1964 caused the most significant damage due to ground liquefaction since the modern practice of geotechnical earthquake engineering was begun. Subsequent to this event, Japanese researchers conducted field and laboratory studies to try to understand and explain this phenomenon. In some studies, researchers collected sets of soil data that had been obtained prior to the earthquake and then returned to those same locations to measure the changes that had occurred (Kawakami and Asada (1966), Kishida (1966), Ohsaki (1966), and Watanabe (1966)). This same procedure was also used after the 1968 Tokachioki earthquake (Ohsaki (1970) and Kishida (1970)) and the 1978 Miyagiken-Oki earthquake (Ishihara et al. (1980)). Figure 68 compares the grain size distribution curves of the Niigata sands that liquefied to those of the sand samples taken from the Wolf River test sites. It can be seen that the two sands have similar grain size characteristics and that they both fall within the size range defined as most liquefiable by Ishihara et al. (1989). Figure 69 and Figure 70 show the comparison of grain size distribution curves for the Wolf River sand samples relative to the sands at the sites of the Tokachioki and Miyagiken-Oki earthquake studies, respectively, with similar comparison results.

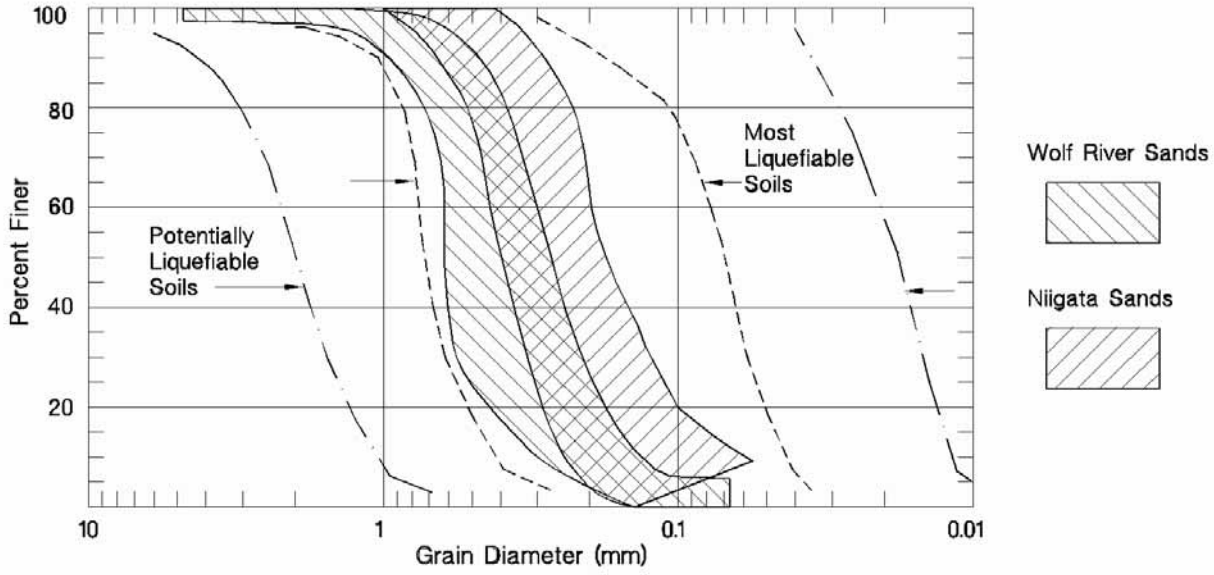

Figure 68. Comparison of grain size distribution curves for Niigata and Wolf River sands

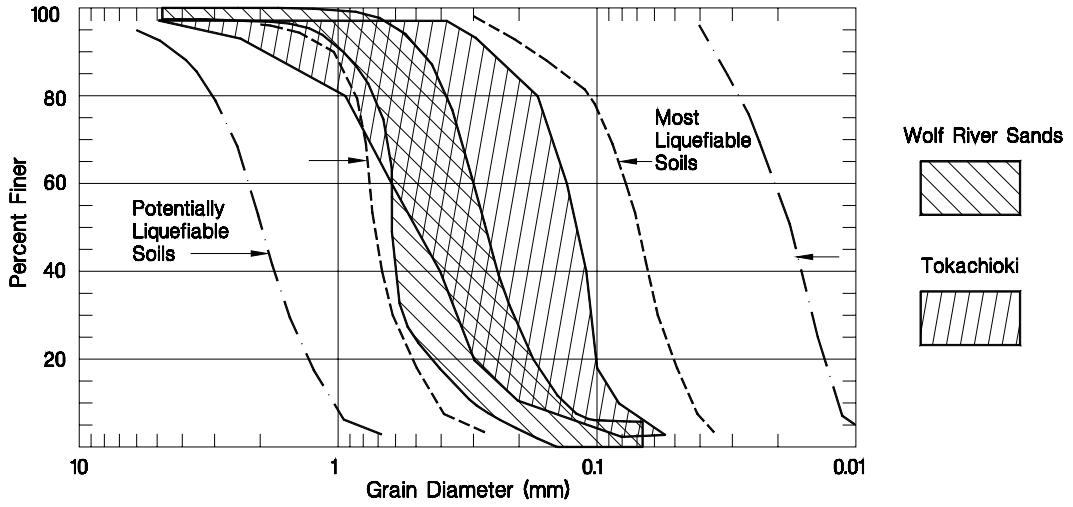

Figure 69. Comparison of grain size distribution curves for Tokachioki and Wolf River sands

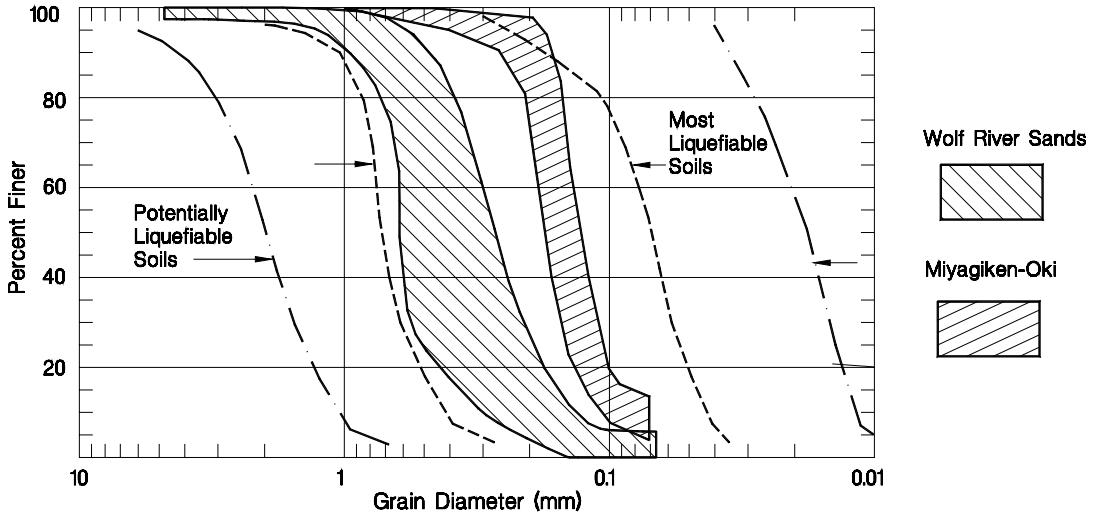

Figure 70. Comparison of grain size distribution curves for Miyagiken-Oki and Wolf River sands

Some of the data gathered by Japanese researchers before and after the earthquakes is in the form of Standard Penetration Test (SPT) N values, i.e. blows measured per foot. The SPT was the most common and accepted field test for measuring the strength of soil deposits at the time of the Niigata earthquakes. Plotting N values from sites of liquefaction before and after the earthquake events in the above cited references leads to the graph shown in Figure 71. Taken over the entire 15 m depth investigated, there

appears no clear trend to correlate the N values measured after the earthquakes with those measured before. (Note that depths less than 4 m are not used in the plotting because the ground water surface in Niigata is reported to be at a depth of about 2 m at the time of the shaking. This approach was used to ensure that all of the N values correspond to a saturated condition.) In addition, there is evidence to suggest that the liquefaction did not occur at a depth greater than 15 m and thus N values from depths greater than 15 m are not plotted. Kishida (1966) reports "The sand particles (sic) that came out from the ground during the earthquake were compared with sand particles that were obtained from boring samples. After many kinds of tests that checked grain size distribution, color, mineral texture, and roundness of sand particles, it was estimated that the sand at the depth of about 5-7 meters below the ground level came out during the earthquake at Niigata City (B.R.I. report p.160: 1965)." In addition, Koizumi (1966) writes "Sand eruption was observed at many places in the city during the earthquake. At a certain site some pumice was contained in the ejected sand. A boring was made at that site to take samples by spoon sampler at intervals of 1 m and comparisons were made between the ejected sands in relation to grain size, color, roundness of particles and mineral composition. (Tests were conducted by Dr. M. Ichikawa and Dr. I Cinema of Tokyo Educational University.) The comparison has led to the conclusion that the ejected sands originated only from 3 m to 9 m depth." With this in mind, it is reasonable to separate the data in Figure 71 between those points that represent the N values of sands at depths that liquefied (3 – 10 m) during the earthquake from N values of sands at depths that did not liquefy (10 – 15 m), in order to identify a consistent trend.

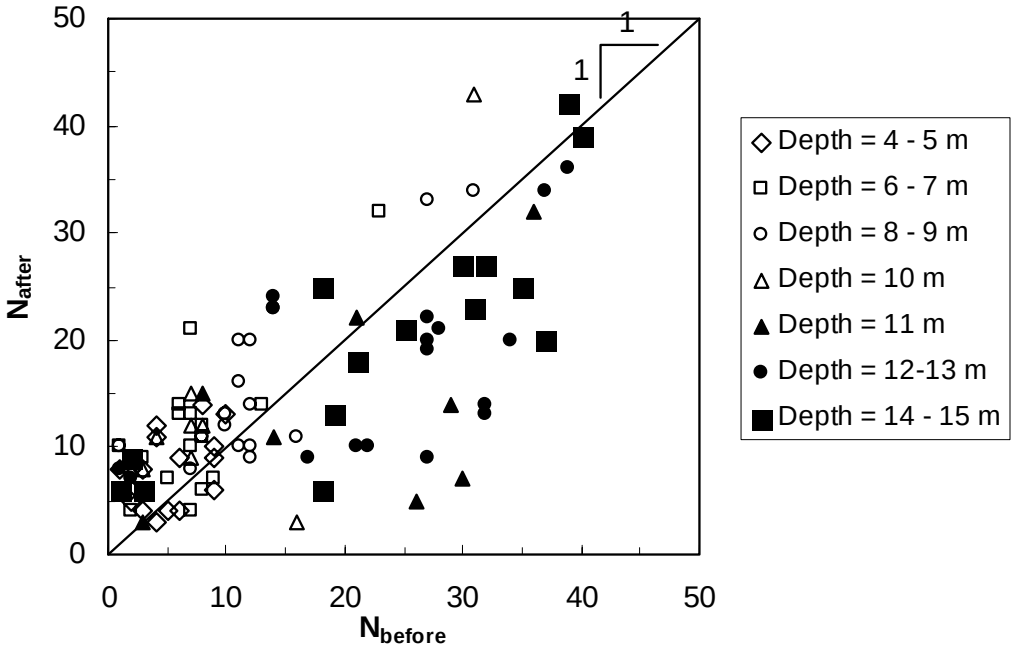

Figure 71. Change in Standard Penetration Test value, N, after the Niigata (1966), Tokachioki (1968), and Miyagiken-Oki (1978) earthquakes

Separating the data at an estimated depth of liquefaction of 10 m leads to the graphs in Figure 72 and Figure 73 below. Figure 72 shows that for depths greater than 10 m where the sands did not liquefy, the N values measured after the earthquake for the most part are less than those measured before, i.e. the sands have been loosened by the action of the earthquake. On the graph in Figure 73, the majority of the data for sands at depths equal to or shallower than 10 m where liquefaction did occur shows that the N value has increased after the soil liquefaction. These observations are in agreement with Koizumi (1966) who states, "Thus, sands which have increased their densities after the earthquake, were unstable during the earthquake, whereas sands which have decreased their densities were stable if the acceleration of the earthquake did not exceed a certain limit." Therefore, it can be stated that for sands that have undergone liquefaction, soil densification occurred as an after-effect of the liquefaction. To quantify the amount of this densification, a best-fit line for the data is plotted in Figure 73 and yields

$$N_{After} = 0.96\ N_{Before} + 3.8 \tag{44}$$

that is, there is an increase in N value of roughly four caused by densification induced by soil liquefaction.

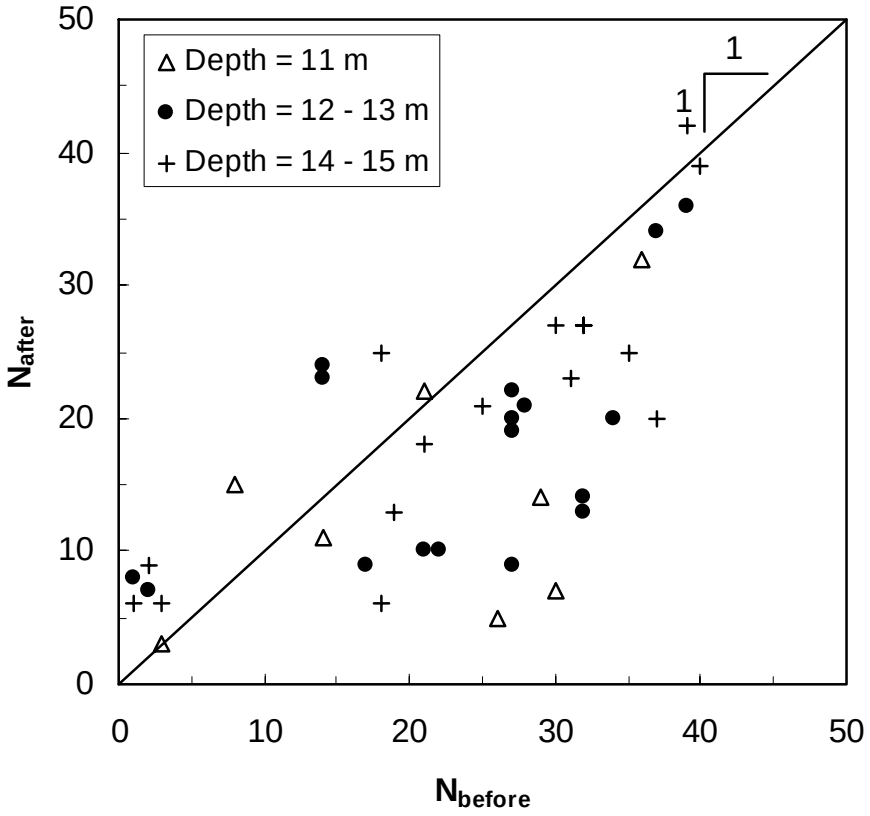

Figure 72. Change in N value due to Japanese earthquake shaking at non-liquefied depths (10 – 15 m)

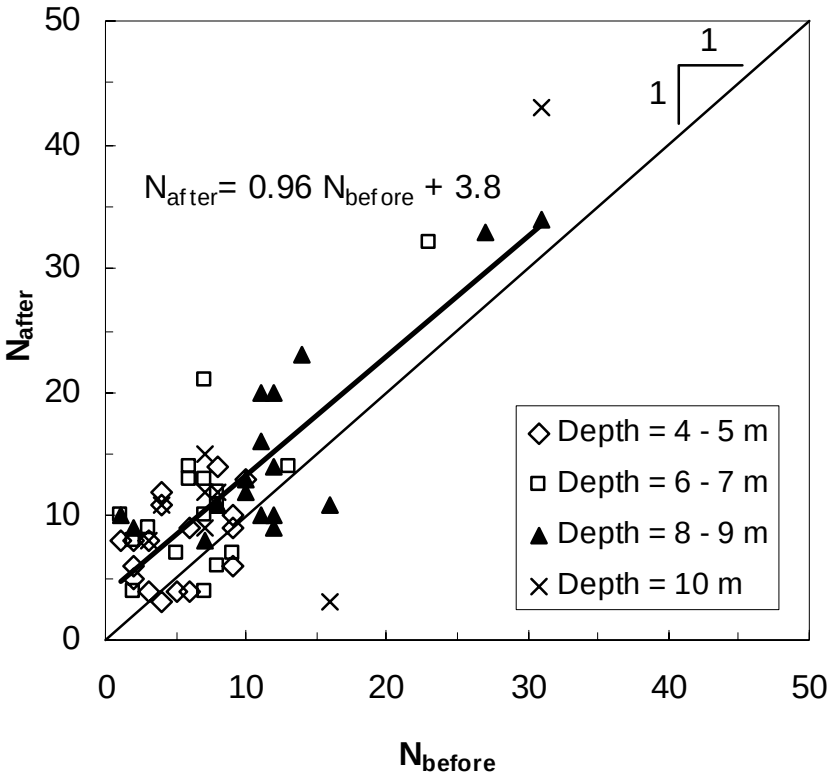

Figure 73. Change in N value due to soil liquefaction at depths of 3 – 10 m during Japanese earthquakes

Change in Void Ratio

Studies describing the change in void ratio caused by earthquake-induced liquefaction are examined for comparison with the results above regarding the change in N value due to soil liquefaction. Hayashi et al. (1966) report the results of laboratory tests in which varying magnitudes of acceleration from a vibration table are applied to saturated sands of varying initial void ratios to determine the magnitude of acceleration required to cause liquefaction. For the sands that exhibited liquefaction, the void ratios after liquefaction were also measured. In every case, the void ratio of the sand decreased due to liquefaction, i.e. densification occurred, and the average decrease in void ratio is equal to 11% from the initial void ratio. Yoshimi (1967) conducted laboratory experiments in which loose, saturated sands were enclosed in a rigid box on a shaking table, covered with an impervious membrane to which a surcharge was applied, and subjected to horizontal vibrations in order to observe the liquefaction phenomenon. Void ratio measurements taken before and after the occurrence of liquefaction of a natural sand deposit (Niigata sand) show an average decrease in void ratio of 13% after the liquefaction. More recently, Kayen et al. (2000) performed non-destructive in-situ testing using ground penetrating radar (GPR) to measure void ratios before and after blast-induced liquefaction at the Treasure Island Test Site. Their results show an average

decrease of 10% in the void ratio measured after the liquefaction from the initial void ratio. The agreement in the results of these studies despite their widely different test methods gives confidence in the assumption that soil liquefaction results in a 10% decrease in void ratio from the initial void ratio.

Relating Liquefaction Decrease in Void Ratio to Increase in N Value

The 10% decrease in void ratio can be converted to an equivalent increase in N value to adjust N values measured after field liquefaction. The result can be compared with the change observed in Figure 73 and Equation (44). A 10% decrease in void ratio can be expressed in a form equivalent to the increase in N value given in Equation (44). Equation (45) shows the resulting relationship between the void ratio after liquefaction, e_{After}, in terms of the void ratio before liquefaction, e_{Before}.

$$e_{After} = 0.9\, e_{Before} \tag{45}$$

Relative density, D_r, is defined by Terzaghi et al. (1996) as

$$D_r = \frac{e_{max} - e}{e_{max} - e_{min}} \tag{46}$$

where

e_{max} is the void ratio corresponding to the loosest state of a soil, equal to 1.36 for submerged Niigata sand (Yoshimi 1967),
e_{min} is the void ratio corresponding to the densest laboratory-obtainable state of a soil, equal to 0.66 for submerged Niigata sand (Yoshimi 1967)
e is the in-situ void ratio of the soil.

Thus, from Equation (46) and Yoshimi (1967), the relative density of Niigata sand can be expressed as

$$D_r = \frac{1.36 - e}{0.70} \tag{47}$$

Relative density, D_r, can be estimated from the standard penetration value, N_{60}, using the following equation (USACE 1993):

$$D_r \approx \left(\frac{N_{60}}{60} \right)^{0.5} \tag{48}$$

where relative density is expressed as a decimal value ($0 < D_r < 1.0$). The N values used for the examination of densification due to liquefaction (performed during this study and described previously) were all recorded in Japan. According to Seed et al. (1985), Japanese values of N can be converted to standardized N_{60} values by:

$$N_{60} = N_m \frac{ER_m}{60} \tag{49}$$

where N_m is the SPT N value for the method used and ER_m is the estimated rod energy for the method used. In Japanese practice, ER_m is either equal to 78% for the free-fall hammer release method or 67% for the rope and pulley with special throw hammer release method, yielding correction ratios of 1.30 and 1.12, respectively (Seed et al. 1985). In addition, Seed et al. (1985) report that Japanese SPT results should be further corrected for borehole diameter and hammer blow frequency effects, namely, Japanese values of N_{60} should be multiplied by 0.9 to give equivalent values of N_{60} measured in the United States. This correction will account for differences in testing procedures used in the two countries, namely, lower hammer blow frequency and smaller diameter of drill holes in the Japanese Standard Penetration Tests. Combining these two correction factors from Seed et al. (1985) yields an overall correction factor of 1.17 or 1.01 for converting Japanese values of N_{60} to U. S. values of N_{60}, depending on the test method used. It is not known which testing methods were used in the Japanese studies described previously and it is likely that both methods were used. For this study it will be assumed that the reported values of Japanese N_{60} should be increased by approximately 10% to give U.S. equivalent values of N_{60}. The 10% increase is an average between the correction factors of 1.17 and 1.01 proposed by Seed et al. (1985). Thus, for Japanese values of N_{60}, Equation (48) becomes

$$D_r \approx \left(\frac{1.1 * N_{60}}{60} \right)^{0.5} \tag{50}$$

Combining the two expressions for relative density given in Equations (47) and (50) and solving for *e* in terms of N_{60} yields:

$$e = 1.36 - 0.70 \left(\frac{1.1 N_{60}}{60} \right)^{0.5} \tag{51}$$

Similarly, combining Equations (47) and (50) and solving for N_{60} in terms of *e* yields:

$$N_{60} = 54.5 \left(\frac{1.36 - e}{0.70} \right)^2 \tag{52}$$

Table 12 and Table 13 show the results when Equations (52) and (51), respectively, are applied to determine the relationship between the increase in SPT N value and the decrease in void ratio caused by liquefaction. In Table 12, the increase in N value caused by liquefaction-induced densification as determined from the Japanese field data (performed during this study and described previously) is applied to calculate the corresponding decrease in void ratio, *e*, using Equation (51). As shown, this results in a decrease in void ratio ranging from 7.5 % to 3.3%, depending on the initial value of N_{60}.

Table 12. Comparison of measured increases in SPT N value after 1966 Niigata earthquake to decrease in void ratio, *e* calculated using Equation (52)

N_{60} Before	N_{60} After	*e* Before	*e* After	Decrease in *e*
2	5.7	1.226	1.134	7.5%
20	23	.936	0.905	3.3%

In Table 13, a 10% decrease in void ratio, as reported in the void ratio studies described above (Hayashi et al. 1966, Yoshimi 1967, and Kayen et al. 2000) and illustrated in Equation (45), is applied to an initial value of N = 20 using Equation (51). This results in an expected increase in N value of 47% (21 to 31). This increase from 21 to 31 blows is in agreement with the data plotted in Figure 73.

Table 13. Comparison of decrease in void ratio, *e*, measured in void ratio studies to increase in SPT N value calculated using Equation (51)

e Before	*e* After	Decrease in *e*	N_{60} Before	N_{60} After	Increase in N60
.923	.831	10%	21	31	1.47 (47%)

APPENDIX E

GROUND MOTION ATTENUATION AND SITE RESPONSE MODEL

From a paleoliquefaction site, the a_{max} or range of a_{max} required for triggering liquefaction at a selected magnitude can be estimated as described above. In the back-analysis, a_{max} is varied until a factor of safety of unity is achieved for an assumed value of magnitude. In the previous back analysis, a magnitude of 7.5 was assumed. To estimate the earthquake magnitude that will yield the back-calculated a_{max} for a paleoliquefaction site, a ground motion attenuation and site response analysis must be conducted. This analysis models the seismic waves that radiate from the earthquake source and propagate through the bedrock and to the paleoliquefaction site. A site response analysis models the vertical propagation of the seismic waves from the bedrock through the soil column under the site. The resulting back-calculated magnitude is used to calculate a new magnitude scaling factor for the CPT-based liquefaction back-analysis. If the new magnitude scaling factor is different from the magnitude scaling factor assumed in the back analysis, the back-analysis is repeated until the assumed magnitude in the liquefaction back-analysis converges with the magnitude estimated from the ground motion attenuation and site response analyses.

As illustrated schematically in Figure 74, seismic waves originate at a fault rupture. The waves radiate away from the rupture or earthquake source through the bedrock and eventually reach the bedrock beneath the paleoliquefaction site. At the paleoliquefaction site, the seismic waves propagate upwards through the softer sediments. The amplitude and frequency content of the seismic waves change (are amplified or attenuated) as they travel vertically through the various soils between the bedrock and the ground surface.

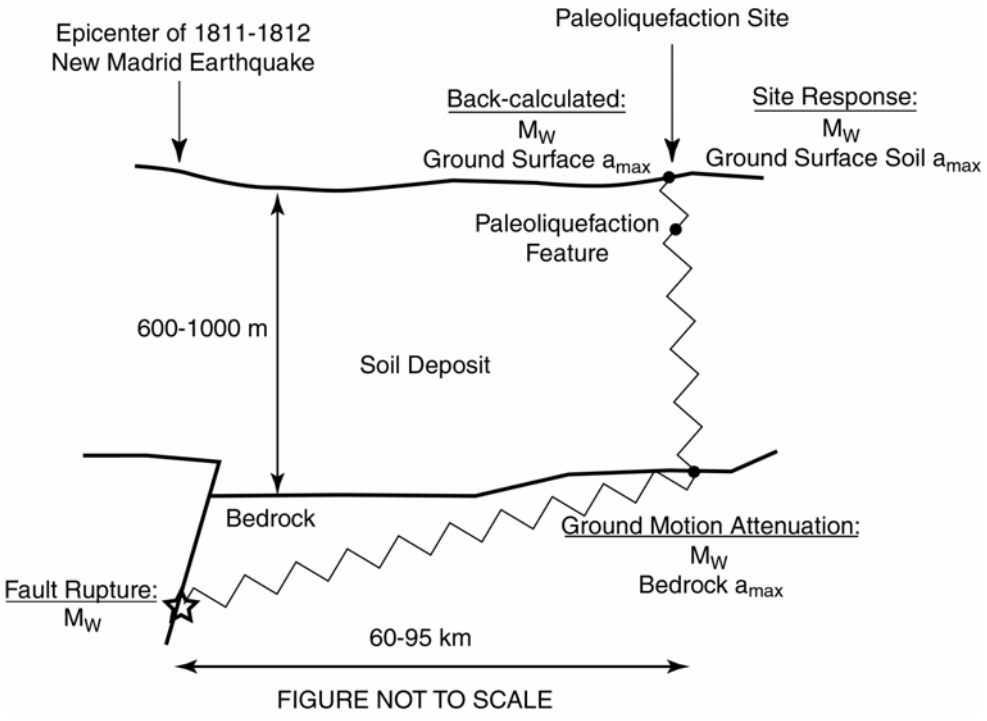

Figure 74. Schematic of paleoliquefaction back analysis

To estimate the peak ground acceleration at a specific site resulting from an earthquake of a given magnitude, a ground motion attenuation and site response analysis must be conducted. The three main steps in the attenuation and site response analyses are: (1) the earthquake source must be modeled, (2) the path that the seismic waves travel from the source to the site must be characterized, and (3) and the effect of the soil deposits on the site response analysis above the bedrock must be assessed.

Because of the lack of earthquake records for large earthquake magnitudes originating in the NMSZ, it is common to use synthetic earthquake records in attenuation and site response analyses. These synthetic earthquake records are developed from semi-empirical source, path, and site models and used to study the seismic behavior of sites in the NMSZ.

The Fourier amplitude spectrum of an earthquake motion is calculated using the model parameters described below. If synthetic time histories are required for analysis, the Fourier spectrum is applied to a randomly-generated signal of band-limited, finite-duration white noise (Boore 2003). If time histories are not required, peak ground motion parameters (peak ground acceleration, velocity, or displacement and spectral accelerations, velocities, or displacements) can be estimated from the Fourier amplitude spectrum using random vibration theory. The calculations involved in applying random vibration theory have the advantage of not requiring the computationally-intensive step of converting the earthquake motion from the frequency domain to the time domain. A thorough discussion of the background of random vibration theory and its application to seismology is given by Boore (2003). The computer program SMSIM (**S**tochastic **M**odel **SIM**ulation), developed by Boore (1996), performs the calculations necessary to calculate peak ground acceleration using random vibration theory, the Fourier amplitude spectrum, and the input parameters described below.

The main components of the Fourier amplitude spectrum for any given earthquake are (a) the Fourier amplitude spectrum of the earthquake at the source, (b) the effect of the bedrock material properties and bedrock quality on this spectrum, (c) the effect of the site characteristics on the spectrum. In general, the frequency content of an earthquake record at any site can be expressed using the equation

$$A(f, M_0, R) = S(f, M_0) \cdot D(f, R) \cdot P(f) \cdot G(f) \tag{53}$$

where $A(f,M_0,R)$ is the total Fourier amplitude spectrum at the paleoliquefaction site which depends on the following four factors: (1) $S(f,M_0)$ is the frequency spectrum of the motion at the earthquake source, depending only on seismic moment, M_0; (2) $D(f,R)$ is the attenuation of the frequency spectrum from source to site which is the effect that the path from the source to the site has on the amplitude of the spectrum, a function of hypocentral distance, R; (3) $P(f)$ is a low-pass filter that removes the high frequency

energy from the signal; and (4) *G(f)* is the effect of the soil profile at the site. Each of the four components of the model are discussed below.

Frequency Spectrum At the Earthquake Source

The single-corner model, called the Brune model after Brune (1970 and 1971), is the most commonly-used model for characterizing an the source frequency spectrum of an earthquake. The Brune model assumes a circular fault rupture whose seismic energy attenuates as a function of $1/\omega^2$, where ω is the angular frequency. The Brune model is a point-source model and does not consider the dimensions of the fault. The model is described mathematically as follows:

$$S(f, M_0) = C \cdot (2\pi f)^2 M_0 \frac{1}{1 + \left(\frac{f}{f_c}\right)^2} \tag{54}$$

where C is a constant, M_0 is the seismic moment, f is frequency, and f_c is the corner frequency. The corner frequency is the frequency above which the amplitude spectrum is constant (see Figure 75).

$$C = \frac{R_{\phi\theta} F V}{4\pi\rho\beta^3 R_0} \tag{55}$$

where $R_{\phi\theta}$=0.55 is the radiation pattern, F=2 is the free-surface amplification, V=0.71 is a factor that partitions the energy into two horizontal components, ρ is the mass density, β is the shear wave velocity of the rock at the source, and R_0=1 km is a reference distance (Boore 2003).

An important component in the Brune model is the corner frequency, f_c, above which the Fourier amplitude is constant, defined as

$$f_c = 4.9 \times 10^6 \beta \left(\frac{\Delta\sigma}{M_0}\right) \tag{56}$$

where β is the shear wave velocity of the rock at the source, $\Delta\sigma$ is the stress drop in bars, and M_0 is the seismic moment. Catchings (1999) proposes a value of β = 3.52 km/s to represent the shear wave velocity of the bedrock in the upper Mississippi embayment. The stress drop parameter is a measure of the high-frequency energy available to create seismic waves (Atkinson and Beresnev 1997) and is discussed further below.

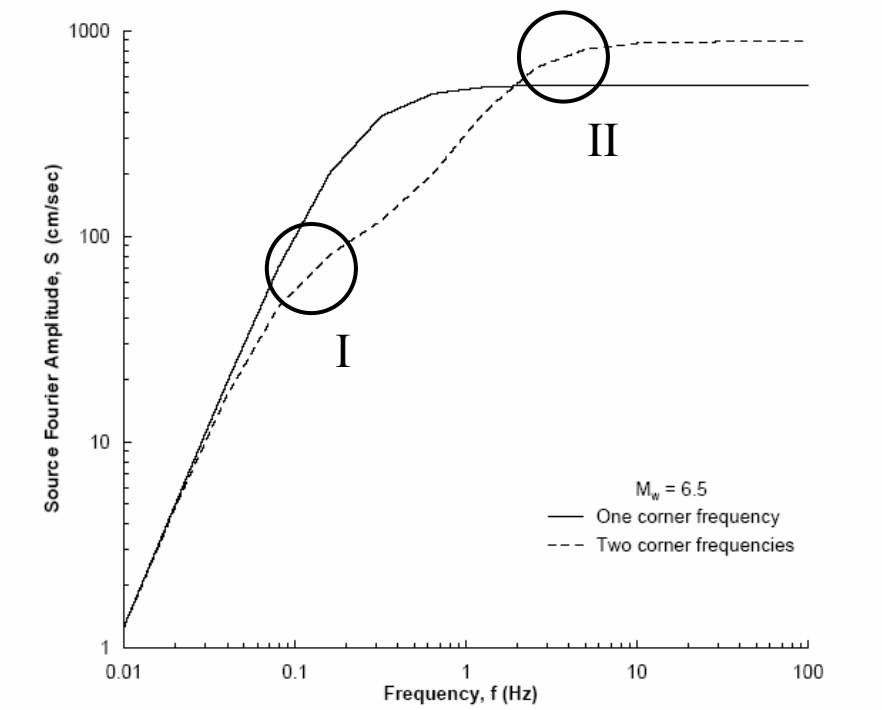

Figure 75. Brune single-corner source model and Atkinson and Boore (1995) two-corner source model (from Romero and Rix 2001)

Seismic moment is a measure of the size of an earthquake based on the energy released by the fault rupture and is defined as a function of the bedrock material properties and dimensions of the fault rupture:

$$M_0 = \mu AD \tag{57}$$

where μ is the rupture strength of the bedrock that is being faulted, A is the area over which the rupture occurs, and D is the average fault slip (Hanks and Kanamori 1979). Seismic moment is related to the more commonly-used moment magnitude, M_W, by an empirical relationship from Hanks and Kanamori (1979):

$$M_W = \frac{2}{3}\log M_0 - 10.7 \tag{58}$$

Stress drop was originally defined as the ratio of the fault slip displacement to the fault dimension. Presently, the stress drop must be inferred from seismic measurements such as source duration, corner frequency, or spectral amplitudes. Because the stress drop is only inferred and not measured directly, it is typically varied to calibrate source models with field measurements (Atkinson and Beresnev 1997). Attempts by different individuals to estimate the stress drop for an actual earthquake using different methods can yield drops from 25 bars to 500 bars, depending on the interpretation of the earthquake and the meaning of the stress drop parameter (Atkinson and Beresnev 1997).

A widely-used value for the stress drop, originally proposed by Hanks and McGuire (1981), is 100 bars. Hanks and McGuire (1981) arrived at this value by calibrating the Brune source model using California earthquakes. Romero and Rix (2001) use 110 bars as their reference stress drop but perform additional analyses using motions generated with a 150-bar stress drop source model. The US National Seismic Hazard maps utilize as one of their source models for the Central and Eastern US earthquakes a 150-bar stress drop (Frankel et al. 1996 and 2002) to account for the possibility of earthquakes with larger stress drops, like those measured for the magnitude 5.9 Saguenay, Quebec (1988) earthquake with a stress drop of 655 bars and the magnitude 4.7 New Madrid, MO (1989) earthquake with a stress drop of 229 bars (Toro et al. 1997). The analysis presented below also uses a 150-bar Brune source model to calculate the source spectrum of the ground motion. For this study, the bedrock mass density and shear wave velocity, 2.8 g/cm^3 and 3.52 km/s respectively, from Catchings (1999), also utilized by Romero and Rix (2001), are used herein.

Atkinson and Boore (1995) propose a two-corner source model (see Figure 75) where the values of the two corner frequencies depend on earthquake magnitude. The empirical Atkinson and Boore (1995) model is modeled mathematically as the sum of two Brune models and better characterizes the frequency content of intraplate earthquakes in the range of one to 10 Hz. The empirical earthquake data used to relate the locations of the two corner frequencies (see Figure 75) have magnitudes ranging from four to seven. Because the magnitudes relevant to the calculations in this study are larger than four to seven, the Brune model is assumed for the source spectrum with a stress drop of 150 bars instead of the empirical two-corner frequency model from Atkinson and Boore (1995).

Attenuation of Frequency Spectrum From Source To Site

The *D(f,R)* term in Equation (53) captures the effect of the path as the seismic waves travel from the source to the paleoliquefaction site. *D(f,R)* consists of an anelastic (or inelastic) attenuation term, D_a, and a geometric spreading term D_g.

$$D(f,R) = D_a(f,R) * D_g(R) \tag{59}$$

The anelastic diminution is the reduction in amplitude and frequency due to intrinsic losses as the seismic waves travel through the bedrock, expressed as

$$D_a(f,R) = \exp\left(\frac{-\pi f R}{\beta \cdot Q(f)}\right) \tag{60}$$

where $Q(f)=680f^{0.36}$ is the rock quality factor given by Atkinson and Boore (1995) for eastern North America.

The geometric spreading is the reduction in amplitude as the seismic waves travel further from the source. It is a function of hypocentral distance and is characterized by Atkinson and Boore (1995) as follows:

$$
\begin{aligned}
D_g(R) &= \frac{1}{R} && \text{for R<70 km} \\
D_g(R) &= \frac{1}{70} && \text{for } 70 \le \text{R} \le 130 \text{ km} \\
D_g(R) &= \frac{1}{70}\left(\frac{130}{R}\right)^{0.5} && \text{for R} \ge 130 \text{ km}
\end{aligned}
\tag{61}
$$

Herrman (2000) also presents a ground motion attenuation model for the New Madrid Seismic Zone. Because the Herrman (2000) model has not been as validated as extensively as the Atkinson and Boore (1995) model, the later was chosen for this study. The Atkinson and Boore (1995) model also was one of the models used in developing the US National Seismic Hazard Maps (Frankel, et al. 1996), as well as the one chosen by Romero and Rix (2001). There is no practical difference between the two models at distances smaller than 50 km (see Figure 76). However, there is a small difference at distances greater than 100 km (see Figure 76). All of the analyses performed in this study are at hypocentral distances less than 100 km.

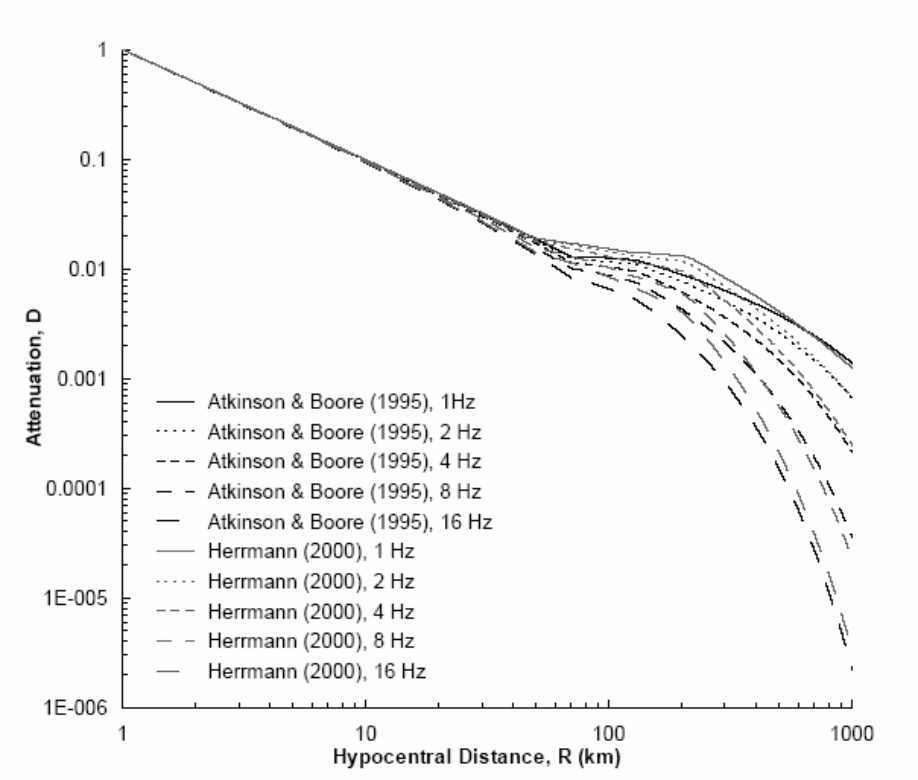

Figure 76. Comparison of attenuation models from Atkinson and Boore (1995) and Herrmann (2000) (from Romero and Rix (2001))

Of the back-analyses conducted in this study, the Wolf6 site provides the best estimate of ground shaking because it is a site of marginal liquefaction. Wolf6 is located the farthest south of the sites examined. Because of the greater epicentral distances (140 km and 175 km) associated with the two northernmost epicenters and the fact that the southernmost epicenter, located at Blytheville, AK is thought to have been the first event, an epicenter located at Blytheville, AK is initially assumed for the back-analyses conducted herein. An earthquake sufficient to trigger liquefaction at Wolf6 would also likely be sufficient to trigger liquefaction at sites at the two southernmost NMSZ sites studied herein. While the Wolf6 marginal liquefaction site does not indicate which event caused the marginal liquefaction feature there, the no liquefaction site of Wolf4 can indicate the magnitudes that were not exceeded by any earthquake event that caused ground shaking at Wolf4.

Because the Walker and Nodena Farms sites are dated to be pre-1811-1812 features and have a large degree of uncertainty because of their age and the severity of the liquefaction features, the back-analyses at those sites are performed assuming the Blytheville epicenter.

Low Pass Filter

The low-pass filter, *P(f)* in Equation (53), has a significant effect on the calculated value of a_{max} and is required to dampen the high frequency energy from the frequency spectrum calculated using the above source and path models. This reduction in amplitude of the higher frequencies could be an effect of the source or the site as discussed by Boore (2003) and Atkinson and Boore (1998). Atkinson and Boore (1995) recommend the f_{max} filter proposed by Hanks (1982)

$$P(f) = \left(1 + \left(\frac{f}{f_{max}}\right)^{8}\right)^{-0.5} \tag{62}$$

where f_{max} is the largest frequency present in the time history. Atkinson and Boore (1995) use f_{max}=50 Hz to avoid artificially diminishing the high frequency amplitudes and state that earthquake spectra from Eastern North America typically do not have data for frequencies above 20 Hz. In addition, Atkinson and Boore (1995) show that the upper corner frequency of most accelerometers is in the 20-50 Hz range.

Another type of low pass filter, usually called a κ filter, is proposed by Anderson and Hough (1984). The *k* filter reduces the high-frequency energy by

$$P(f) = \exp(-\pi\kappa f) \tag{63}$$

where κ is the slope of the Fourier spectrum at high frequencies. Anderson and Hough (1984) propose that κ is a function of the site geology. Herrmann and Akinci (2000) recommend κ of 0.048 for soil sites in the Mississippi embayment, while Frankel et al. (1996 and 2002) use a κ of 0.01 for firm rock sites in Eastern North America in developing the US National Seismic Hazard Maps. The value of κ=0.01 from Frankel et al. (1996 and 2002) is based on measurements made in a firm rock profile in South Carolina. EPRI (1993) recommends κ=0.006 for hard rock profiles and κ=0.048 for soil profiles. Romero and Rix (2001) use κ=0.02 for their NEHRP BC rock boundary analyses, κ=0.006 for their NEHRP Rock A (hard rock) analyses, and κ=0.048 for their soil site analyses.

The value of κ appears to increase with epicentral distance (Anderson and Hough 1984), but because the increase is small and dependent on the site properties it is often disregarded. Thus, the value of κ is usually assumed to be independent of epicentral distance and is assumed constant herein.

The stochastic simulations of the earthquake source and path for this study are calculated for a hard rock (NEHRP Rock A) profile. Therefore, a value of κ=0.006 from EPRI (1993) is used in order to be consistent with the definition of a hard rock profile (Rock A) in Romero and Rix (2001). Figure 77 shows the variation of a_{max} for the hard rock profile as a function of distance and magnitude developed herein as calculated using SMSIM and the input parameters described above.

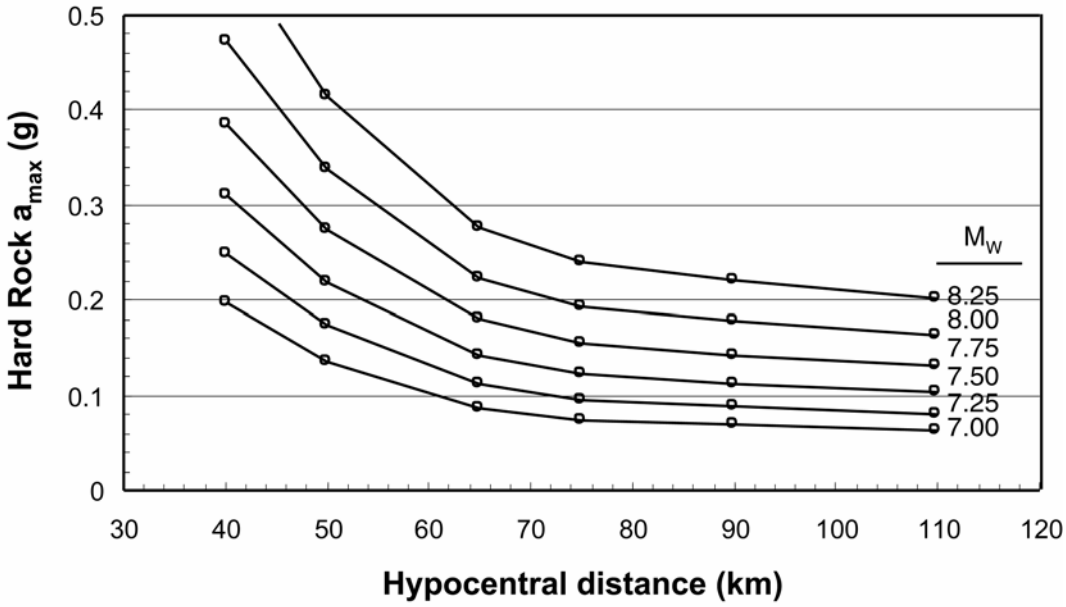

Figure 77. Variation of a_{max} with distance for varying magnitudes calculated using SMSIM for the Hard Rock profile used by Romero and Rix (2001)

Site Amplification Spectrum

The site amplification term, *G(f)* in Equation (53), captures the effect that the soil profile at a site has on the frequency spectrum and Fourier amplitude of the motion. This term in the Fourier amplitude model can be set equal to unity if a separate site response analysis is conducted. Results from a separate site response analysis are used in this study and thus *G(f)* is set equal to unity in the SMSIM analyses herein.

REFERENCES

Anderson, J.G. and Hough, S.E. (1984). "A model for the shape of the Fourier amplitude spectrum of acceleration at high frequencies." *Bulletin of the Seismological Society of America*. Vol. 74, No. 5, pp. 1969-1993.

Arulanandan, K., Yogachandran, C., Meegoda, N.J., Ying, L., and Zhauji, S. (1986). "Comparison of the SPT, CPT, SV and electrical methods of evaluating earthquake induced liquefaction susceptibility in Ying Kou City during the Haicheng Earthquake." *Use of In Situ Tests in Geotechnical Engineering*, ASCE Geotechnical Special Publication No. 6, 389-415.

Atkinson, G.M. and Beresnev, I. (1997). "Don't Call It Stress Drop." *Seismological Research Letters* Vol. 68 No. 1 pp. 3-4.

Atkinson, G.M. and Boore, D.M (1995). "Ground-Motion Relations for Eastern North America," *Bulletin of the Seismological Society of America*, Vol. 85, No. 1, pp. 17-30.

Atkinson, G.M. and Boore, D.M. (1998). "Evaluation of Models for Earthquake Source Spectra in Eastern North America." *Bulletin of the Seismological Society of America*, Vol. 88, No. 1, pp. 917-934.

Barnes, A. A., (2000). *An interdisciplinary study of earthquake-induced liquefaction features in the New Madrid seismic zone, central United States*. M. S. Thesis, Auburn University, Alabama.

Bennett, M.J. (1989). "Liquefaction analysis of the 1971 ground failure at the San Fernando Valley Juvenile Hall, California." *Bulletin of Association of Engineering Geologists*, 26(2), 209-226.

Bennett, M.J. (1990). "Ground deformation and liquefaction of soil in the Marina District." *Effects of the Loma Prieta Earthquake on the Marina District, San Francisco, California*, Dept. of the Interior, U.S. Geological Survey, Open File Report 90-253, 44-79.

Bennett, M.J., McLaughlin, P.V., Sarmiento, J.S., and Youd, T.L. (1984). "Geotechnical investigation of liquefaction sites, Imperial Valley, California." *Open-File Rep. No. 84-252*, US Geological Survey, Menlo Park, CA.

Bennett, M.J., Ponti, D.J., Tinsley, J.C. III, Holzer, T.L., and Conaway, C.H. (1998). "Subsurface geotechnical investigations near sites of ground deformation caused by the January 17, 1994, Northridge, California, earthquake." *Open-File Report 98-373*, US Geological Survey, Menlo Park, CA.

Bennett, M.J. and Tinsley, J.C (1995). *Geotechnical Data From Surface and Subsurface Samples Outside of and Within Liquefaction-related Ground Failures Caused by the Octover 17, 1989, Lome Prieta Earthquake, Santa Cruz and Monterey Counties, California.* USGS Open-file Report OFR-95-663.

Boore, D.M. (1996), *SMSIM - FORTRAN Programs for Simulating Ground Motions from Earthquakes: Version 1.0*, U.S Geological Survey Open-File Report 96-80-A.

Boore, D.M. (2003). Simulation of ground motion using the stochastic method, *Pure and Applied Geophysics* vol. 160 pp. 635--675.

Boore, D. M. (2000). *SMSIM Fortran Program for Simulating Ground Motions from Earthquakes: Version 1.87 Users' Manual*. U. S. Geological Survey No. 73.

Boulanger, R.W., Mejia, L.H., and Idriss, I.M. (1997). "Liquefaction at Moss Landing during the Loma Prieta Earthquake," *Journal of Geotechnical and Geoenvironmental Engineering*, Vol. 123, No. 5, pp. 453-464.

Bray, J.D., Önalp, A., Durgunoglu, H.T., and Stewart, J. (2000). *Ground Failure and Building Performance in Adapazari, Turkey* <http://peer.berkeley.edu/turkey/adapazari/phase1/index.html>. Accessed 22 February 2004.

Broughton, A. T., Van Arsdale, R. B., and Broughton, J. H. (2001). "Liquefaction Susceptibility Mapping in the City of Memphis and Shelby County, Tennessee." *Engineering Geology.* Vol. 62, No. 1-3, pp. 207-222.

Brune, J.N. (1970), "Tectonic Stress and the Spectra of Seismic Shear Waves from Earthquakes," *Journal of Geophysical Research*, Vol. 75, No. 26, pp. 4997-5009.

Brune, J.N. (1971), "Correction," *Journal of Geophysical Research*, Vol. 76, p. 5002.

Catchings, R. D. (1999). "Regional Vp, Vs, Vp/Vs, and Poisson's Ratios across Earthquake Source Zones from Memphis, Tennessee, to St. Louis, Missouri." *Bulletin of the Seismological Society of America*. Vol. 89, No. 6, pp. 1591-1605.

Charlie, W. A., Rwebyogo, M. F. J., and Doehring, D. O. (1992). "Time-Dependent Cone Penetration Resistance due to Blasting." *Journal of Geotechnical Engineering* Vol. 118 No. 8 pp. 1200-1215.

Clark, J. I., Zhu, F., Paulin, M., Jeffries, M. G., Rogers, B. T., Charlie, W. A., Rwebyogo, M. F. J., and Doehring, D. O. (1993). "Time-Dependent Cone Penetration Resistance Due to Blasting; Discussion and Closure." *Journal of Geotechnical Engineering* Vol. 119 No. 12 pp. 2007-2013.

Dobry, R., Ladd, R. S., Yokel, F. Y., Chung, R. M., and Powell, D. (1982). "Prediction of Pore Water Pressure Buildup and Liquefaction of Sands During Earthquakes by the Cyclic Strain Method." *NBS Building Science Series 138*, US Department of Commerce, 152 pages.

EPRI (1993), Guidelines *for Determining Design Basis Ground Motions*, Palo Alto, CA, Electric Power Research Institute, Vol. 1, EPRI TR-102293.

Frankel, A.D., Mueller, C., Barnhard, T., Perkins, D., Leyendecker, E.V., Dickman, N., Hanson, S., and Hopper, M (1996). *National Seismic-Hazard Maps: Documentation*, USGS Open-File Report 96-532.

Frankel, A.D., C. Peterson, M.D., Mueller, C., Haller, K.M., Wheeler, R.L., Leyendecker, E.V., Wesson, R.L., Harmsen, S.C., Cramer, C.H., Perkins, D.M., and Rukstales, K.S. (2002), *Documentation for the 2002 Update of the National Seismic Hazard Maps*, USGS Open-File Report 02-420.

Goto, H. (1968). "Damage to Civil Engineering Construction: Electric Power Facilities." In Kawasumi, H. and Committee (eds.) *General Report on the Niigata Earthquake of 1964* pp. 517-524.

Green, R. A. (2001). *Energy-Based Evaluation and Remediation of Liquefiable Soils.* Ph.D. thesis Virginia Polytechnic Institute and State University Blacksburg, VA 394 pages.

Green, R.A. (2004). Personal communication.

Gutenberg, B. and Richter, C. (1956). "Magnitude and Energy of Earthquakes." *Annali de Geofisica* Vol. 9 pp. 1-15.

Hanks, T.C. (1982), "f_{max}," *Bulletin of the Seismological Society of America*, Vol. 72, No. 6, pp. 1867-1879.

Hanks, T.C. and Kanamori, H. (1979). "A Moment Magnitude Scale." *Journal of Geophysical Research* Vol. 84, pp. 2348-2350.

Hanks, T.C. and McGuire, R.K. (1981), "The Character of High-Frequency Strong Ground Motion," *Bulletin of the Seismological Society of America*, Vol. 71, No. 6, pp. 2071-2095.

Hayashi, S., Kubo, K. and Nakase, A. (1966). "Damage to Harbour Structures by the Niigata Earthquake." *Soils and Foundations* Vol. 6 No. 1 pp. 89-112.

Herrmann, R.B. (2000). *Ground Motion Scaling from Earthquakes in the New Madrid Seismic Zone*. <http://www.eas.slu.edu/People/RBHerrmann/GroundMotion/>.

Accessed November 14, 2003.

Herrmann, R.B. and A. Akinci (2000), *Mid-America Ground Motion Models*, http://www.eas.slu.edu/People/RBHerrmann/MAEC/maecgnd.html. Accessed January 16 2004.

Idriss, I. M. and Sun, J. I. (1992). *SHAKE91: A Computer Program for Conducting Equivalent Linear Seismic Response Analyses of Horizontally Layered Soil Deposits*, University of California, Davis.

Ishibashi, I. and Zhang, X. (1993). "Unified Dynamic Shear Moduli and Damping Ratios of Sand and Clay," *Soils and Foundations*, 33(1), pp. 182-191.

Ishihara, K., Kawase, Y., and Nakajima, M. (1980). Liquefaction Characteristics of Sand Deposits at an Oil Tank Site During the 1978 Miyagiken-Oki Earthquake. Soils and Foundations The Japanese Society of Soil Mechanics and Foundation Engineering Vol. 20 No. 2 pp. 97-111.

Ishihara, K., Kokusho, T., and Silver, M. L. (1989). "Recent Developments in Evaluating Liquefaction Characteristics of Local Soils." *State-of-the-Art Report Proc. 12th International Conference on Soil Mechanics and Foundation Engineering* Rio de Janiero, Brazil Vol. 4 pp. 2719-2734.

Joshi, R. C., Achari, G., Kaniraj, S. R., and Wijeweera, H. (1995). "Effect of Aging on the Penetration Resistance of Sands." *Canadian Geotechnical Journal* Vol. 32 No. 5 pp. 767-782.

Juang, C.H. (2002). *Soil Liquefaction in the 1991 Chi-Chi Earthquake*. < http:// www.ces.clemson.edu/chichi/TW-LIQ/Homepage.htm>. Accessed 22 February 2004.

Juang, C.H., Yuan, H., Lee, D.-H., Lin, P.-S. (2003). "Simplified Cone Penetration Test-based Method for Evaluating Liquefaction Resistance of Soils," *Journal of Geotechnical and Geoenvironmental Engineering*, Vol. 129, No. 1, pp. 66-80.

Kawakami, F., and Asada, A. (1966). "Damage to the Ground and Earth Structures by the Niigata Earthquake of June 16, 1964." *Soils and Foundations* Vol. 6 No. 1 pp. 14-30.

Kayen, R. E., Barnhardt, W. A, Ashford, S., and Rollins, K. (2000) "Non-destructive Measurement of Soil Liquefaction Density Change by Crosshole Radar Tomography, Treasure Island, California." *Proceedings of the Sessions of Geo-Denver 2000,* Geotechnical Special Publication No 110, American Society of Civil Engineers, Computer Simulation of Earthquake Effects, pp. 52-65.

Kayen, R. E., and Mitchell, J. K. (1997). "Assessment of Liquefaction Potential During Earthquakes by Arias Intensity." J*ournal of Geotechnical and Geoenvironmental Engineering* Vol. 123 No. 12 pp. 1162-1174.

Kayen, R. E., Mitchell, J. K., Seed, R. B., Lodge, A., Nishio, S., and Coutinho, R. (1992). "Evaluation of SPT-, CPT-, and Shear Wave-based Methods for Liquefaction Potential Assessments using Loma Prieta Data." *Proc., 4th Japan-U.S. Workshop on Earthquake Resistant Design of Lifeline Facilities and Countermeasures for Soil Liquefaction*, NCEER-92-0019, Nat. Ctr. For Earthquake Engrg., Buffalo, N. Y., pp. 177-192.

Kishida (1966). "Damage to Reinforced Concrete Buildings in Niigata City with Special Reference to Foundation Engineering." *Soils and Foundations* Vol. 6 No. 1 pp. 71-88.

Kishida (1970). "Characteristics of Liquefaction of Level Sandy Ground During the Tokachioki Earthquake." *Soils and Foundations* Vol. 10 No. 2 pp. 103-111.

Koizumi, Y. (1966). "Changes in Density of Sand Subsoil Caused by the Niigata Earthquake." *Soils and Foundations* Vol. 6 No. 2 pp. 38-44.

Kulhawy, F. H. and Mayne, P. W. (1990). *Manual on Estimating Soil Properties for Foundation Design*, Final Report 1493-6, El-6800, Electric Power Research Institute, Palo Alto, CA.

Liao, T., Mayne, P.W., Tuttle, M.P., Schweig, E.S., Var Arsdale, R.B. (2002). "CPT site characterization for seismic hazards in the New Madrid seismic zone." *Soil Dynamics and Earthquake Engineering* Vol. 22, pp. 943-950.

Liao, T., Zavala, G., McGillivray, A., Camp, B., and Mayne, P.W. (2001). *Results of Cone Penetration Tests Performed in Marked Tree, AR*. Georgia Tech. Research Corporation Project Nos. E-20-F47/F34.

Lunne, T., Robertson, P. K., and Powell, J. J. M. (1997). *Cone Penetration Testing in Geotechnical Practice*. Blackie Academic and Professional/SPON Publishers, New York/UK, 312 pages.

Meigh, A. C. (1987). *Cone Penetration Testing: Methods and Interpretation*. Butterworths, London.

Mesri, G., Feng, T. W., and Benak, J. M. (1990). "Postdensification Penetration Resistance of Clean Sands". *Journal of Geotechnical Engineering* Vol. 116 No. 7 pp. 1095-1115.

Mitchell, J.K., Lodge, Angela, L., Coutinho, R.Q., Kayen, R.E., Seed, R.B., Nishio, Shinya, and Stokoe, K.H., III. (1994). "Insitu test results from four Loma Prieta earthquake liquefaction sites: SPT, CPT, DMT, and shear wave velocity." *Report No. UCB/EERC- 94/04*, Earthquake Engineering Research Center, Univ. of California, Berkeley, CA, April.

NCEER (1997). *Proceedings of the NCEER Workshop on Evaluation of Liquefaction Resistance of Soils*. Edited by Youd, T.L. and Idriss, I.M. Technical Report No. NCEER-97-0022. December 31, 1997.

NEHRP Recommended Provisions for the Development of Seismic Regulations for New Buildings (1997), Prepared by Building Safety Council for Federal Emergency Management Agency, Washington, D.C., Part 1 - Provisions.

Nuttli, O. W. (1974). *The Mississippi Valley Earthquakes of 1811 and 1812*. U. S. Geological Survey Earthquake Information Bulletin Vol 6 No 2 pp

Obermeier, S.F., J.R. Martin, A.D. Frankel, T.L. Youd, P.J. Munson, C.A. Munson, and E.C. Pond (1993). *Liquefaction evidence for one or more strong Holocene earthquakes in the Wabash Valley of southern Indiana-Illinois, with a preliminary estimate of magnitude*. U.S. Geological Survey Professional Paper 1536, 27p.

Obermeier, S. F., and Pond, E. C. (1999). "Issues in Using Liquefaction Features for Paleoseismic Analysis." *Seismological Research Letters*, Vol. 70, No. 1, pp. 34-58.

Ohsaki, Y. (1966). "Niigata Earthquakes, 1964 Building Damage and Soil Condition." *Soils and Foundations* Vol. 6 No. 2 pp. 14-37.

Ohsaki, Y. (1970). "Effects of Sand Compaction on Liquefaction During the Tokachioki Earthquake." *Soils and Foundations* Vol. 10 No. 2 pp. 112-128.

Olson, S.M., Obermeier, S.F., and Stark, T.D. (2001). "Interpretation of Penetration Resistance for Back-analysis at Sites of Previous Liquefaction." *Seismological Research Letters*, Vol. 72, No. 1, pp. 46-59.

Olson, S. M., and Stark, T. D. (1998). "CPT Based Liquefaction Resistance of Sandy Soils." *Geotechnical Earthquake Engineering and Soil Dynamics III*, Proceedings of a Specialty Conference, Geo-Institute of the American Society of Civil Engineers, Geotechnical Special Publication No. 75, Vol. 1, pp. 325-333.

Penick, J., Jr. (1976) The *New Madrid Earthquakes of 1811-1812*. Columbia, Missouri: University of Missouri Press, 181 pp.

Pond, E. C. (1996) *Seismic Parameters for the Central United States Based on Paleoliquefaction Evidence in the Wabash Valley*. Ph.D. thesis Virginia Polytechnic and State University, Blacksburg, VA 583 pages.

Pond, E. C. and J. R. Martin (1997). "Estimated magnitudes and accelerations associated with prehistoric earthquakes in the Wabash valley region of the central U.S." *Seismological Research Letters*, 68, 611-623.

Rix, G. J., and Stokoe, K. H. II (1991). “Correlation of Initial Tangent Moduli and Cone Penetration Resistance,” *Calibration Chamber Testing*, A. B. Huang, Ed., Elsevier, pp. 351-362.

Robertson, P. K. (1990). "Soil Classification Using the Cone Penetration Test." *Canadian Geotech. Journal*, Vol. 27 No. 1 pp. 151-158.

Robertson, P. K., and Wride, C. E. (1998). "Evaluating Cyclic Liquefaction Potential Using the Cone Penetration Test." *Canadian Geotechnical Journal*, Vol. 35 No. 3 pp. 442-459.

Romero, S.A., and Rix, G.J. (2001). *Ground Motion Amplification of Soils In the Upper Mississippi Embayment*. Mid-America Earthquake Center. Report No. GIT-CEE/GEO-01-1.

Seed, H. B., and Idriss, I. M. (1971). "Simplified Procedure for Evaluating Soil Liquefaction Potential." *Journal of the Soil Mechanics and Foundations Division*, Proceedings of the American Society of Civil Engineers, Vol. 97 No. SM9 pp. 1249-1273.

Seed, H. Bolton, Tokimatsu, K., Harder, L. F., and Chung, R. M. (1985). "Influence of SPT Procedures in Soil Liquefaction Resistance Evaluations." *Journal of Geotechnical Engineering*, Vol. 111 No. 12 pp. 1425-1445.

Seed, H.B., Wong, R.T., and Tokimatsu, K. (1986). "Moduli and Damping Factors for Dynamic Analyses of Cohesionless Soils." *Journal of Geotechnical Engineering*, 112(GT11), pp. 1016-1032.

Shibata, T. and Teparaksa, W. (1988). “Evaluation of liquefaction potentials of soils using cone penetration tests.” *Soils and Foundations*, 28(2), 49-60.

Silva, W.J. and K. Lee (1987), *WES RASCAL Code for Synthesizing Earthquake Ground Motions*, US Army Engineer Waterways Experiment Station, Report 24, Miscellaneous Paper S-73-1.

Sowers, G. F., and Hedges, C. S. (1966). "Dynamic Cone for Shallow In-Situ Penetration Testing". *ASTM Special Technical Publication No. 399* Fifth Pacific Area National Meeting American Society for Testing and Materials pp. 29-38.

Stark, T. D. and Olson, S. M. (1995). "Liquefaction Resistance Using CPT and Field Case Histories." *Journal of Geotechnical Engineering* Vol. 121 No. 12 pp. 856-869.

Suzuki, Y., Tokimatsu, K., Koyamada, K., Taya, Y., and Kubota, Y. (1995). “Field correlation of soil liquefaction based on CPT data.” *Proc., International Symposium on Cone Penetration Testing (CPT ’95)*, Vol. 2, Linköping, Sweden, October, 1995, pp. 583-588.

Terzaghi, K., Peck, R. B., and Mesri, G. (1996). *Soil Mechanics in Engineering Practice.* Third Edition. John Wiley and Sons, Inc.

Toro, G.R., Abrahamson, N.A., and Schneider, J.F (1997). "Model of Strong Ground Motions from Earthquakes in Central and Eastern North America: Best Estimates and Uncertainties." *Seismological Research Letters* Vol. 1 pp. 41-57.

Tuttle, M. P., (1999). *Late Holocene Earthquakes and Their Implications for Earthquake Potential of the New madrid Seismic Zone, Central United States*. PhD Thesis, University of Maryland, College Park.

Tuttle, M., Law, K.T., Seeber, L., and Jacob, K. (1990). "Liquefaction and ground failure induced by the 1988 Saguenay, Quebec, earthquake." *Canadian Geotechnical Journal*, 27, 580-589.

Tuttle, M, J., Sims, K., Dyer-Williams, R. Lafferty III, and Schweig, E. S. III (2000). *Dating of Liquefaction features in the NMSZ.* NUREG/GR-0018.

U. S. Army Corps of Engineers, Technical Engineering and Design Guides No. 7 (1993). *Bearing Capacity of Soils*. ASCE Press, New York, New York, p. 20.

Vaughn, J.D. (1994). *Paleoseismological Studies in the Western Lowlands of Southeast Missouri*. Contracted report for USGS award number 14-08-0001- G1931.

Watanabe, T. (1966). "Damage to Oil Refinery Plants and a Building on Compacted Ground by the Niigata Earthquake and Their Restoration." *Soils and Foundations* Vol. 6 No. 2 pp 86-99.

Yoshimi, Y. (1967). "An Experimental Study of Liquefaction of Saturated Sands." *Soisl and Foundations* Vol. 7 No. 2 pp. 20-32.

Youd, T.L. and Bennett, M.J. (1983). "Liquefaction sites, Imperial Valley, California." *Journal of Geotechnical Engineering Division, ASCE*, 109(3), 440-457.

Youd, T.L., Bray, J.D., Önalp, A., Durgunoglu, H.T., and Stewart, J. (2000). *CPT Liquefaction Investigations, Adapazari, Turkey*. <http://peer.berkeley.edu/turkey/adapazari/phase2/index.html>. Accessed 22 February 2004.

Youd, T. L., Idriss, I. M., Andrus, R. D., Arango, I., Castro, G., Christian, J. T., Dobry, R., Finn, W. D. L., Harder, L. F. Jr., Hynes, M. E., Ishihara, K., Koester, J. P., Liao, S. S. C., Marcuson, W. F. III, Martin, G. R., Mitchell, J. K., Moriwaki, Y., Power, M. S., Robertson, P. K., Seed, R. B., and Stokoe, K. H. II. (2001). "Liquefaction Resistance of Soils: Summary Report from the 1996 NCEER and 1998 NCEER/NSF Workshops on Evaluation of Liquefaction Resistance of Soils." *Journal of Geotechnical and Geoenvironmental Engineering*, Vol. 127 No. 10 pp. 817-833.